GAS PHASE (C-H-O) CARBIDIZATION OF IRON FROM HEMATITE AT 625 °C

by

Jesús Ramón López Hércules

ProQuest LLC.
789 East Eisenhower Parkway
P.O. Box 1346
Ann Arbor, MI 48106 – 1346

A thesis submitted to the Faculty and Board of Trustees of The Colorado School of Mines in partial fulfillment of the requirements for the degree of *Doctor of Philosophy in Metallurgical and Materials Engineering.*

Golden, Colorado
Date : 11/19/98

Signed : _____
Jesús Ramón López Hércules

Approved: _____
Dr. Gerard P. Martins
Thesis Advisor

Golden, Colorado
Date: 11/19/98

_____
Dr. John J. Moore
Professor and Head Department of
Metallurgical and Materials
Engineering.

ABSTRACT

Iron carbide (cementite), produced by gas-phase carbidization, is likely to become a significant feedstock for EAF steelmaking as the new millennium is approached. Nucor Steel and Qualitech Steel are two corporations in the U.S. who have committed significant investment in its future. The primary objective of the research was the contribution to the knowledge base on the intrinsic reaction-kinetics and associated mechanisms of the carbidization of iron to cementite. In addition, thermodynamic analyses were conducted in regard to the solid phase equilibrium configuration in which amorphous carbon rather than graphite was the stable condensed carbon-phase. Metastable gas-phase configurations, based on the postulate of low intrinsic gas-phase equilibration rates for methanation were also examined.

The thermodynamic analysis in regard to gas-phase saturation with respect to amorphous (Dent) carbon, $C_{(am)}$, rather than graphite, indicated that at selected low temperatures (800-900°K), the boundary delineating the undersaturated from the saturated gas-phase, provides an increased undersaturated field when $C_{(am)}$ is the equilibrated condensed carbon-species. In addition, when CH_4 is excluded from the contacting gas-phase (meta-stable gas-phase) the Fe_3C field now envelops the tie line along which a specified Y_{H_2} / Y_{CO} ratio is located. This meta-stable gas-phase feature, in principle, would indicate that Fe_3C could be produced with gas mixtures of $Y_{H_2} / Y_{CO} \rangle 3$, whereas a stable ($CH_4$, CO, CO_2 H_2O, H_2) gas-phase analysis would have predicted Fe as the stable iron-species.

The contribution to the elucidation of the reaction-kinetics and mechanisms of conversion of iron (the product of reduction of reagent-grade hematite) to cementite consisted of the development of a rate equation based on adsorption of CO and H_2 onto the surface of the solid reactant. This reaction-rate model incorporates the following

mechanistic steps: adsorption equilibria between H_2 and CO in the gas-phase and also on the surface species; dissociation of the surface CO by two paths - a surface Boudouard reaction and a surface water-gas reaction - which produce a carbon surface-species and ultimately, an intrinsically high-rate conversion reaction between the carbon and the iron surface to produce cementite.

The parameters of the rate-equation were obtained from experiments (at 625 °C, 898 °K) conducted with CO-Ar and CO-H_2 gas mixtures. The composition of the CO-H_2 gas mixtures covered the range from "pure" CO (no H_2 present) to low mole fraction of CO ($Y_{CO} = 0.05$).

The reaction-rate equation developed in conjunction with the measurements of the fractional conversion of Fe to Fe_3C, $\chi_{Fe}(t)$ was:

$$\chi_{Fe}(t) = \lambda \cdot r''_{Fe_3C(PCO,PH_2)} \cdot t$$

in which,

$$\lambda = \frac{3M_a S_o}{m_{Ao}}$$

$$\lambda \cdot r''_{Fe_3C(PCO,PH_2)} = k'_{3.15}\left[\frac{(K_{3.13}\cdot p_1)^2}{\left(1+(K_{3.13}\cdot p_1)^{1/2}+(K_{3.14}\cdot p_2)^{1/2}\right)^4}\right]+$$

$$k'_{3.16}\left[\frac{(K_{3.13}\cdot p_1)}{\left(1+(K_{3.13}\cdot p_1)^{1/2}+(K_{3.14}\cdot p_2)^{1/2}\right)^2}\right]\left[\frac{(K_{3.14}\cdot p_2)}{\left(1+(K_{3.13}\cdot p_1)^{1/2}+(K_{3.14}\cdot p_2)^{1/2}\right)^2}\right]$$

and,

$$K_{3.13} = 1.33 \pm 0.08 \text{ atm}^{-1}$$

$$K_{3.14} = 0.35 \pm 0.02 \text{ atm}^{-1}$$

$$\lambda \cdot k_{3.15} = k'_{3.15} = 0.66 \pm 0.03 \text{min}^{-1}$$

$$\lambda \cdot k_{3.16} = k'_{3.16} = 21 \pm 1.5 \text{ min}^{-1}$$

$$p_{1(2)}[\equiv] \text{ atm.}$$

The quantity λ incorporates the Fe stoichiometry of Fe_3C, molecular weight of Fe, the initial mass of iron and the "surface area" of the precursor iron . The latter quantity can not be determined explicitly since it is embedded in the heterogeneous reaction-rate constants of $k'_{3.15}$ and $k'_{3.16}$.

There was evidence, similar to that reported by Conejo in an earlier investigation, that there are two regions of rate-behavior associated with the conversion process. Specifically, the rate of conversion for conversions above 80% proceeded at lower a rate. The demarcation between these regions was well defined in the work by Conejo.

The analysis of the conversion data from the experiments conducted so as to establish the parameters of the rate equation uncovered a discrepancy between the gravimetric and Mössbauer analyses. The Mössbauer analysis indicated higher conversions than the gravimetric analysis. This paradox was traced to sample preparation associated with the comminution of the reaction product.

The experiments conducted with CO-H_2 gas-mixtures revealed that carbon precipitation was initiated on the surface of the reaction product when the conversion of iron to carbide was in excess of 95%. Also apparent from these experiments was that Fe_3C rather than Fe catalyzed the deposition of a condensed-phase carbon-species. This latter conclusion was based on the results of experiments conducted with "pure" CO where precipitation of carbon was not initiated until the cementite in the reaction product was greater than 95%.

Ancillary conclusions based on the overall suite of experiments conducted were that: a) gas-phase equilibria with a CO-H_2 feed gas, where the prominent species: CH_4, CO, CO_2, H_2O and H_2 would be forecast, does not appear to take place in the reactor system (quartz tube with sample boat) employed; and, b) methane, the carbon-bearing species in the CH_4-H_2 gas mixtures, did not produce carbidization of iron (obtained by primary reduction of reagent-grade hematite).

In regard to the accomplishments of the research conducted, it is clear that contributions have been made in regard to consideration of amorphous carbon rather than graphite in thermodynamic analyses of the Fe-C-H-O system. Also, a thermodynamic analysis should examine meta-stable configurations - both solid-phases as well as the gas-phase. Although the reaction-kinetics rate equation is a significant and valuable contribution, an additional contribution will be required in regard to the "high conversion" region during the carbidization of iron. Also, the precipitation of carbon which is observed as complete conversion is approached, will require an investigation where the gas-phase composition is systematically controlled (in conjunction with gas-chromatographic analyses) to resolve this issue. The role of sulfur species (H_2S or SO_2) in the carbidizing gas-mixture, in controlling carbon precipitation, is another topic which has been receiving significant attention recently, and will no doubt warrant a research effort to elucidate (quantitatively) the mechanisms involved.

TABLE OF CONTENTS

LIST OF FIGURES

LIST OF TABLES

ACKNOWLEDGMENTS

I would like to thank my advisor; Dr. Gerard Martins, for the support to conduct this research and his willingness to share his vast knowledge. In addition, I would like to thank Dr.Don Williamson from Physics Department for conducting the Mössbauer analyses and for his professionalism as a member of my thesis committee, and Dr. John Hager for his continual interest in this research. Also, I thank Dr. John Moore and Dr. Gene Woosley for serving on my thesis committee.

I would like to acknowledge the emotional support of my family while completing my studies; my wife, Gledys Maria Valdez Guevara and our three children (Jesús, Daniela and Karem) who provided me with a reason to research for new ideas.

My studies at Colorado School of Mines would not have been possible without the financial support provided by a scholarship awarded by the Venezuelan government through Universidad Nacional Experimental Politecnica "Antonio Jose de Sucre" UNEXPO, Conicit - Consejo Nacional de Ciencia y Tecnología. Additionally, teaching assistantships were provided by the Department of Metallurgical and Materials Engineering of Colorado School of Mines.

This thesis is dedicated to my parents, Jesús and Mercedes, to my wife, Gledys and to our three children, Jesús, Daniela and Karem, who continually expressed encouragement, patience and support during my academic career.

CHAPTER 1
INTRODUCTION

Particulate iron carbide (cementite) produced by gas-phase carbidization has, during the last five years, emerged as a viable feedstock for electric-furnace steelmaking by serving as a replacement for direct reduced-iron (DRI) pellet as well as scrap iron. It is envisioned that it also offers the potential as a feedstock for direct steel-production. Today, there exists a demand for environmentally adequate, energy efficient (and therefore less expensive) methods for producing steel.

Iron carbide is now viewed as a new iron source in the iron and steelmaking industries because of the many benefits associated with its utilization, including: (1) low levels of tramp elements making it useful as an alternative to high quality iron scrap,for which there is short supply on the market, or as a diluent for reviving low-grade scrap; (2) the relatively high carbon-content of cementite providing an auxiliary heat source; (3) it is non-pyrophoric, unlike reduced iron; (4) the particulate product can accommodate rapid injection into the bath; and, (5) it has been discovered that, with its use, lower nitrogen levels in steel can be realized.

Furthermore, in conjunction with modern post-combustion technology, which is capable of supplying more than 65% of the energy requirements, iron carbide feedstock has the potential to significantly decrease energy consumption and the need for coal injection in electric arc furnace (EAF) steelmaking.

1.1 Background and Perceived Justification of the Research.

The potential that iron carbide offers as a steelmaking feedstock was highlighted in 1994 by U.S. Steel Corporation. It was reported that "iron carbide's potential calls for

immediate exploration of this product" (McManus, 1994). This assessment was made in the light of ongoing activities in "re-engineering" the steel industry with the objective of achieving increased throughput and reduced coke consumption. These efforts have led to DRI, hot-briquetted iron (HBI) and high-carbon DRI becoming important feedstock not only for the (EAF) but also for the iron blast furnace. Nonetheless, iron carbide's impact on the industry still appeared to be exciting .

Although it is claimed by Hylsa that their high-carbon DRI pellets (~ 4wt% C) can significantly improve the performance of EAF's (Scriefer, 1995) (compared to using standard DRI with coal injection), iron carbide's advantage as a feedstock lies in its higher carbon content (~ 6wt% C) as well as its physical form (particulate) which allows it to dissolve readily when injected into the bath of the furnace. Both products offer energy savings over addition of carbon by coal injection. In contrast to coal injection, where combustion of a portion of the charge takes place in the freeboard above the bath and the heat generated is lost to the furnace walls and roof, the energy transfer is confined to the bath. Furthermore, the use of these high-carbon iron feedstocks is well suited to current post-combustion technology. An additional aspect for consideration is that there is still some uncertainty as to whether the carbon in high-carbon DRI is present as iron carbide (Fe_3C) or "free" carbon precipitated from the gas phase.

It is apparent that alternative steelmaking technologies are being assessed and implemented by the steel industry worldwide. There is little doubt that iron carbide will play a prominent role in these developments as the steel industry embarks into the 21st century.

Current technologies related to post-combustion and a pioneering iron-carbide plant, built and placed in operation by Nucor are now reviewed, so that the impact of iron carbide feedstock on the iron and steelmaking industries can be assessed.

1.1.1 Post Combustion in Steelmaking.

In EAF steelmaking, high energy efficiency during smelting is achieved by employing modern post-combustion technology, which is capable of supplying more than 65% of the energy requirement (Fruehan, 1996 and Gregory *et al.*, 1996). The underlying principle of post-combustion technology is that oxidation of CO to CO_2 produces three times the energy (enthalpy) compared to that of the primary oxidation of carbon. The off-gases evolved from the molten-steel/slag bath – CO and H_2 produced during the early stage of the melt cycle – are entrained in multiple low-velocity oxygen-injectors and oxidized to CO_2 and H_2O by combustion in the freeboard.

However reactions, such as :

$$CO_{2(g)} + C \text{ (or } \underline{C} \text{)} = 2CO_{(g)} \quad \text{.....(1.1)}$$
$$H_2O_{(g)} + C \text{(or } \underline{C}) = CO_{(g)} + H_{2(g)} \quad \text{.....(1.2)}$$

are both endothermic, and can indirectly decrease the overall efficiency of the off-gas heat recovery. This may be a result of the recirculating gas flow-field in the furnace whereby CO_2 and H_2O can react with carbon in the char or metal droplets of the foaming slag. In addition, it has been demonstrated that H_2O reacts with carbon in the metal droplets by almost an order-of-magnitude higher rate than does CO_2. This behavior may provide an explanation for the reduction in heat-release by post-combustion observed in systems that employ injection of high-volatility coals, where H_2O is then the major combustion-product.

1.1.2 Post-Combustion Technology applied to Iron-Carbide Based Steelmaking.

The high carbon content (6%) of iron-carbide feedstock will obviously decrease energy consumption and consequently the need for coal injection in EAF steelmaking. Since it is a particulate product, its solution-melting-rate in the bath will be higher than

that of scrap or pellets. In addition, the carbon monoxide off-gas evolution rate would be expected to be uniform, thereby mitigating the control strategy required for (oxygen-injection) post-combustion. Indeed, it is reported that Nucor plans to reactivate its joint venture U.S. Steel-Praxair iron carbide direct-steelmaking project, once their iron carbide plant in Trinidad is operating at steady full-capacity.

1.1.3 Nucor's Commercial Iron Carbide Process.

The process converts hematite (0.1 to 1 mm) in a fluidized-bed reactor (Garraway, 1996). The fluidized bed is designed to operate at 570 °C and 300 kPa(g). Production is 900 tonne/day of Fe_3C from 53 tonne/hour of ore, with 550,000 m^3/hour (NTP) of process gas (composition 60% CH_4, 34% H_2, 2% CO and 1% H_2O; remainder is CO_2 and N_2). Three stages have been identified in the conversion process to carbide. During Stage 1 the primary reduction of Fe_2O_3 to Fe_3O_4 occurs. In Stage 2, progressive reduction of Fe_3O_4 to Fe is achieved. In the third and final stage, carbidization of Fe to Fe_3C occurs due to the available C in the CH_4, and CO gas species. The overall stoichiometry is illustrated by the reaction :

$$3\,Fe_2O_{3(s)} + 5H_{2(g)} + 2CH_{4(g)} = 2Fe_3C_{(s)} + 9H_2O_{(g)} \quad \text{.....(1.3)}$$

It appears, based on Mössbauer analyses, that after a certain conversion level of iron has occurred (and before complete conversion to Fe), conversion of iron to carbide is initiated (at approximately 33% of the overall reaction-time) (Stephens *et al.,* 1993). The rate is relatively low at first, followed by transition to a much higher rate. Ultimately, the rate tapers off as the asymptotic conversion of 90% Fe_3C is approached at the end of the time-period for which the reaction-progress was tracked. The plant production has progressively increased (relative to the design capacity) since the July, 1994 start-up. "Reaction times have decreased to 24 hours from a high of about 84 hours. As of May 1996, production was 14,500 tonne during 18 months of operation" (Garraway, 1996).

Performance trials at Nucor Steel-Crawfordswille plant have provided results which substantiate the promise offered by iron carbide use in EAF's. Reduction of residual elements such as Cu, Ni, Cr, Mo and Sn in heats has been realized, apparently due to improved retention of carbide in the bath. In addition, nitrogen levels have been reduced beyond that predicted as being solely due to dilution. The intrinsic characteristic of carbon-monoxide evolution in the bath when this feedstock is injected may be responsible for enhanced nitrogen-flushing from the bath.

1.2 Scope of the Research Topic.

The formation of iron carbide from a carbon-bearing feed-gas species such as CO and CH_4 at temperatures above 800 °C has been cited in previous investigations and several processes have been developed in order to define optimum operating-conditions. The carbon-bearing gas-species introduces the potential risk of deposition of carbon which must be assessed on the basis of thermodynamic and kinetic analyses.

The pioneering work of Stelling (1958) claimed that the formation of iron carbide from iron oxide (Fe_2O_3) with a CO-CO_2 gas mixture at low temperatures (700 °C) was possible. Although the potential for decomposition of CO is predicted on the basis of thermodynamic considerations, it was demonstrated that the rate of the gas-solid carbidization reaction is intrinsically higher than that for carbon deposition. Several gas phase and gas-solid reactions participate in the formation of iron carbide (Fe_3C) from the iron precursor (Fe_2O_3 or Fe). Kinetic considerations allow for the realization that, in some situations, the gas phase species configuration may be metastable.

An example of this phenomenon is well documented for reduction of iron oxides by carbon monoxide in the gas phase in the shaft of an iron blast-furnace, where the temperatures are in the range 350 to 550 °C. At these temperatures the equilibrated gas-phase composition corresponds to a species distribution where the CO concentration is significantly lower than that actually present. In addition, this hypothetical, equilibrated

gas-phase composition provides for conditions where the stable solid phase is Fe. Consequently, in order for the reduction sequence: $Fe_2O_3 \rightarrow Fe_3O_4 \rightarrow Fe$ to occur, the intrinsic heterogeneous-rate of carbon deposition from the gas phase by CO decomposition must be significantly smaller than that of CO consumption by the reduction reactions where Fe_2O_3 and subsequently Fe_3O_4 are converted.

A similar situation arises when the feed gas is comprised of CO and H_2. At temperatures below 600°C, where methane is stable, the mechanism of carbidization, without carbon deposition due to CO decomposition, must incorporate the kinetically viable gas-phase methanation reaction:

$$CO_{(g)} + 3H_{2(g)} + = CH_{4(g)} + H_2O_{(g)} \quad \text{.....(1.4)}$$

Recently, Conejo (1995), studied carbidization of iron oxide (reagent grade 99.40 % Fe_2O_3) with CO/H_2 gas mixture, at 625°C. It was found that the reaction proceeded stage-wise where the Fe_2O_3 was first reduced to Fe_3O_4 followed by reduction to FeO and ultimately iron; subsequently, the iron was carbidized to form Fe_3C and as the degree of carbidization approached 100%, free-carbon deposition was initiated. The rate of carbidization was dependent on the mole-fraction ratio of the $CO-H_2$ gas mixture supplied. The iron carbide produced by the experiments conducted was primarily cementite (θ carbide, Fe_3C), which was identified by Mössbauer and XRD analysis. One experiment was described where χ carbide ($Fe_{2.5}C$) was obtained as a reaction product.

The formation of amorphous carbon on iron and nickel surfaces has been observed at temperatures below 900 °K (627 °C). This form of carbon is the thermodynamically stable phase, rather than graphite, at these temperatures. A thermodynamic window where conditions for cementite stability are achieved, without compromising the undersaturation "carbon" in the gas phase, is provided based on the theory that the boundary delineating carbon saturation is defined by amorphous carbon.

More recently, Hayashi and Iguchi (1997) reported results on "a process for producing stable iron carbide" in the temperature range 873 to 1273 °K with H_2-CH_4 gas mixtures and, in the temperature range 823 to 1223 °K with H_2-CO gas mixtures (the free carbon content was reported to be less than 5% in the total product, with 95% in iron carbide). In each case the gas phase contained sulfur-bearing species (H_2S precursor) at low sulfur activity based on Fe/FeS equilibrium (0.1-0.7). It was claimed that traces of gaseous "sulfur" promotes iron-carbide stability in preference to free carbon and metallic iron. The sulfur species adsorbed onto the iron surface is considered to serve a dual role. It inhibits precipitation of carbon, while at the same time it stabilizes iron carbide (Fe_3C) by allowing substantial bulk carburization of iron.

1. 3 Objectives of this Research

The primary objective of this research was to contribute to the development of a comprehensive knowledge-base on the gas-phase carbidization of hematite. This was accomplished, in conjunction with the literature review conducted, by: a) developing stable and metastable equilibrium phase-field diagrams based on both rectangular and equilateral-triangle displays for the ternary gas-phase component; b) developing a reaction-kinetics model, based on co-adsorption of CO and H_2, to describe the conversion-time profile of Fe to Fe_3C; and, c) conducting controlled laboratory-scale experiments for converting Fe_2O_3 to Fe_3C with a gas-phase reactant in order to corroborate and calibrate the kinetics model.

Specifically, the focus of the research has been to:

i) Develop and incorporate the phase boundaries for <u>amorphous</u> carbon in the ternary gas-phase-component (C-H-O) composition diagrams featured in the previous research contribution to this topic provided by Conejo, and to include metastable phase-fields associated with non-equilibrium species distribution in the gas-phase.

ii) Conduct experiments where the conversion of Fe_2O_3 to Fe_3C with CO-H_2 and CH_4-H_2 gas mixtures, are achieved. In conjunction with these experiments, perform gravimetric analyses so as to quantify the conversion-time behavior for the system. Include "base-line" experiments for CO-H_2 gas mixtures, in order to re-establish the intrinsic conversion rate-behavior observed by Conejo.

iii) Corroborate the quantitative conversion-time behavior determined by gravimetric analysis with Mössbauer spectroscopy analysis, and conduct x-ray diffraction analyses so as to provide for qualitative and semi-quantitative assessment of the gravimetric-analyses data.

1.4 Organization of the Thesis.

Chapter 1 of this thesis provides background information on the topic selected for the research. The scope of the research topic is presented and the objectives of the research are then outlined. The chapter is concluded with this section on the organization of the thesis. Chapter 2 contains a review of the information, available in the open literature, on carbidization (carburization) of iron oxides (including iron). The range of topics covered include thermodynamic and reaction-kinetics aspects associated with these conversion processes. In Chapter 3, theoretical frameworks are developed which provide the basis for analyzing and interpreting the system behavior, in concert with the results of the experiments conducted. Details on the equipment utilized and the experiments conducted, as well as the procedures employed, are described in Chapter 4. The results of the experiments and a forecast of the expected behavior are presented in Chapter 5. Analyses and interpretation of these results are also provided. Finally, in Chapter 6, the outcome of the research is summarized by providing a critical discussion of the accomplishments achieved. In addition, conclusions derived from the research conducted are enumerated. This concluding chapter also includes recommendations for additional research which appear to be warranted.

CHAPTER 2
LITERATURE REVIEW

This chapter summarizes the information retrieved from the open literature on a range of topics pertinent to the research conducted for this thesis. The topics included are: reduction and carbidization of iron oxides, deposition of carbon and the role of sulfur in the precipitation of carbon from carbon-bearing gas mixtures. In Section 2.1, information is provided on reaction characteristics of iron ores with H_2 and CO as reducing gases. In Section 2.2, the thermodynamics and kinetics of iron carbide formation are reviewed. Section 2.3 consists of a condensed knowledge base on: deposition of carbon, the role of sulfur on carbon precipitation, and mechanisms which provide for an understanding of filamentous-carbon formation.

2.1 Reduction of Iron Oxides.

During the conversion of iron oxides to cementite, reduction (partial or complete) must precede carbidization. In this section, the salient features inherent to the reduction of hematite to metallic iron, when H_2 and CO are the reductant gases, are outlined.

2.1.1 Structural Characteristic of Iron Oxides and Ores .

Structural characteristics of the most important oxides of iron are listed in Table 2.1, namely: hematite (Fe_2O_3), magnetite ($FeO{\cdot}Fe_2O_3$) and wüstite ($Fe_{1-x}O$) which is only thermodynamically stable above 560 °C. Also, some of the important iron-ore minerals are listed in Table 2.2.

Table 2.1 Structural Characteristic of Iron Oxides (Edström, 1953).

Oxide	Structural Feature	Density ($g.cm^{-3}$)	Specific molar volume (per mole of Fe) ($cm^3.mole^{-1}$)
wüstite $Fe_{1-x}O$	Cubic. Na Cl type Fe ions in octahedral interstices contains 5-11% Fe vacancies.	5.728 (22 % O) 5.613 (24 % O) nominal 5.71	12.58
Magnetite Fe_3O_4	Cubic. Spinel type Unit cell contains 64 tetrahedral and 32 octahedral interstices	5.10 - 5.18	14.9 - 15.13
Hematite Fe_2O_3	α- Fe_2O_3 is rhombohedral. Corundum type β- Fe_2O_3 is cubic. Spinel type	5.24	15.24

Ionic radii are Fe^{2+}= 0.75 Å, Fe^{3+}= 0.60 Å O^{2-}= 1.40 Å (After Pauling)

Table 2.2 Iron Ore Minerals (Roe, 1957).

Name	Chemical Composition	% Iron & Sp. Gr.	Crystal System & Color
Goethite	$Fe_2O_3.H_2O$	62.9 4.3	rhombohedral; yellow, red brown, black.
Hematite (Alpha form; non-magnetic)	Fe_2O_3	70.0 4.9-5.3	hexagonal- rhombohedral; red, black steel gray.
Martite or Gamma hematite. (magnetic)	Fe_2O_3	70.0 4.8-5.3	cubic; iron black often tarnished.
Magnetite	$FeO.Fe_2O_3$	72.4 5.16-5.18	cubic; iron black, many associations, strongly magnetic.
Siderite	$FeCO_3$	48.2 3.83-3.88	hexagonal- rhombohedral; gray, brown, white yellow.
Pyrite	FeS_2	46.5 4.95-5.10	cubic; brass yellow.

The name "martite" is often assigned to the rarely found natural-variety of hematite which results from oxidation of magnetite. Martite type ores may contain residual magnetite; this characteristic has been exploited for the recovery of martite in plants processing magnetite ores. The material has been synthesized by wet chemical methods,

since the 50's, in the form of a powder for recording tapes, discs and the like. A thermal process by which this magnetic ferric oxide can be produced consists of reduction of (alpha) hematite to magnetite at 500°C with hydrogen followed by (the slow) re-oxidation, at 200-250 °C, with air. It is stable at normal ambient temperatures (25-30 °C), and is converted back to the alpha form when heated above 650 °C in air.

2.1.2 Reduction Process.

The reduction processes by which iron oxides are converted to lower oxides are influenced by the reducing-gas composition, temperature, and structural properties, including porosity, of the resulting products. Kawasaki *et al.* (1962), proposed the following sequential events as providing for mechanisms by which reduction occurs, for reduction temperatures higher than 560 °C (i.e. where wüstite is a thermodynamically-stable phase in the conversion process).

The scheme is for a state during the conversion process when an outer porous layer of iron is present in the assemblage followed by the oxides of wüstite, magnetite and the precursor hematite.

1. Diffusion of reactant gas from the bulk gas stream to reaction sites
2. Adsorption of reactant gas at the wüstite interface.
3. Chemical reaction, resulting in phase boundary oxide-conversion reactions:Fe_3O_4/ $Fe_{1-x}O$ and Fe_2O_3/ Fe_3O_4.
   In conjunction with "chemical reaction":
   a) Ionic (Fe^{2+}, O^{2-}) and electron diffusion within a dense wüstite layer
   b) Ionic (Fe^{2+}, O^{2-}) and electron diffusion within a dense magnetite layer
4. Desorption of the product gas(es).
5. Diffusion of product gas(es) to the bulk gas stream.

Lien *et al.* (1971) provided the following guidelines for identifying "rate-controlling mechanisms", when they exist under limiting conditions, based upon apparent activation-energies:

Molecular Gaseous Diffusion:	~2-3 kcal . mol^{-1}
Phase-Boundary/Chemical-Reaction:	~10-15 kcal . mol^{-1}
Solid-State Diffusion :	~30-40 kcal . mol^{-1}

During the initial stages of the reduction of hematite to iron, the reduction-rate is typically much higher than during the later stages, due to what may be considered as direct contact of the reactant gas with the reactant solid. The rate of chemical reaction, in principle, subsequently becomes limited by the supply of reactant gas by diffusion through the porous product-layer and is manifested by a mechanism which is identifiable as gaseous-diffusion. In the final stages of the reduction, both the intrinsic chemical-reaction rate and solid state-diffusion rate become rate-limiting, depending on the temperature of the system.

2.1.3 Reduction of Hematite by H_2-CO Gas Mixtures.

Reduction of both dense and porous briquettes of pure iron oxides with H_2, CO and mixtures of both gases were studied over the temperature range of 800 to 1100 °C (El-Geassy, *et al.* 1977). It was observed, that the reduction rate increased when both temperature and hydrogen content of the gas-mixtures were increased. The reduction of dense briquettes with H_2 is controlled by the intrinsic chemical-reaction rate. Both the intrinsic chemical-reaction rate and gaseous-diffusion rate play a role in determining (controlling) the reduction rate when CO or CO-H_2 mixtures were employed. The activation energies measured for reduction with H_2 was 12.8 kcal/mol whereas it was 7.55 kcal/mol for CO. Reduction of porous briquettes was found to be gas-diffusion controlled

for both gases. The activation energies obtained were 5.14 and 2.28 kcal/mol, for H_2 and CO respectively. The apparent activation-energy was found to increase linearly with increase in gas composition, while the overall reduction-rates increased exponentially with increase gas composition. The reduction rate with H_2 was clearly higher than that with CO, whereas a mixture of two gases resulted in an intermediate rate.

In addition to results on reduction, the general behavior when CO was present in the gas phase was also reported. Iron carbide and free carbon were detected by x-ray analysis for products obtained from experiments conducted at below 900 °C. At higher temperatures only iron carbide was detected. They presented the following hypotheses for iron carbide formation: (1) Below 900 °C, fine-grain carbon deposited by the Boudouard reaction: $2CO_{(g)} = CO_{2(g)} + C_{(s)}$, reacts with freshly formed iron to produce iron carbide; (2) Above 900 °C, carbidization of the reduced iron is achieved via the reaction: $3Fe_{(s)} + 2CO_{(g)} = Fe_3C_{(s)} + CO_{2(g)}$.

2.2 Iron Carbide.

Cementite is not the only carbide phase which can be produced. With suitable thermodynamic and kinetic conditions, other carbide phases can also be obtained. Both thermodynamic and kinetic aspects of iron carbide formation from iron oxides by carbidizing gas-species have been studied by several investigators. The results of these studies are now presented.

2.2.1 Thermodynamic and Kinetic Details of Iron Carbide Formation.

A thermodynamic analysis of the C-H-O system in the context of formation of iron carbide indicates that there is a "risk-potential" for deposition of carbon. This carbon can be produced by the dissociation of carbon monoxide, which produces elemental carbon, $C_{(\alpha)(a)}$. This primary species can polymerize to form amorphous carbon, $C_{(\beta)(a)}$ and graphitic carbon $C_{c(s)}$, dissolve into the bulk of metal, or form a metal carbide $C_{(\gamma)(a)}$. The

dissolved carbon can re-precipitate and form whiskerlike, or vermicular, carbon C_v (Bell, 1987).

The decomposition of hydrocarbons is more complex than that of carbon monoxide according to the Boudouard reaction, and leads to a wide variety of partially hydrogenated species, CH_x and C_nH_n, as well as $C_{(\alpha)(a)}$. The hydrogen-containing fragments can lose hydrogen to produce $C_{(\alpha)(a)}$, polymerize to produce coke, or incorporate hydrogen to produce gaseous hydrocarbons. Furthermore, coke can also be formed during hydrogenation of CO since hydrogen addition to $C_{(\alpha)(a)}$ can lead to the necessary precursor.

Conejo (1995) conducted an investigation of conversion of reagent-grade hematite-powder to cementite, with H_2-CO gas mixtures. The mole fraction ratios studied, Y_{H_2} / Y_{CO}, ranged between 3 to 7, and the reaction temperatures were between 600 to 640 °C. It was found that free carbon was always formed as the conversion of metallic iron into iron carbide (cementite) approached "completion". This carbide appeared to promote the catalytic decomposition of carbon monoxide. An unexpected discovery was that when H_2-CH_4 gas mixtures, with mole-fraction ratios (Y_{H_2} / Y_{CH_4}) of 7 and 5, were employed at 630 °C, only reduction to iron was found to have occurred. This behavior was attributed to "non- equilibrium conditions" in the TGA reactor and to "kinetic limitations" of methane decomposition on the surface of the nascent reduced-iron.

2.2 2 Crystal Structure of the Carbides of Iron.

Several studies on iron carbide characterization have been conducted by X-ray diffraction, Mössbauer effect spectroscopy (MES), transmission electron microscopy (TEM) and scanning electron microscopy (SEM).

Hägg carbide, also reported in the literature as χ-carbide (Fe_2C) and iron percarbide ($Fe_{20}C_9$), is isostructural with Mn_5C_2 and Pd_5B_2 and has the formula Fe_5C_2 (Senateur, 1967). There are close similarities between Hägg carbide, Fe_5C_2, and cementite Fe_3C. Both structures have the feature that each carbon atom is near the center of a trigonal prism of iron atoms. In Hägg carbide the trigonal prisms are joined to form double layers parallel to the shorter unit cell edges, while in cementite only single layers are similarly oriented. The average magnetic-moment per iron atom is larger for cementite than for Hägg carbide (Senateur, 1967).

The structure and morphology of precipitated carbide obtained for a martensitic steel, containing 1.13%C and tempered at 120°C for 1-100 days, were studied by electron microscopy and selected-area-diffraction (Hirotsu and Nagakura, 1972). The carbide in this system was found to be orthorhombic with lattice parameters a = 4.704 ± 0.016, b= 4.318 ± 0.005 and c = 2.830 ± 0.006 Å. Referred to as η-carbide of iron, or η-Fe_2C, it is isomorphous with Co_2C and Co_2N. The structure is similar to, but different from, the structure of hexagonal ε-carbide, which has long been believed to precipitate during the first stage of tempering. The η-carbide has plate-like features with thickness of 30-50 Å and precipitates periodically along dislocations with an interval of about 100 Å.

The crystallographic structure of synthetic iron-carbide has been analyzed so as to provide predictions of the X-ray diffraction patterns corresponding to these ideal lattices (Dirand and Afqir, 1983). These diffraction patterns were systematically compared with actual patterns from carbides extracted from a low silicon-manganese steel at various stages of tempering. A mechanism of the structural transformation-sequence was proposed which incorporates, to begin with, martensitic shearing ($\alpha' \rightarrow \varepsilon$) followed by diffusion of the interstitial atoms ($\varepsilon \rightarrow \eta$) and finally "chemical twinning" ($\eta \rightarrow \chi$) with simultaneous diffusion of the matrix atoms. The transformation ($\chi \rightarrow \theta$) occurs progressively through variations in the periodicity of the twinned structure. The

crystallographic coherency between the various carbides and the matrix were determined and verified by electron microscope diffraction patterns.

The morphologies and types of carbide formed from martensite in a 1.22C Fe-alloy, tempered at 523, 573 and 623 °K, were investigated with the aid of TEM and MES (Ma. *et al.*, 1983). Carbides with three morphologies were discovered: on twins within the martensite plates; in the matrix of the twin-free areas of the martensite plates; and, along the interfaces of the martensite plates. Chi-carbide (χ-carbide) was associated with each carbide morphology in specimens tempered at 573 °K. Cementite (θ-carbide) together with χ-carbide was observed in specimens tempered at 623°K. The transformation of the 25% retained austenite in as-quenched specimens was related to the χ carbide formed at the martensite-plate interfaces during tempering. MES measurements of the magnetic transition-temperatures of the carbides show diffuse transitions, but support the hypothesis that χ-carbide is the dominant carbide in the tempering temperature-range examined.

Cementite, the most common iron-carbide, exhibits the highest hardness of the constituents of plain carbon steel. However, it does not possess a high melting-point. Jackson (1973) cites a melting point of approximately 1200 °C. He also identified two primary phase-fields for both cementite and graphite equilibrium with a liquid. The Fe-C phase diagram published by Chipman (1974) is reproduced in Figure 2.1. The metastable phase cementite may be observed at temperatures below 727 °C and for %C less than 6.67. In addition, metastable χ-carbide ($Fe_{2.2}C$), is indicated at temperatures below 230 °C and %C less than 8.9. A compilation of the structure and composition of iron carbides is provided in Table 2.3

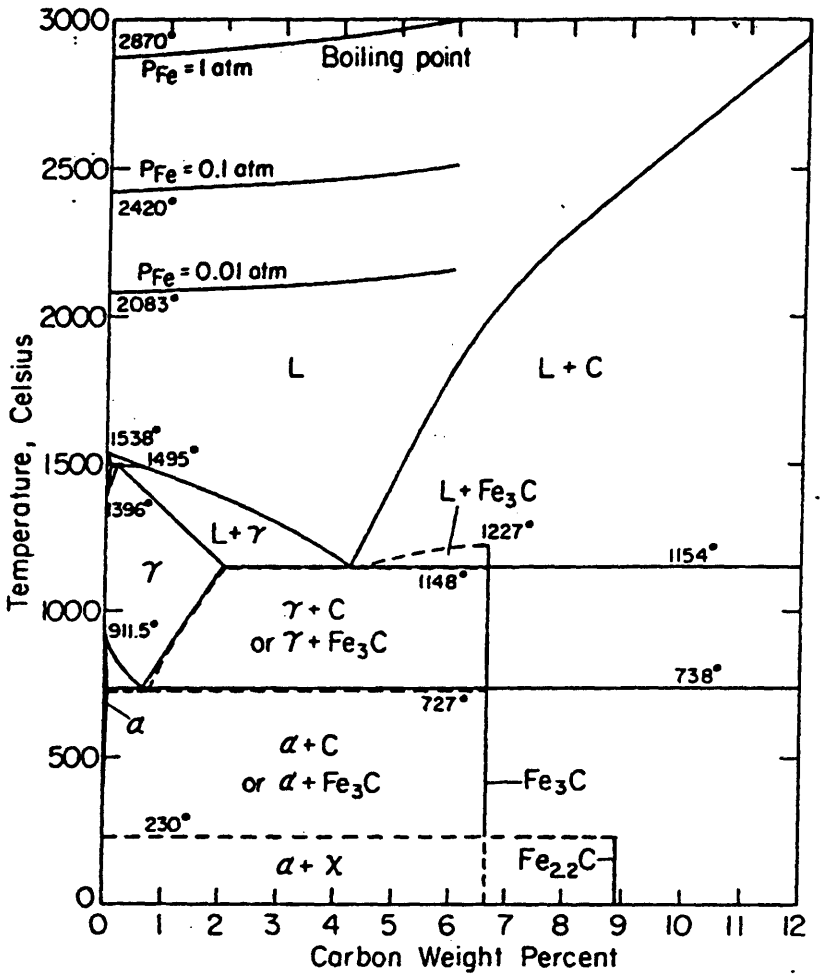

Figure 2.1 Fe-C System at 1 atm. pressure (Chipman, 1974)

Table 2.3 Lattice parameter, carbon concentration, and crystallographical data of the iron carbide phase and solid solution. From Königer *et al.* (1997).

phase	Composition	Carbon concentration (at. %)	Bravais lattice	Lattice parameter (nm) (a RT)
iron	α-Fe		bcc	a =0.28663
Austenite	γ-Fe	0.....8.3	fcc	a =0.3572+0.00078 (at.%C)
Martensite	α'-Fe(C)	0.....8.3	bct	a =0.28664-0.00028 (at.%C) c / a =1+0.0096 (at. %C)
Cementite	θ- Fe_3C	25.0	Orthorh.	a =0.45248 b =0.50896 c =0.67443
Hägg-Carbide	χ-Fe_5C_2	28.6	Monoclinic	a =1.1562 b =0.4573 c =0.5060 β =97.74°
ε-carbide	ε-Fe_2C_{1-x}	29.4 (at $Fe_{2.4}C$)	Hex.	a =.2754 c =.43486 (at $Fe_{2.4}C$)
η-carbide	η-Fe_2C	33.0	Orthorh.	a =0.4704 b =0.4318 c =0.2830

2.2.3 Previous Research on Carbidization of Iron Oxides.

There are several schemes by which iron carbides have been produced. A compilation of these processes was presented by Conejo (1995) and reproduced here, with one addition, in Table 2.4. The addendum is the recent research where a sulfur bearing species is added to the carbidizing gas-phase (Hayashi and Iguchi, 1997).

2.3 Carbon Deposition.

The formation of iron carbide by contact with a reducing and carbidizing gas-phase has the risk-potential, based on a thermodynamic assessment, for deposition of carbon. The mechanism of carbon deposition from carbon-bearing gas mixtures consists of several steps; the adsorption of the gas-species is one of the steps in the mechanism sequence. A necessary requirement is a catalytic surface by which the gas-solid reaction is promoted.

2.3.1 Thermodynamic and Kinetic Details of Carbon Deposition from CH_4 and CO.

The mechanism of carbon deposition from CO must incorporate more than just chemisorbed atoms (Dent *et al*, 1945). The atoms must link together and build up into crystallites of carbon without destroying the activity of the catalyst surface for the propagation of the process. The rate at which carbon atoms are chemisorbed onto the surface is more rapid than the rate at which they are hydrogenated to methane. They must then also link together at a rate which is appreciable higher than the rate of their hydrogenation to methane.

Pring and Farlie (1912), in their paper on the methane equilibrium cited the research conducted by Mayer and Altamayer (1907). Whereas the work conducted by Spring and Farlie was conducted in the temperature range 1200 to 1500°C, that of Mayer and Altamayer was a much lower temperature investigation where measurements were

Table 2.4 Methods for the production of iron carbide (after Conejo, 1995)					
Investigator	Year	Reduction gas and temperature	Carburizing gas and temperature	Precursor material	Solid product
Cohn and Hofer	1950	H_2 400-500°C	CO 100-350°C		Fe_2C Fe_3C
Mayer	1951		CO /CO_2 570-690°C	Fe Catalyst	
Stelling	1957	CO (H_2) 400-500°C	CO (H_2) 570-690°C	Particulate iron oxide Fe_2O_3	Fe_2C
Gray and Leroy	1975	CO 510-540 ° C		Particulate iron oxide Fe_2O_3	Fe_3C
Stephens	1977	H_2/CH4 480-700°C	H_2/CH4 480-700°C	Particulate iron oxide Fe_2O_3	Fe_2C Fe_3C
Okamura	1987	H_2 300-400°C	CO or CO/H_2 250-400°C	Acicular FeOOH	Fe_5C_2
Hayashi and Iguchi	1997	H_2/CH_4/H_2S 600-1000°C CO/H_2/H_2S 550-950°C	H_2/CH_4/H_2S 600-1000°C CO/H_2/H_2S 550-950°C	Particulate iron oxide Fe_2O_3	Fe_3C

made at temperatures between 250 and 850°C. The significance of this lower temperature investigation is that it is one of the earliest references to amorphous carbon in the context of carbon condensation from a gas phase containing carbon-bearing species.

Mayer and Altamayer (1907) conducted measurements of the gas-phase composition when methane and hydrogen were equilibrated in contact with "carbon", over the temperature range 250 to 850°C.

For the reaction :

$$C_{(s)} + 2H_{2(g)} = CH_{4(g)} \quad \ldots\ldots\ldots\ldots\ldots\ldots\ldots\ldots\ldots\ldots\ldots\ldots\ldots\ldots \quad (2.1)$$

where $C_{(s)}$ refers to amorphous carbon, and is designated as $C_{(\beta)(a)}$.

With assigning a value of 18,500 cal for the heat of formation of methane at absolute zero, the equilibrium constant for Reaction 2.1 was correlated to the data acquired, and the following equation obtained:

$$\log(K) = \frac{4{,}050}{T} - 3.027 \cdot \log(T) - 6.424 \cdot 10^{-4} \cdot T + 4.617 \quad \ldots\ldots\ldots\ldots\ldots\ldots (2.2)$$

$K\ [\equiv]\ atm^{-1}$; $523 < T\ (°K) < 1023$

Three decades later, in 1945, Dent *et al* conducted measurements of the gas composition in equilibrium with the concomitant solid-phase. This extensive research project encompassed both CH_4/H_2 and CO/O_2 equilibration with a condensed carbon-phase on a catalyst (Ni or Mo on an Al_2O_3 support) surface. The temperature range of these studies was 410 to 515°C for the C-H system and 250 to 900°C for the C-O system. A significant contribution was that the discovery that the Gibbs free-energy of the condensed solid-phase, relative to if it were hypothetically graphite, was independent of the gas-phase species that were introduced to effect the equilibration. Thus, it was found

that the gas-phase composition in equilibrium with this low-temperature phase of condensed-carbon was at higher carbon-potential than if carbon in the form of graphite were the equilibrated solid-phase.

The investigation conducted by Dent *et al* (1945) obtained measurements of the equilibrium state associated with the reaction:

$$CH_{4(g)} = C_{(s)} + 2H_{2(g)} \qquad \text{..... (2.3)}$$

at 410 and 525 °C. The measurement technique consisted of passing, at a low flow-rate, a mixture of CH_4 and H_2 over the catalyst, the composition being slightly richer in CH_4 than the expected "equilibrium composition" based on graphite. The same method was used at 250 to 900 °C for the C-O system, and the corresponding equilibrium state associated with the reaction:

$$2CO_{(g)} = CO_{2(g)} + C_{(s)}) \qquad \text{..... (2.4)}$$

The results of the measurements revealed a higher standard (Gibbs) free-energy change than that for the corresponding values of Kp_{gr} for equilibration with graphite as the condensed phase.

The measured equilibrium constants were calculated from:

$$K_p = \left[\frac{Y_{H_2}^2}{Y_{CH_4}}\right] \cdot P_{tot} \qquad \text{..... (2.5)}$$

for the Reaction (2.3); and,

$$K_p = \left[\frac{Y_{CO_2}}{Y_{CO}^2}\right] \cdot \frac{1}{P_{tot}} \quad \text{..... (2.6)}$$

for the Reaction (2.4) Y_i is the mole fraction of the species I, and, P_{tot} is the total pressure of the gas phase.

The difference in the standard free-energy change is then given by:

$$\Delta(\Delta G°) = -RT\ln(Kp)_{ob} + RT\ln(Kp)_{gr} \quad \text{..... (2.7)}$$

Dent *et al* (1945)'s compilation for the $\Delta(\Delta G°)$ values varied from 0 to 5000 kcal for the temperature range corresponding to 800 down to 350°C. More recently, Rostrup-Nielsen, (1975 –originally published in 1912) conducted similar, but less extensive, experiments to that of Dent *et al* (1945). Both CO and CH_4 decomposition on a Ni catalyst were studied. Results similar to Dent *et al* (1945) were reported except that $\Delta(\Delta G°)$ values computed from the gas-phase composition analysis were lower.

Rao and López (1985) studied the distribution of precipitated free-carbon and carbon dissolved in sponge-iron obtained by direct reduction of pellets of hematite in H_2-CH_4 gas mixtures at 800°C and at ambient pressure of 1 atm. Thermal decomposition of methane occurred and carbon dissolved in Fe was observed. In addition there was evidence of superficial carbon deposits on the iron as well as the reactor walls.

2.3.2 Correlation of Hematite to Iron Conversion Process-Parameters on the Catalytic Activity of iron for Carbon Deposition.

The temperature of reduction of hematite to iron has a significant effect on the subsequent carbon-deposition rate associated with decomposition of carbon monoxide (Turkdogan and Vinters, 1974). This behavior is apparent in Figure 2.2 for carbon deposition at 400, 600 and 1000 °C, for a CO pressure of 1 atm with 660 mg of Fe. The

iron "catalyst" was obtained by H_2-reduction of hematite ore granules at the temperature indicated in parentheses. It is observed that for temperatures of 400 and 600 °C at which

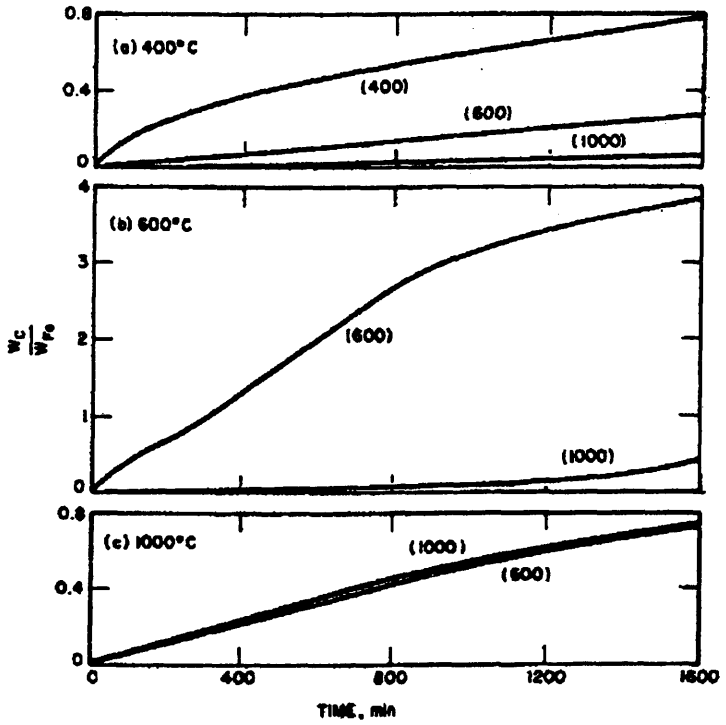

Figure 2.2. Dependency of catalytic activity of hydrogen-reduced hematite-ore granules on the reduction temperature (°C) indicated in brackets. Displayed are: Ratio of carbon-deposited relative to the mass of iron "catalyst" as a function of time, for a CO gas phase at a total pressure of 0.4 atm., at temperatures: a) 400, b) 600 and c) 1000 °C, w_{Fe} = 660mg (after Turkdogan and Vinters 1974)

carbon deposition was measured, the deposition rate decreased with increasing temperature-of-reduction at which the iron was prepared. The decreased pore surface area of iron which occurs at higher reduction temperatures may be responsible for the behavior observed. At the highest deposition temperature of 1000 °C, the reduction temperature is less critical because the higher surface-area pore structure of the iron obtained by reduction of the oxide at 600 °C, rapidly coarsens upon reheating to 1000 °C during the carbon deposition measurements. The rates of catalyzed gas-phase reactions are dependent on the characteristics, including physical condition, of the catalytic surface. In Figure 2.3 it is seen that the rate of carbon deposition at 600°C , for CO at a pressure of 1 atm, in contact with 660 mg of Fe, is highly dependent on the type of hematite from which the catalytic iron-surface was derived. It was noted that although the pore surface-area of iron obtained by the reduction of specular hematite was smaller than that obtained by the reduction of porous hematite, the rate of carbon deposition was higher with the iron from the specular hematite compared to that for the iron from the porous hematite.

2.3.3 Morphological Structure of Deposited Carbon.

The two modifications of carbon devoid of hydrogen, that have been identified on metal surfaces, are carbidic carbon and graphitic carbon (Bell *et al*, 1987). Carbidic carbon consists of isolated carbon atoms ($C_{(\alpha)}$), whereas graphitic carbon consists of one or more, sheets of carbon in which the carbon atoms exhibit sp^2 coordination. Enthalpy measurements have been made for $C_{(\alpha)(a)}$ and $C_{(c)(s)}$ on Ni , Fe and Ru. It is observed that $C_{(\alpha)(a)}$ exhibits a positive heat-of-formation relative to bulk graphite, and that graphitic overlayers on a metal exhibit a slightly negative heat-of-formation relative to bulk graphite.

Carbon filaments grown by decomposition of CO-H_2 mixtures on pure-iron catalyst

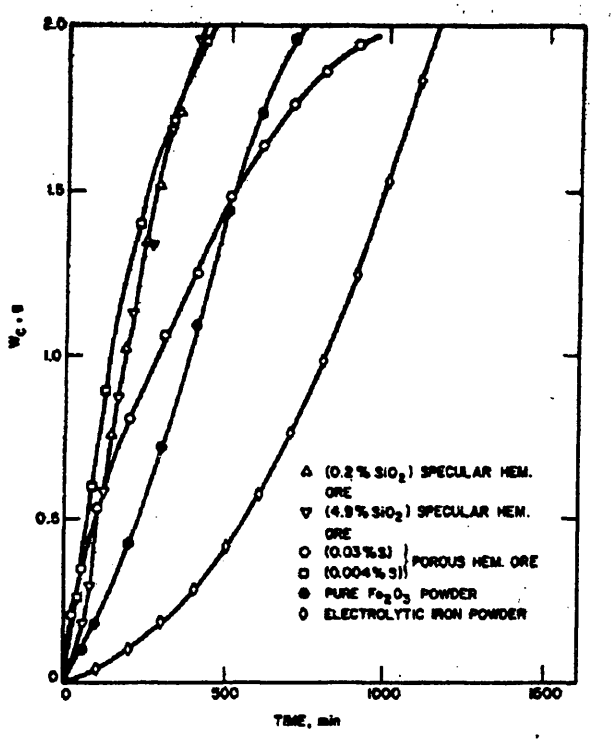

Figure 2.3 Mass of carbon deposited as a function of time onto iron (660 mg) derived from precursors (the precursor hematites were reduced with hydrogen; temperature unspecified). Conditions: 600°C; CO gas only; 1 atm total pressure (after Turkdogan and Vinters 1974).

have a uniform structure, where the layers of graphitic carbon are stacked on top of each other in a similar manner to a deck of cards. The graphitic nature of the carbon filaments is controlled to a large degree by the wetting properties that exist between the metal and deposit. The formation of carbon filaments with a high degree of crystalline perfection has been shown to be due to the existence of a strong interaction between the two components (metal and carbon deposited) (Kim *et al.*, 1992). This condition is achieved in situations where the interstitial spacing in the metal faces matches the interatomic distance of the carbon-carbon bond of graphite. Carbon filaments produced with a given bimetallic catalyst were found to become more graphitic as the hydrogen content of the reactant gas was increased. It is plausible that the higher hydrogen content of the feed gas promotes the reconstruction of the bimetallic particles, and thereby generate faces where precipitation of carbon in the form of graphite would be favored

Experiments conducted by Turkdogan and Vinters (1974) at 600°C with carbon monoxide at 1 atm in contact with 660 mg of iron catalyst, revealed that the catalyst was almost completely converted to cementite during a period of approximately one day. A mass increase of 2.4 g of carbon was recorded. The results were confirmed from X-ray diffraction patterns obtained for the reaction product, which was found to consist primarily of iron, cementite (Fe_3C) and graphite. The results of pore surface area measurements made on selected samples indicated that these areas, for unit mass of carbon in the sample, were essentially independent of the proportion of the total iron in the composite reaction-product. Thus, the pore surface-area of the carbon deposit was determined to be essentially that of graphite associated with the composite. The pore surface-area of the deposit (35.9 m^2/g) was observed to be several times greater compared to 6.2 m^2/g for the iron catalyst.

2.3.4 The Role of Sulfur on Carbon Formation.

Sulfur bearing species (SO_2, H_2S) have been found to modify significantly the precipitation behavior of carbon onto iron. This topic has been studied both in the context of catalyst (nickel) deactivation and the catalytic effect of iron (or iron carbide) on the decomposition of carbon monoxide.

Reforming Gas Equilibrium. In the context of steam reforming of natural gas (primaily CH_4), sulfur in the gas phase retards the rate of carbon formation on the catalyst more so than the reforming rate (Rostrup-Nielsen, 1984). Nucleation of carbon occurs when the surface species on the catalyst are in equilibrium with the gas phase, while at the same time the gas-phase conditions correspond to carbon supersaturation, thereby providing the potential for carbon formation.

Since methane is the primary gas species in the feed, carbon deposition is most likely to occur as a result of decomposition of this carbon-bearing species via the reaction:

$$CH_{4(g)} = C_{(s)} + 2H_{2(g)} \quad \text{.....(2.8)}$$

from which:

$$a_c^{Hyp} = K_{p(2.8)} \cdot \frac{p_{CH_4}}{\left(p_{H_2}\right)^2} \quad \text{.....(2.9)}$$

where :

a_c^{Hyp} is the hypothetical carbon activity associated with the gas phase,

p_i is the partial pressure of the species i indicated (CH_4 or H_2) present in the system,

$K_{p(2.8)}$ is the equilibrium constant for the reaction.

Furthermore,

$$K_{p(2.8)} = \frac{\left(\overline{p}_{H_2}^{eq}\right)^2}{\left(\overline{p}_{CH_4}^{eq}\right)} \quad \ldots\ldots\ldots\ldots\ldots\ldots\ldots\ldots\ldots\ldots\ldots \quad (2.10)$$

where $\overline{p}_{H_2}^{eq}$ and $\overline{p}_{CH_4}^{eq}$ are the respective equilibrium partial-pressure associated with equilibration of carbon on the surface of the catalyst. It is apparent that at equilibrium $a_c = 1$, and that this activity is referenced to graphite as the condensed phase (rather than carbon dis-sorbed in the nickel catalyst).

Rostrup-Nielsen (1977) defines the quantity ($-\Delta G_a$) as the "affinity" for the Reaction (2.8) to precipitate carbon, based on the partial pressure of H_2 and CH_4 present (independent of whether they correspond to an equilibrated gas phase). This in defined as:

$$-\Delta G_a = R\ T \ln\left(K_{p(2.8)} \cdot \frac{p_{CH_4}}{p_{H_2}^2}\right) \ldots\ldots\ldots\ldots\ldots\ldots\ldots\ldots\ldots\ldots\ldots\ldots\ldots (2.11)$$

Since in reforming operation steam is introduced with the feed, two reactions are required to describe the equilibria in the gas phase. These reactions may be selected as:

$$CH_{4(g)} + H_2O_{(g)} = CO_{(g)} + 3H_{2(g)} \ \ldots\ldots\ldots\ldots\ldots\ldots\ldots\ldots\ldots\ldots\ldots\ldots (2.12)$$

$$CO_{(g)} + H_2O_{(g)} = CO_{2(g)} + H_{2(g} \ \ldots\ldots\ldots\ldots\ldots\ldots\ldots\ldots\ldots\ldots\ldots\ldots (2.13)$$

Another affinity ($-\Delta G_e$) is then defined for Reaction (2.8) (the precipitation reaction) based on an equilibrated gas phase (as controlled by Reactions (2.12) and (2.13). This is defined as:

$$-\Delta G_e = R\ T \ln\left(K_{p(2.8)} \cdot \frac{p_{CH_4}^{eq}}{p_{H_2}^{eq}}\right) \ldots\ldots\ldots\ldots\ldots\ldots\ldots\ldots\ldots\ldots\ldots\ldots\ldots (2.14)$$

It should be noted that the partial pressures in Equation (2.14) can be different from their over-bar counter part in Equation (2.10). Carbon can be expected to be nucleated when the catalyst is in equilibrium with the gas phase, while at the same time the equilibrated gas phase is supersaturaed with respect to carbon (a_c^{Hyp} >1, ($-\Delta G_a$) = ($-\Delta G_e$)>0).

However, under conditions far removed from gas-phase equilibrium and where the kinetics of the system are interactive, the intrinsic rate of gasification of adsorbed carbon atoms can result in a depression of the steady-state carbon activity, a_c^s, at the surface of the catalyst and carbon-free operation can be achieved (a_c^s<1), in spite of a_c^{Hyp}>1 ($-\Delta G_a$ >0). This behavior also can occur in a situation where ($-\Delta G_e$)>0. The steady-state activity, a_c^s, depends on sulfur coverage (proportional to $(1-\theta_s)^2$):

$$a_c^s = \frac{a_c^{Hyp}(1-\theta_s)^2}{6.17\times 10^4 \cdot exp(-7760/T)\cdot (Y_{H_2O}/Y_{H_2})\cdot \sqrt{p_{H_2}}} \quad \text{(Rostrup-Nielsen, 1984)} \quad ...(2.15)$$

where

T is the temperature of the catalyst (°K).

p_{H_2} is the initial partial pressure of hydrogen in the system (atm.)

Y_{H_2O} / Y_{H_2} is the mole fraction ratio of water and hydrogen in the feed gas.

θ_s is sulfur coverage as a fraction of saturation.

a_c^{Hyp} is the hypothetical carbon activity in the gas phase

It should be apparent that at the onset of carbon formation a_c^s=1 .

The impact of sulfur coverage of a "catalyst" surface on nucleation of carbon is also reflected by the morphology of carbon. Above a certain coverage (θ_s ~ 0.7-0.8), carbon in the form of whiskers is not formed. This threshold value corresponds to observations by Erley and Wagner (1978). Sulfur was found to completely eliminate the

dissociative adsorption of carbon monoxide into adsorbed carbon atoms at a coverage θ_1= 0.33 (θ_1 is the sulfur coverage expressed as sulfur atoms per nickel surface-atom) which is equivalent to $\theta_s \approx 2 \times 0.33 \approx 0.7$. It is seen, on inspecting the information listed in Table 2.5, that above a certain sulfur coverage there are still sites available for the reforming reactions whereas sites for carbon formation have been passivated.

Table 2.5 Optimum Sulfur Content for Sulfur-Passivated Reforming (Rostrup-Nielsen,1984).

Experiment No.	1	2	3	4
S in feed, Vol ppm H_2S	28	14	5	1
(Y_{H_2S} / Y_{H_2})x 10^6 feed	90.9	45.5	16.2	3.2
θ_s (fd. gas basis) 850°C	0.91	0.87	0.83	0.75
θ_s (eq. gas basis) 850°C	0.86	0.83	0.78	0.70
CH_4 (dry exit), vol%	0.71	0.70	0.36	-
Duration, h	47	42	95	5
Carbon formation	No	No	No	Yes

Carbon-free operation has been demonstrated above a critical level of sulfur coverage on the catalyst, for gas-phase conditions that would otherwise result in carbon formation (Rostrup-Nielsen,1984). Sulfur-passivated reforming, as practiced in this process, eliminates the risk of carbon formation by ensemble control. In principle, potential nickel sites for carbon formation are blocked while a sufficiently large number of

sites for the reforming reactions are maintained (Udengaard *et al.*, 1992). As a result, the kinetic balance between the carbon-forming reactions and the reforming reactions is shifted in favor of reforming. This effect is achieved by adding sulfur to the process feed-gas. The sites which participate in the reforming reaction are of smaller size than those required for the formation of carbon. When incorporating sulfur into the surface, the larger-size sites disappear, but a sufficiently large fraction of the smaller-size sites (to provide for a significant rate of the reforming-reaction) will remain. Recent advances in surface science have provided a basis for a detailed understanding of this phenomenon.

SO_2 and Decomposition of Carbon Monoxide. The role of sulfur dioxide on carbon deposition from carbon monoxide has been studied (SO_2 composition from 20 to 10,000 ppm by volume) at 600°C on 660 mg hydrogen-reduced iron (Olson and Turkdogan, 1974). The results are displayed graphically in Figure 2.4.(a). It is seen that there is no apparent difference in the deposition behavior when the gas phase was either pure CO or a mixture containing 20 ppm SO_2. However, for SO_2 contents of 40 ppm and higher, the deposition-rate is greatly reduced during the elapsed time of the experiments. Furthermore, as the carbon deposition rate decreased with increasing SO_2 content of the gas mixture, the sulfur content of the solid phase increased from 0.013% in 900 min. for a gas composition of 20 ppm SO_2, to 31.5% in 350 min. for 10,000 ppm SO_2. The latter concentration corresponds to the conversion of approximately all of the iron to FeS. Consequently, the observed weight gain is a combination of carbon accumulation and formation of FeS.

The pronounced retardation of the carbon deposition rate due to SO_2 in the gas phase is also apparent in Figure 2.4.(b). However, the prominent feature of this display is that in experiment "f", once the iron sample had been conditioned for 2 minutes with 10,000 ppm, the weight gain was significantly lower than for the experiment "e" with the same concentration of SO_2 except that the SO_2 was maintained throughout the run.

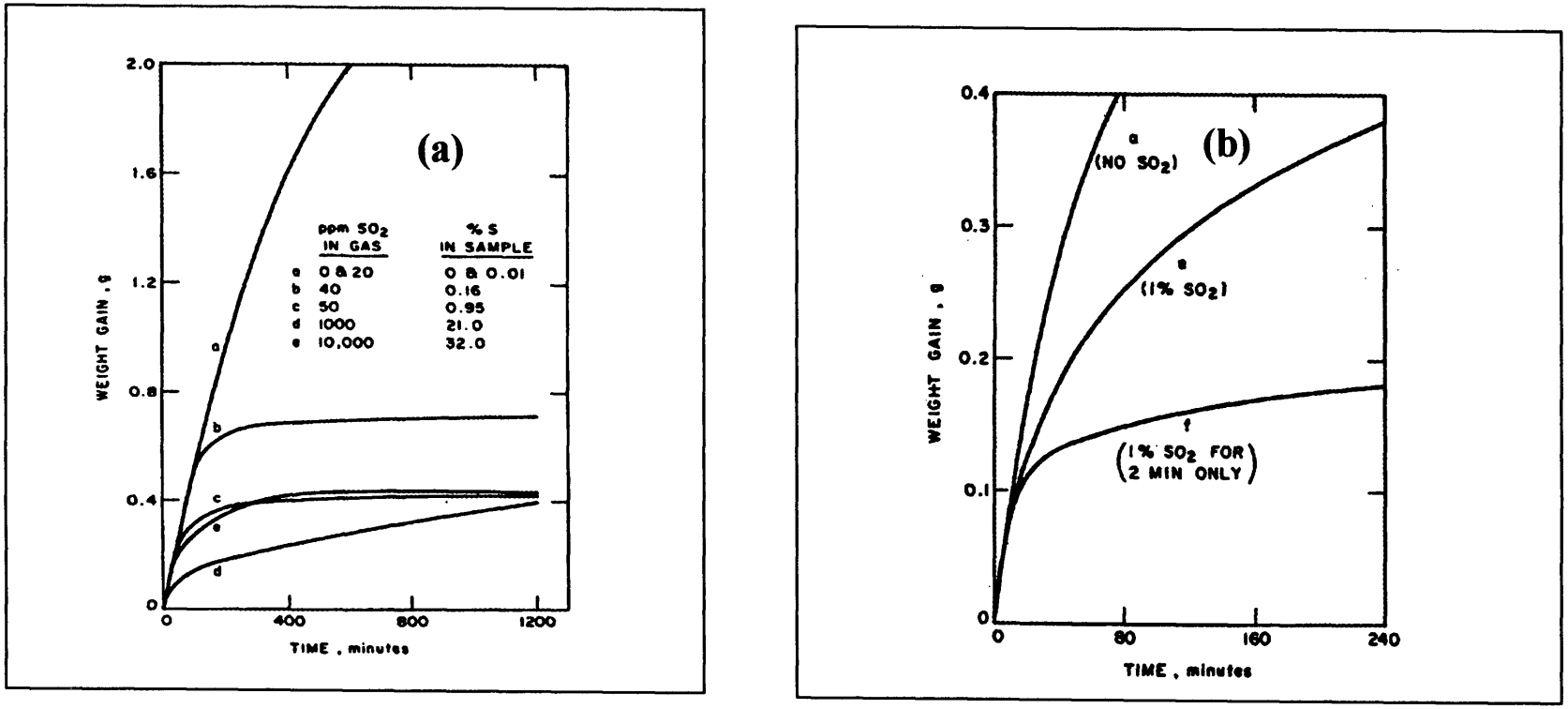

Figure 2.4 **(a)** Time dependent weight increase on 660 mg hydrogen-reduced iron obtained from hematite-ore granules. Conditions: CO-SO_2 gas mixture; 1 atm. total pressure; 600°C. **(b)** Redisplay of information presented in (a) together with response for condition where the SO_2 in the gas mixture for run "f" (10,000 ppm SO_2) was discontinued after 2 minutes. (after Olson and Turkdogan, 1974).

It is therefore apparent that the increased weight gain of the sample in the experiment "e" was due to FeS formation. The initial (2 minutes) SO_2 treatment of the iron catalyst was sufficient to significantly retard carbon formation. In the experiment "f", lasting 230 min, the sample contained 0.15 % sulfur. The x-ray examination of soot samples obtained from experiments in CO-SO_2 mixtures revealed that the carbon deposited was primarily in the form of cementite.

H_2S and Decomposition of Carbon Monoxide. Hydrogen sulfide in the gas phase can also retard the rate of carbon deposition from carbon monoxide. This has been studied at 600°C for H_2S concentrations from 25 to 250 ppm. (Olson and Turkdogan, 1974). In Figure 2.5, weight gain is shown as a function of time for samples exposed to several H_2S-containing gas mixture for 60 minutes and then contacted with CO. The results of similar experiments are shown in Figure 2.6 for an exposure time of 240 min. In both experiments the weight gain was reduced by the presence of H_2S although an acceleration of rate of weight gain was observed in several cases after the flow of H_2S had ceased. X-ray analysis of the all these samples indicated that cementite was a principal constituent. On comparison of the behavior displayed in Figure 2.4.(a) and Figure 2.7, it is apparent that there is little difference in the effect of SO_2 and H_2S on carbon deposition.

Several experiments were also conducted with H_2S concentrations up to 250 ppm in 50/50 CO-H_2 gas-mixtures. In Figure 2.7 the rate of weight gain as a function of time is shown for samples exposed to these mixtures for the duration of each experiment. X-ray analysis showed that predominant phase in the deposit was cementite. On comparing the results for the CO-H_2-H_2S mixture in Figure 2.7 with those for CO-H_2 in Figure 2.6, it can be seen that while the curves for 250 ppm H_2S are similar, the weight gain for 50 ppm H_2S in the CO-H_2-H_2S mixture is much greater than that for the corresponding CO-H_2S mixture.

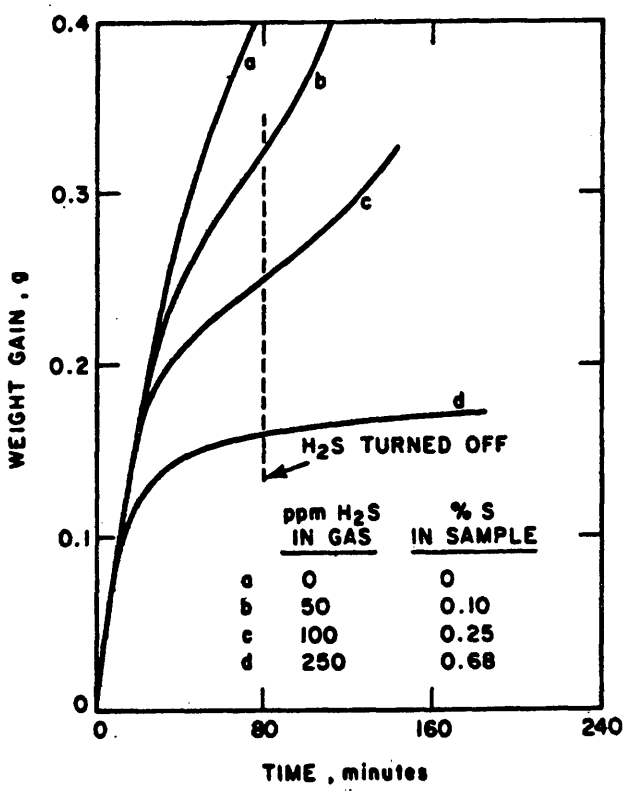

Figure 2.5 Time dependent weight increase for experiments similar to those conducted for display in Figure 2.4.(b), except that the gas-phase sulfur-species was H_2S instead of SO_2. The catalytic-activity-recovery behavior was examined by discontinuing the H_2S in the gas-mixture supplied after the time inducted (80 minutes) (after Olson and Turkdogan, 1974).

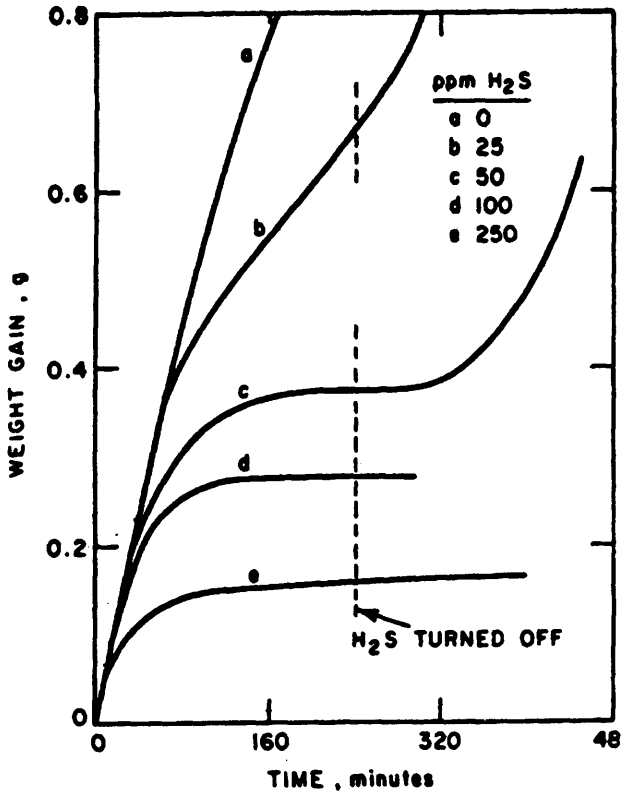

Figure 2.6 Time dependent weight increase for experiments similar to those conducted for display in Figure 2.5, except that the catalytic-activity-recovery behavior was examined by discontinuing the H_2S in the gas-mixture supplied at 240 minutes instead of 80 minutes (after R. G. Olson and E..T. Turkdogan, 1974).

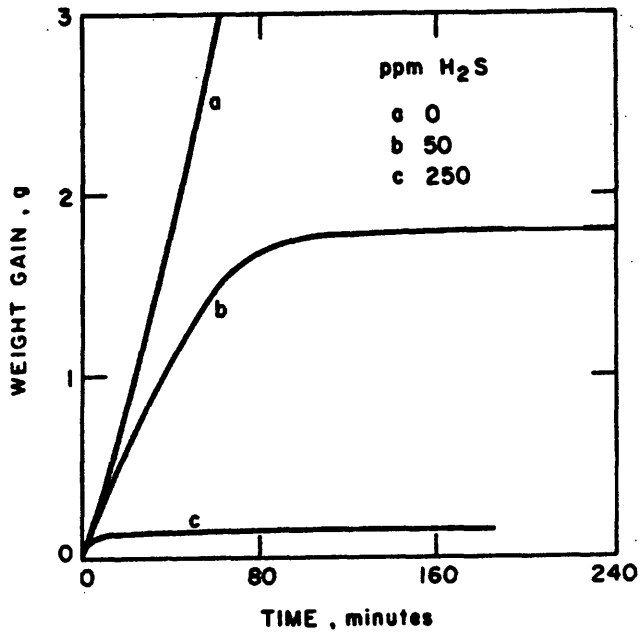

Figure 2.7 Time dependent weight increase on 660 mg hydrogen-reduced iron obtained from hematite-ore granules. Conditions: $CO-H_2-H_2S$ gas mixture(CO/H_2) = 1); 1 atm total pressure; 600 ° C (after Olson and Turkdogan, 1974).

2.3.5 Filamentous Carbon Formation.

During carbidization, the potential risk of deposition of carbon is an important consideration. The carbon deposit on an iron (or iron carbide) surface contains iron as a constituent.

Driving Force. The driving force for the bulk diffusion of carbon through the metal particle is ascribed either to a temperature gradient or to concentration gradient. Rostrup-Nielsen *et al.*(1977) proposed that the carbon solubility at the gas metal interface differs from that at the metal/carbon interface, since the activity of carbon in the gas phase may be much higher than unit. Sacco *et al.* (1989) suggest that the mass flux originates from the solubility difference between carbon at the α-iron/Fe_3C interface and that between α-iron and carbon itself. Kock *et al.* (1985) propose that the driving force for bulk carbon diffusion is the gradient of the carbon content of sub-stoichiometric carbide, whereby the carbon content decreases in the direction of the metal/carbon interface. Central in the model of Alstrup (1988) is the assumption, proposed by Schouten *et al.* (1977), that the carbon atoms entering the selvedge create a "surface carbide".

A mechanism proposed by Snoeck *et al*, (1997) is schematically represented in Figure 2.8. The surface reactions, such as the cracking or the Bouduoard reaction, produce adsorbed carbon atoms. The isolated surface carbons which are important in the filament formation dissolve into the nickel particle at the gas side, and diffuse to the rear, at the support side. At the front of the nickel particle, a selvedge with high concentration is created because of the segregation behavior of carbon in nickel: the surface is enriched with carbon, and the carbon concentration decreases from the surface concentration to the bulk concentration of interstitially dissolved carbon over a number of atomic layers. Since the concentration of carbon, dissolved in nickel at the gas side of the nickel particle, can exceed the solubility at the support side of the particle, a concentration gradient over

nickel become possible, and therefore, a driving force for the carbon diffusion through the nickel particle is created.

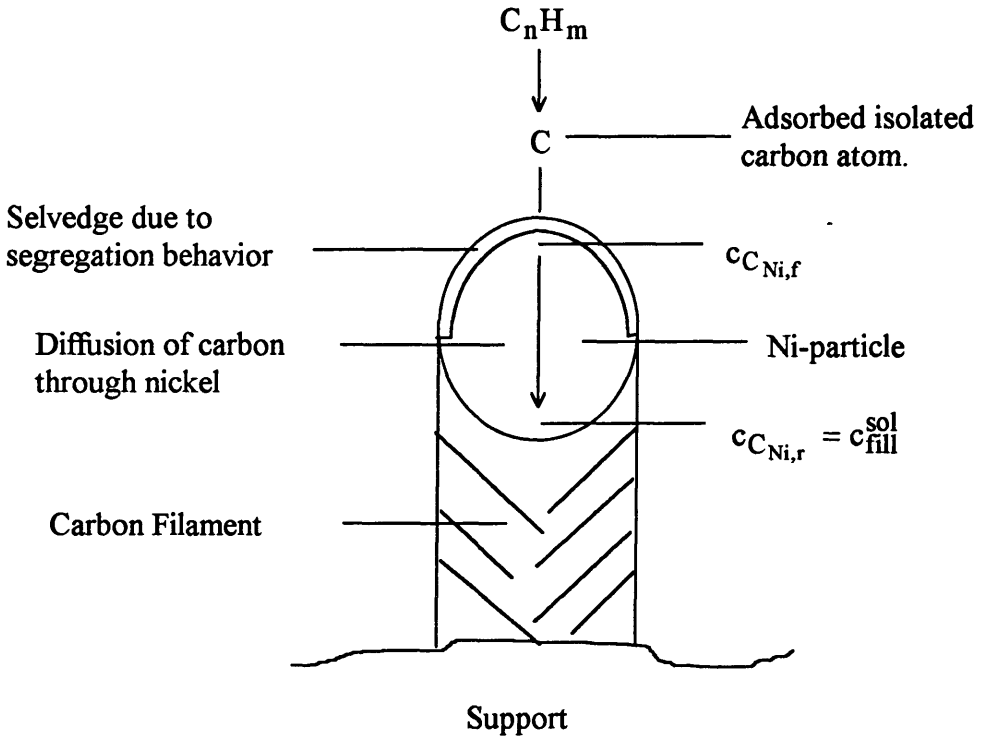

Figure 2.8 Schematic representation of the mechanism of filamentous carbon formation (after Snoeck *et al.*; 1997)

Nucleation of Carbon Filaments. It is found that a uniform concentration of carbon exists in nickel, equal to the gas-phase carbon solubility in nickel and higher than the saturation concentration of filamentous carbon (Snoeck *et al.*,1997). Nucleation of filamentous carbon can take place, provided that supersaturation is sufficiently high. Due to the very high concentration present, the surface coverage by carbon is very high. Consequently, the net rate of the surface reactions is zero, even though an "affinity for carbon formation" exists in the gas phase. After nucleation of a carbon filament, the concentration at the catalyst support side of the particle drops to the saturation concentration of the filamentous carbon, leading to the situation illustrated in Figure 2.8.

Initiation of Carbon Filament Growth and Formation of Hollow Carbon Filament. The nucleation of filamentous carbon requires a supersaturation of carbon in a nickel particle, on the catalyst support followed by reconstruction and faceting of the particle and precipitation of graphitic layers (Alstrup , 1988, Yang *et al.*, 1989 and Kim *et al* ,1992). At low temperature, the rate of nucleation is low compared to the rate of diffusion. Nucleation is uniform over the whole metal/carbon (or support) interface, and the particle is lifted from the support when carbon layers are excreted. Compact filaments are formed, without hollow channels.

At high temperature, nucleation is instantaneous, and intrinsically at a higher rate than the rate of diffusion. Nucleation occurs as soon as supersaturation is reached at the metal/support interface. The difference in diffusional path length causes rapid nucleation and excretion of carbon layers near the metal/gas interface, so that the metal is lifted from the catalyst at these places. Therefore, no driving force is present any longer for nucleation at places with high diffusional path lengths: no carbon excretion will take place there and hollow filaments are obtained. At the places where there is no excretion of carbon, the metal/support interaction must be overcome to lift the particle. This configuration is shown in Figure 2.9.

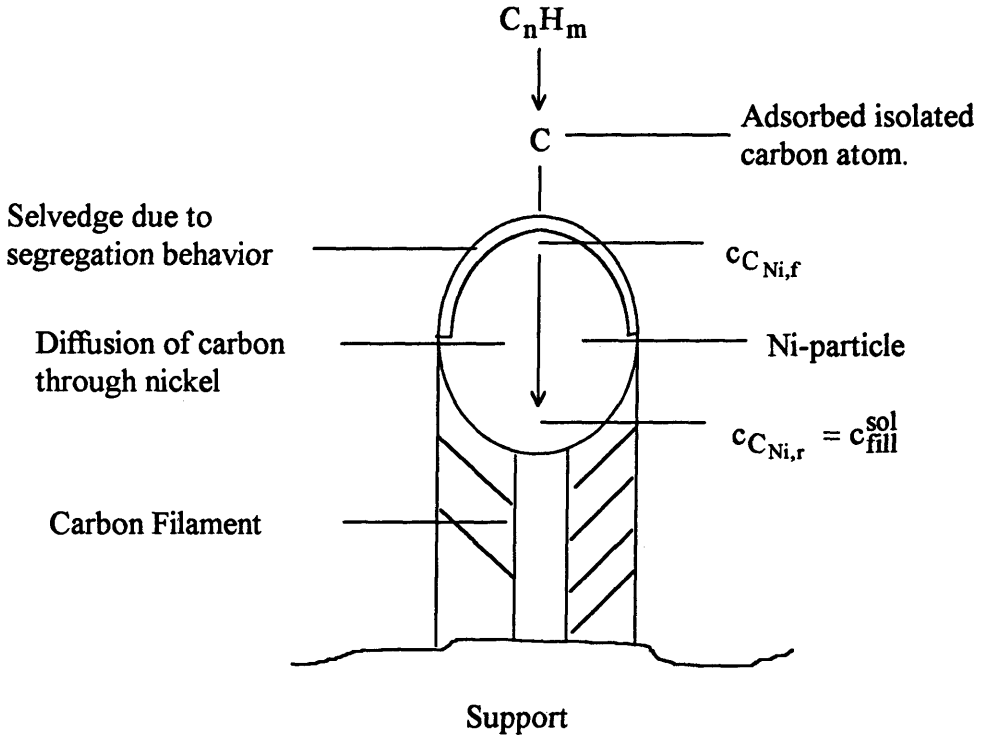

Figure 2.9 Schematic representation of the mechanism of hollow filaments formation (after Snoeck *et al.*; 1997)

Influence of Hydrogen on Carbon Deposition. Walker *et al.* (1959) investigated the formation of filamentous carbon in the iron/CO system and proposed that the presence of a critical amount of hydrogen was necessary to decompose inactive iron carbides into the catalytically active metallic form. Other explanations for this phenomenon have centered around the ability of hydrogen either to maintain a reasonably clean metal surface by gasification of residual carbon species or to mutually enhance the adsorption of CO at the exposed metal. (Park *et al.*, 1997). In addition, hydrogen plays a diverse role in the production of solid carbon —at low levels it exerts a promotional effect on the formation of this product and at concentrations above 30% of the feed-gas it acts as an inhibitor for carbon deposition.

Structure of Filamentous Carbon. Filamentous carbon is formed on small particles, e.g. on supported catalyst or polycrystalline metals having small grain sizes (Yang *et al.*,1989). The size of the particles for the formation of carbon filament are typically less than 0.5 μm. A common characteristic of all carbon filaments is that the metal particle is found in the growing tip of the filaments. The metal particle is usually faceted. Studies on the microstructure indicate that the filaments are graphitic with a fishbone structure and that graphitic layers are stacked parallel to the metal surface.

A type of Fischer-Tropsch and methanation catalyst—carbon-expanded iron— has been developed (Shultz *et al.*, 1961). This material is a form of carbon deposit which often complicates the operation of the conventional catalyst. When examined by electron microscopy these deposits are observed to consist of nuclei of iron to which are attached filaments, consisting primarily of carbon but may contain some finely dispersed iron.

2.3.6 Adsorption Models

The formation of iron carbide from carbon-bearing gas mixtures must include a mechanism by which the carbon in gas phase must to be incorporated in the reaction surface in order to promote the carbidization reaction (iron carbide formation). In this section several adsorption models are presented which the kinetics of formation of carbon, from pure CO and H_2-CO gas mixtures, on a reaction surface.

The Rate of Carbon Formation from CO. Several authors have indicated that the rate of carbon formation at constant temperature, from CO and CH_4 containing gases is solely a function of the carbon activity, a_c, of the gas. Other authors have formulated three variations of kinetic models which are capable of describing the observed kinetics of carbon formation by decomposition of CO on nickel catalysts. One of these models, for isothermal conditions, predicts that the rate of carbon formation is not solely dependent on a_c (Tavares *et al.*,1994).

Kinetic Model 1, claimed by Tøttrup (1976) to adequately describe her kinetic measurements, was based on the following reactions steps:

$$CO_{(g)} + (*) \leftrightarrow *CO \qquad \text{.....(2.16)}$$

$$*CO + (*) \rightarrow *C + *O \qquad \text{.....(2.17)}$$

$$*CO + *O \rightarrow *CO_2 + (*) \qquad \text{.....(2.18)}$$

$$*CO_2 \rightarrow CO_{2(g)} + (*) \qquad \text{.....(2.19)}$$

For conditions where the dissociation of CO is rate-limiting, Tøttrup derived the following expression for the rate of carbon formation, r_c:

$$r_c = k \frac{p_{CO}}{\left[1 + K_A p_{CO} + K_B\left(p_{CO_2} / p_{CO}\right)\right]^2} \qquad \text{.....(2.20)}$$

where

k = $k_{(2.17)}K_{(2.16)}$

K_A = $K_{(2.17)}$ is the equilibrium constant of the chemisorption of CO

K_B is a combination of equilibrium constants.

Optimization of the model parameters allowed for reasonable agreement with the measured kinetic-data.

Sakai *et al.*(1985) modeled the results of kinetic studies by replacing reactions steps (2.17) and (2.18) by the rate-limiting step where the adsorbed CO directly lead to an adsorbed carbon and adsorbed CO_2.

$$*CO + *CO \rightarrow *C + *CO_2 \qquad \text{.....(2.21)}$$

With the same constraints as above, this second model gives the following expression for the rate of carbon formation:

$$r_c = k \frac{p_{CO}^2}{\left(1 + K_A p_{CO}\right)^2} \qquad \text{.....(2.22)}$$

where

k is the product of the rate constant of the rate-limiting step and K_A^2

K_A is the equilibrium constant of the chemisorption of CO.

The third model is similar to the second, except that only one of the two CO molecules reacting with each other to form carbon and CO_2 is chemisorbed before the reaction step. However, it is not possible to distinguish between models 2 and 3 by correlation of the measured rates, since both rate expressions have the same structure.

According to Rosei *et al.* (1983), in the absence of hydrogen, three models can be postulated for CO reaction on a transition metal surface leading to the accumulation of carbon on the surface.

The first step, in all cases, is the adsorption of the CO molecule onto the surface. In Model 1, this step is followed by direct dissociation into adsorbed carbon and oxygen. The third step consists of the reduction of the surface oxygen with CO and production of CO_2 which instantaneously desorbs. These reactions are:

$$CO_{(g)} + (*) \leftrightarrow *CO \qquad \text{.....(2.23)}$$

$$*CO + (*) \rightarrow *C + *O \qquad \text{.....(2.24)}$$

$$CO_{(g)} + *O \rightarrow CO_2 + (*) \qquad \text{.....(2.25)}$$

In the second model, two adsorbed CO molecules react forming CO_2 and an adsorbed carbon atom:

$$CO_{(g)} + (*) \leftrightarrow *CO \qquad \text{.....(2.26)}$$

$$*CO + *CO \rightarrow *C + CO_{2(g)} \qquad \text{.....(2.27)}$$

Finally, the third model incorporates an additional reaction where an adsorbed CO molecule reacts with CO in the gas phase producing CO_2 and surface carbon, according to:

$$CO_{(g)} + (*) \leftrightarrow *CO \qquad \text{.....(2.28)}$$

$$*CO + CO_{(g)} \rightarrow *C + CO_{2(g)} \qquad \text{.....(2.29)}$$

In principle all three model can work, although disproportionation of CO ($2CO_{(g)} \rightarrow *C + CO_{2(g)}$) is thermodynamically favored. It was found that only Model 1 provides adequate correlation to different sets of experimental data corresponding to a wide range of total pressures.

The Rate of Carbon Formation and Carbidization from CO and H_2.

Recently Tavares *et al.* (1994) developed a kinetic model to the observed kinetics of carbon formation from CO, based on the elementary steps:

$$CO_{(g)} + (*) \leftrightarrow *CO \qquad \text{..... (2.30)}$$

$$*CO + *CO \rightarrow *C + *CO_2 \qquad \text{.....(2.31)}$$

$$*CO_2 \rightarrow CO_{2(g)} + (*) \qquad \text{.....(2.32)}$$

. The rate expression was developed on the basis that reaction step (2.31) is rate-controlling, reaction step (2.30) is at quasi-equilibrium, reaction step (2.32) is irreversible due to the absence of CO_2 in the feed, and that the adsorbed species compete for the same type of sites on the surface,

$$r_{(2.31)} = k_{(2.31)} \frac{K_{(2.30)}^2 p_{CO}^2}{\left(1 + K_{(2.30)} p_{CO}\right)^2} \qquad \text{..... (2.33)}$$

where $k_{(2.31)}$ is the rate constant of reaction step (2.31)

and $K_{(2.30)}$ is the equilibrium constant of the reaction step (2.30)

The simplest way of accounting for the presence of hydrogen atoms on the surface in this model would be to add a hydrogen chemisorption step, (Tavares *et al;*1996). This reaction is:

$$H_{2(g)} + 2(*) \leftrightarrow 2*H \qquad \text{..... (2.34)}$$

When reaction step (2.26) is considered to be in quasi-equilibrium and hydrogen atoms compete with CO molecules for the same surface sites, the rate expression for carbon is now:

$$r_c = r_{(2.31)} = k_{(2.31)} \frac{K_{(2.30)}^2 p_{CO}^2}{\left(1 + K_{(2.30)} p_{CO} + K_{(2.34)}^{1/2} p_{H_2}^{1/2}\right)^2} \qquad \text{.....(2.35)}$$

where $K_{(2.34)}$ is the equilibrium constant of reaction step (2.34).

These authors concluded that hydrogen coadsorbed with CO onto nickel significantly weakens the chemisorption-bond energy of CO.

Turkdogan and Vinters (1974) proposed the following rate-controlling reactions for carbon deposition from H_2-CO mixtures onto metallic iron:

$$*H_2 + *CO \rightarrow *H_2O + *C \qquad \text{.....(2.36)}$$

$$2*CO \rightarrow CO_{2(g)} + *C + (*) \qquad \text{..... (2.37)}$$

The carbon formed then migrates across the surface to nucleating centers where cementite and free carbon are deposited.

Conejo (1995) proposed that the rate of cementite formation from iron controlled the following two reaction steps:

$$\alpha Fe_{(s)} + CO_{(g)} \underset{k^{-}_{(2.38)}}{\overset{k^{+}_{(2.38)}}{\rightleftharpoons}} \alpha Fe_{(s)} + {}^{*}CO \qquad \text{.....(2.38)}$$

$$H_{2(g)} + {}^{*}CO \xrightarrow{k_{(2.39)}} {}^{*}H_2O + C \qquad \text{.....(2.39)}$$

The mechanism proposed includes reaction between an adsorbed species (*CO) and a gas species (H_2) to produce a surface carbon-species. This mechanism is referred to as Rideal mechanism (Laidler, 1954). The rate of carbidization, based on the scheme proposed, is given by the following equation :

$$r_{Fe_3C} = r_c = k_{(2.39)} p_{H_2} (1-\theta_1)\theta_1 \qquad \text{.....(2.40)}$$

where

θ_1 = fraction surface-coverage by carbon monoxide

Then, at steady state, the rate of formation of iron carbide is given by the following equation :

$$r_{Fe_3C} = k_{2.39} p_2 \left\{ \frac{1-\alpha^2}{4} + \alpha \sqrt{\left(\frac{1+\alpha}{2}\right)^2 - \beta} - \left[\left(\frac{1+\alpha}{2}\right)^2 - \beta \right] \right\} \qquad \text{...(2.41)}$$

where

$CO \equiv 1$; $H_2 \equiv 2$

$$\alpha = \frac{k^{+}_{2.38} p_1}{k_{2.39} p_2} + \frac{k^{-}_{2.38}}{k_{2.30} p_2} \qquad \text{and} \qquad \beta = \frac{k^{+}_{2.38} p_1}{k_{2.39} p_2}.$$

CHAPTER 3
THEORETICAL ASPECTS

In this chapter the development of both stable and metastable phase stability diagrams for the Fe-C-H-O system are presented. In Section 3.1, the development of stable-phase stability diagrams with a gas phase comprised of C-H-O components are developed. In Section 3.2, the deposition of carbon from CH_4 is explained including amorphous carbon as condensed-solid phase and graphite as well. In Section 3.3, the metastable Fe-C-H-O ternary diagrams are presented on the basis that the equilibrium is achieved in gas phase between H_2 CO, CO_2 and H_2O delineating boundary condition in order to produce iron carbide without potential risk of deposition of carbon. In Section 3.4, an adsorption model for carbidization by H_2-CO gas mixture is proposed. Finally, in Section 3.4, Predictions of the distribution of the iron-bearing phases in the reaction product from measurements of the masses of the precursor Fe_2O_3 and the product are presented

3.1 Stable-Phase Stability Diagrams

In this section, the development of stable-phase stability diagrams is presented. These consist of phase-field boundaries for pairs of iron-bearing solids in contact with a gas phase comprised of C-H-O components and in which the prominent species are CH_4, H_2, CO, CO_2 and H_2O.

3.1.1 Ternary Representation

These diagrams were developed earlier by Conejo (1995). The ternary coordinates represent the components (C-H-O) of the equilibrium gas phase comprised of the species: methane (CH_4), hydrogen (H_2), water vapor (H_2O), carbon monoxide (CO), carbon

dioxide (CO_2). For the species indicated, there is only a limited region on the C-H-O that is directly relevant. This region is shown in Figure 3.1 (Conejo. 1995).

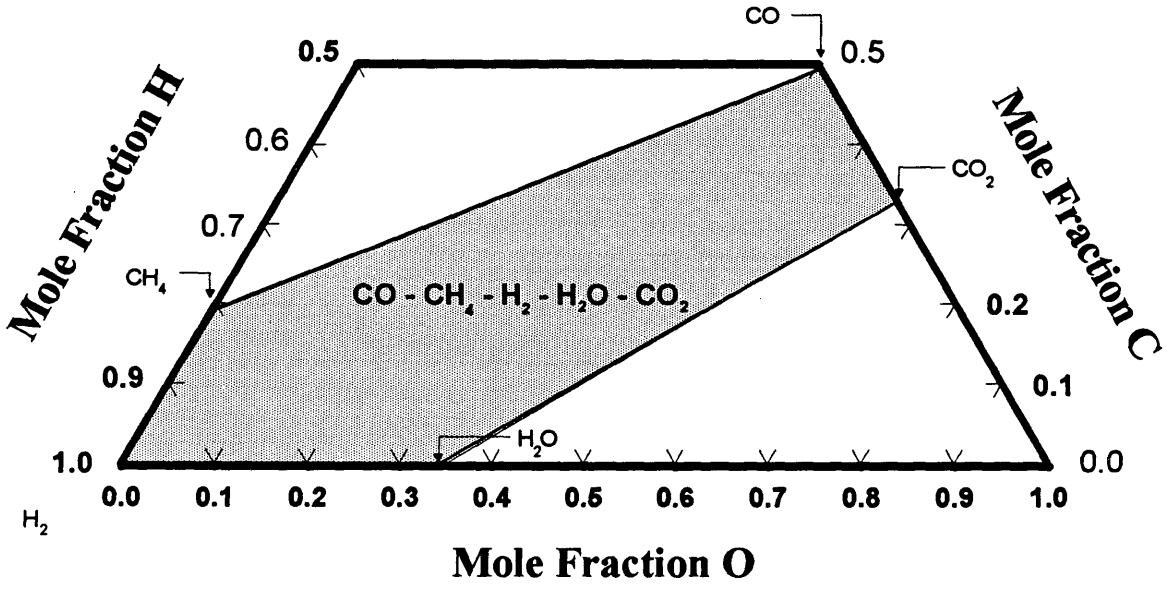

Figure 3.1. Region of analysis in the C-H-O system. where five gas species CH_4, H_2, H_2O, CO and CO_2 are prominent. (from Conejo, 1995)

At a given temperature the stable equilibrium-phase-boundaries between pairs of solid iron-bearing species, Fe/Fe_3O_4, Fe/Fe_3C, Fe_3O_4/Fe_3C are controlled by the equilibrium gas-phase composition. In addition, the saturation boundary for carbon deposition is controlled by equilibration of the carbon-bearing species within the gas phase when carbon is at unit activity. The diagrams developed by Conejo displayed the saturation line for graphite. The diagrams presented in this research incorporate the saturation line for amorphous-carbon since this has been shown to be an important solid species in this system. It should be noted that the phase boundaries for the iron-bearing species are unaffected by the choice of, what in effect is, the reference state for carbon. In the diagrams shown, the Gibbs free energy of formation of all carbon-bearing species, CH_4, CO, CO_2 and Fe_3C are relative to amorphous carbon. Thus the standard Gibbs free-energy changes for any reaction where a carbon-bearing species participates is unchanged.

The method of calculating the equilibrium gas-phase composition has been described in detail by Conejo (1995). Three independent chemical-reactions define the equilibria in the system. Therefore, for a specified total-pressure and temperature the following two gas-phase reactions:

$$CO_{(g)} + H_2O_{(g)} = H_{2(g)} + CO_{2\,(g)} \quad \text{.....(3.1)}$$

$$CO_{(g)} + 3H_{2\,(g)} = CH_{4\,(g)} + H_2O_{\,(g)} \quad \text{.....(3.2)}$$

in conjunction with one of the following reactions which describe the equilibrium between pairs of iron-bearing solid-phase, delineate the phase-field boundary between the two solid-phases selected. At a temperature below 833 °K (560 °C), for example, these are :

$$3Fe_{(s)} + 2CO_{(g)} = Fe_3C_{(s)} + CO_{2(g)} \quad \text{.....(3.3)}$$

$$3Fe_3O_{4(s)} + 5H_{2(g)} + CO_{(g)} = Fe_3C_{(s)} + 5H_2O_{(g)} \quad \text{.....(3.4)}$$

$$Fe_3O_{4(s)} + 4H_{2(g)} = Fe_{(s)} + 4H_2O_{(g)} \quad \text{.....(3.5)}$$

At a temperature above 833 °K (560 °C), in addition to reactions (3.3) and (3.4), above, three additional solid-phase pairs, with "wüstite" as the common phase, must be considered:

$$3Fe_{0.947}O_{(s)} + 3.947H_{2(g)} + 0.947\,CO_{(g)} = 0.947Fe_3C_{(s)} + 3.947H_2O_{(g)} \quad (3.6)$$

$$Fe_{0.947}O_{(s)} + H_{2(g)} = 0.947Fe_{(s)} + H_2O_{(g)} \quad (3.7)$$

$$0.947Fe_3O_{4(s)} + 0.788\,CO_{(g)} = 3Fe_{0.947}O_{(s)} + 0.788CO_{2(g)} \quad (3.8)$$

In order to determine the saturation boundary for amorphous carbon, the third reaction in addition to Reactions (3.1) and (3.2), can be selected as either:

$$C_{\beta(s)} + CO_{2(g)} = 2CO_{(g)} \quad (3.9)$$

$$C_{\beta(s)} + 2H_{2(g)} = CH_{4(g)} \quad (3.10)$$

The thermodynamic database displayed in Tables 3.1 to 3.5 was used. In addition, the data for Gibbs free-energy-of-formation of amorphous-carbon relative to graphite were obtained from the compilation by Dent and are listed in Table A.6.

The two coordinates, which must to be obtained in order to define a point on a phase-field boundary, are determined by selecting one of the gas-phase component coordinates and determining the other by solving the set of equations developed from: i) three component-balances (for carbon, hydrogen and oxygen); ii) three equilibrium-expressions (mass-action relationships) for the three relevant reactions as described previously; and, iii) the requirement that the sum of the mole fractions for the equilibrated gas-species and that of their C-H-O components be invariant and equal to unity. These mole-fraction relationships are :

$$Y_{CH_4} + Y_{CO} + Y_{CO_2} + Y_{H_2} + Y_{H_2O} = 1 \quad \text{.....(3.11)}$$

and,

$$Y_C + Y_H + Y_O = 1 \quad \text{.....(3.12)}$$

The numerical strategy employed is based on the arithmetic-geometric equality, and resulting equations are solved in the iteratively logarithmic domain (Baker,1981).

Three ternary stable-phase stability diagrams are presented in Figures 3.2, 3.3 and 3.4. The features exhibited at two temperatures, 800 °K (527 °C) and 900 °K (627 °C), and two pressure, 0.8 atm and 3.0 atm may be observed in these figures — note that C_{am} is equivalent to $C_{\beta(s)}$. In addition, the phase boundary for the region where Fe_3C is stable and the gas phase is undersatured with respect to amorphous carbon has been replotted on binary Cartesian-axes in order to provide a more detailed view of this region. Included in this supplemental plot, is the mole fraction ratio Y_{H_2} / Y_{CO} relevant to a binary feed-gas mixture comprised of hydrogen and carbon monoxide and employed by Conejo in his experiments. The straight line on the Cartesian-coordinates plot corresponds to the straight line joining the ternary-diagram coordinates (Y_H, Y_O : 1.0, 0.0) and (Y_C, Y_O : 0.5, 0.5). The region below the dashed line representing the saturation boundary for amorphous carbon and identified by P_1-P_2 identifies the gas-phase component composition, which when equilibrated, will provide for stability of Fe_3C while at the same time is undersaturated with respect to $C_\beta(s)$. It should be apparent that, for example in Figure 3.2.b), that a binary H_2/CO feed-gas mixture cannot satisfy simultaneously the requesite carbon and hydrogen contents for the gas phase. In contrast, at 900°K, it can be seen that the point indicated by "A" identifies a point where this can be achieved (Figure 3.3.b). In Figure 3.4 a) and b), it is seen that for the same temperature of 900 °K, but a higher total-pressure of 3 atm, the region has shrunk but the $C_{am}(C_{\beta(s)})$ saturation boundary

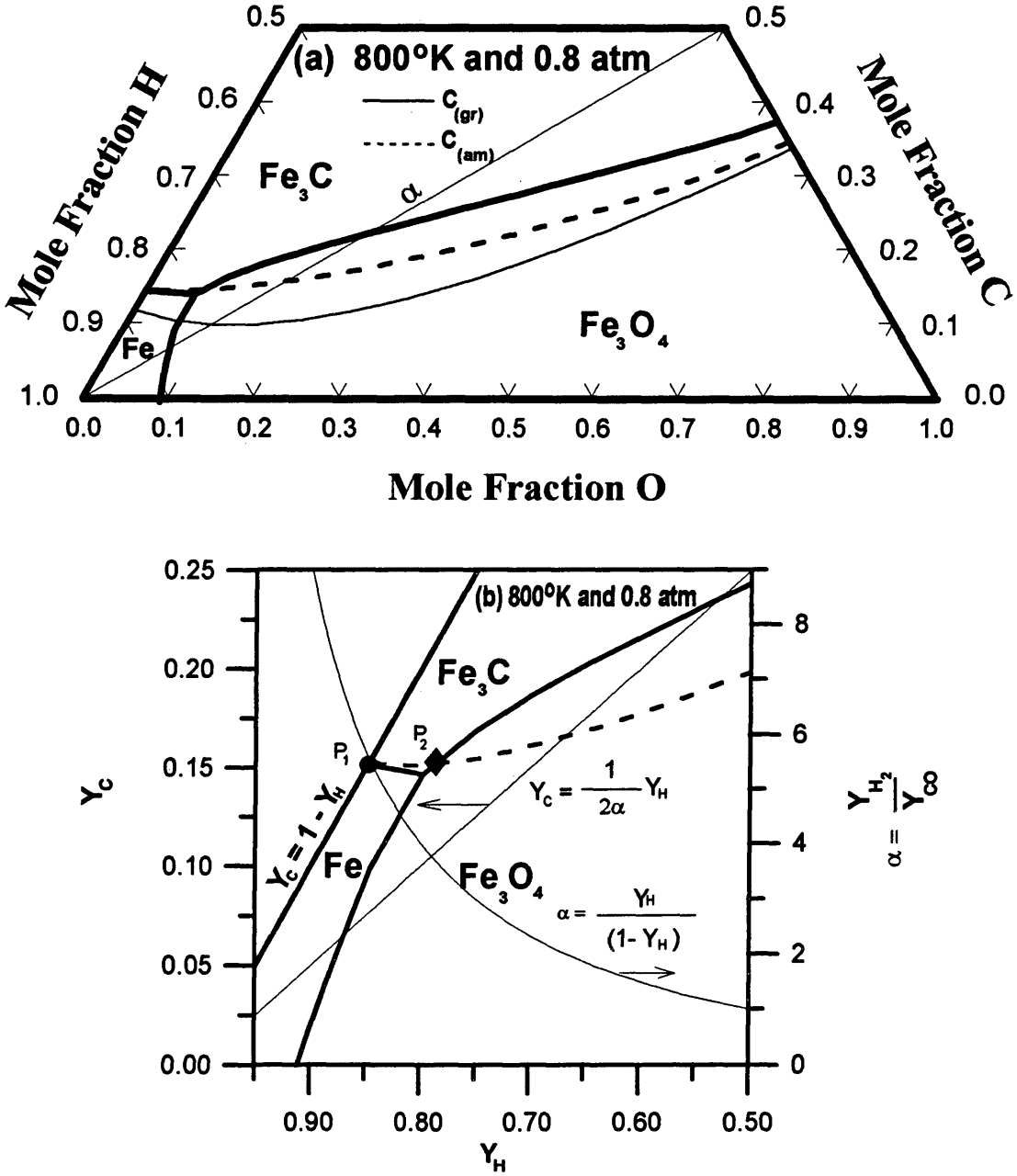

Figure 3.2. Phase Stability Diagram for the System Fe-C-O-H at 0.8 atm and 800 °K. (a) Ternary Diagram and (b) replotted so that mole fraction ratio $\frac{Y_{H_2}}{Y_{CO}}$ can be identified for the limiting values indicate by P_1 and P_2.

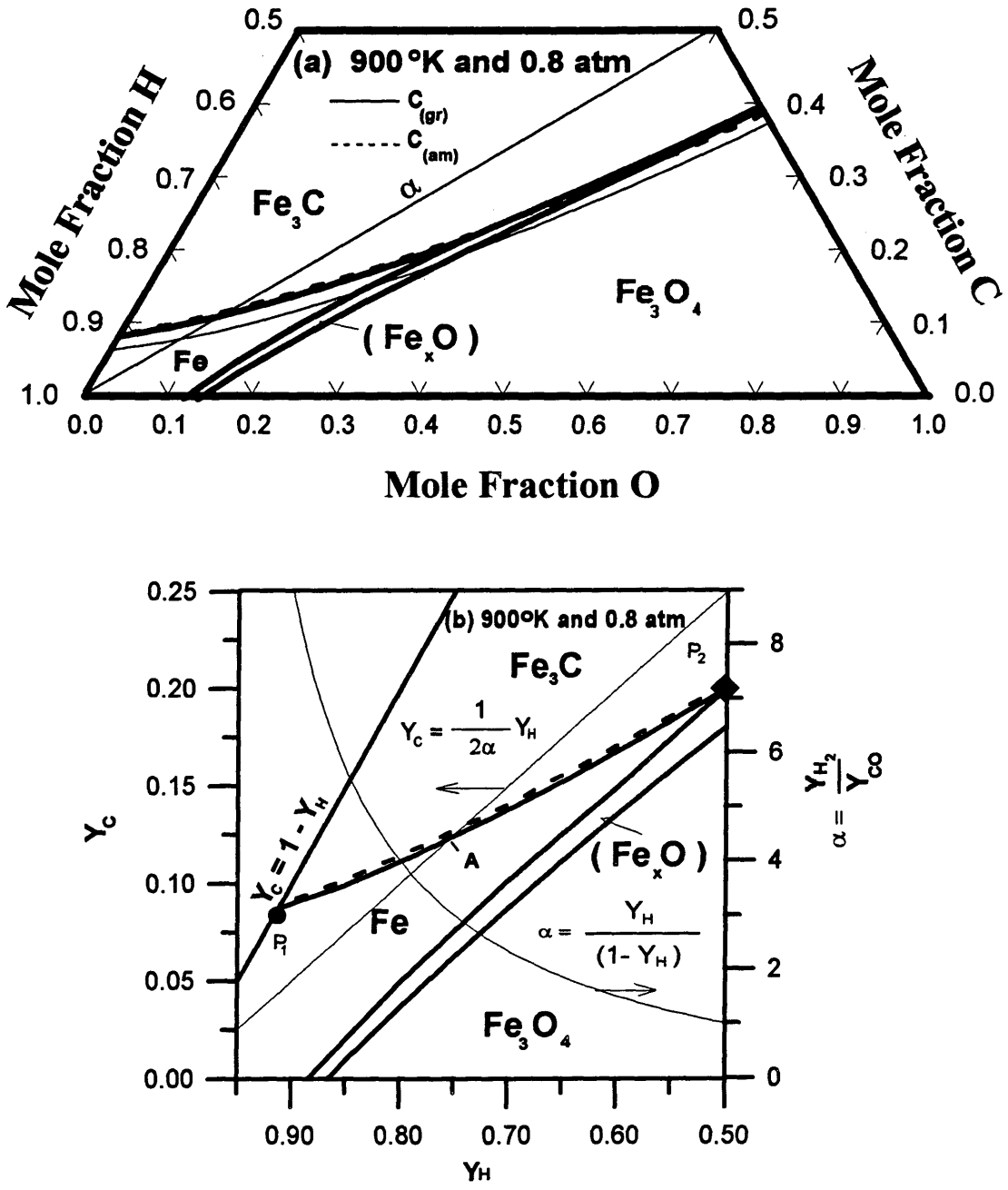

Figure 3.3. Phase Stability Diagram for the System Fe-C-O-H at 0.8 atm and 900 °K. (a) Ternary Diagram and (b) replotted so that mole fraction ratio $\frac{Y_{H_2}}{Y_{CO}}$ can be identified for the limiting values indicate by P_1 and P_2.

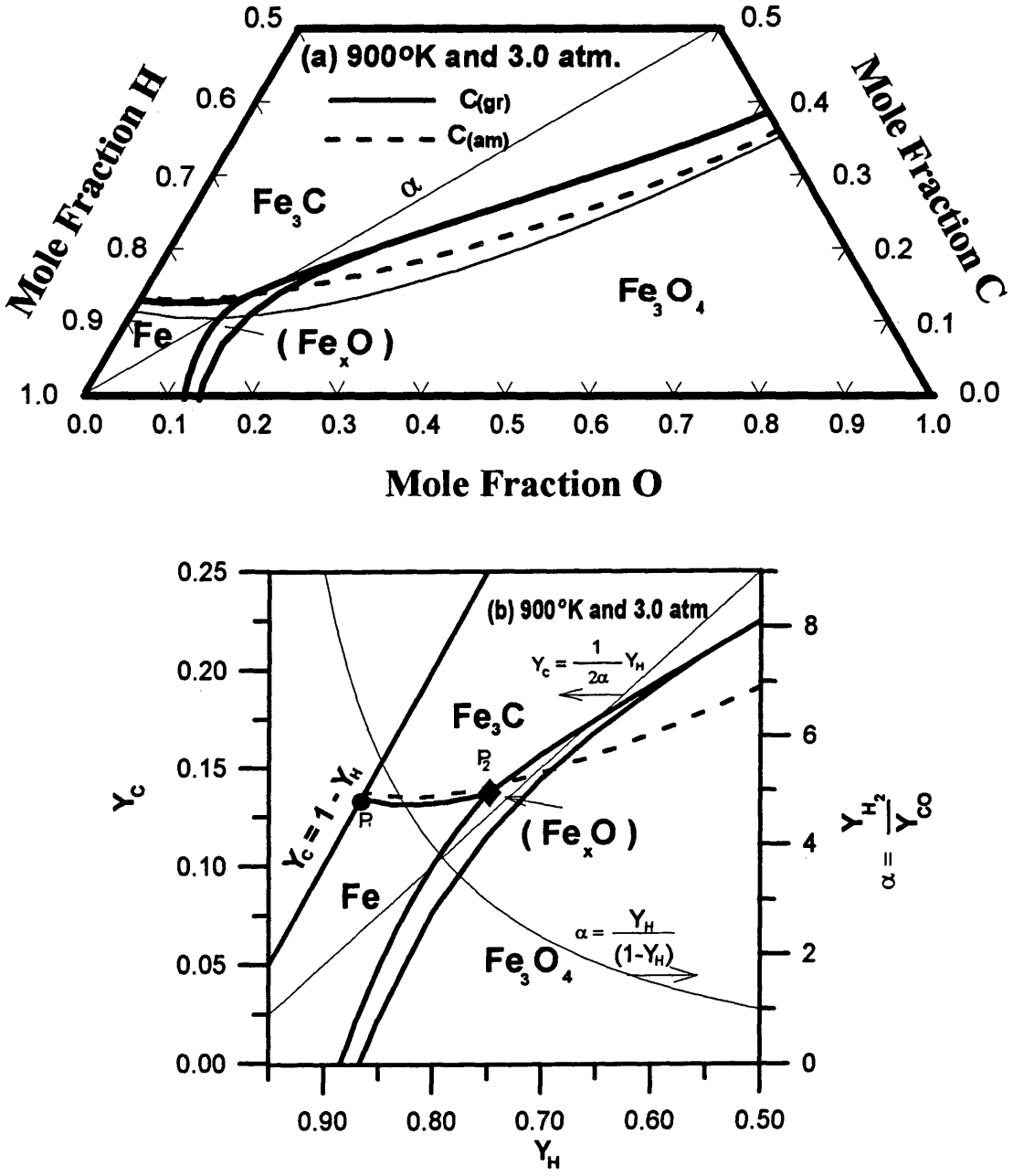

Figure 3.4. Phase Stability Diagram for the System Fe-C-O-H at 3.0 atm and 900 °K. (a) Ternary Diagram and (b) replotted so that mole fraction ratio $\frac{Y_{H_2}}{Y_{CO}}$ can be identified for the limiting values indicate by P_1 and P_2.

is not as close to the Fe(s)/Fe_3C(s) boundary. It is therefore apparent that a thermodynamic phase-stability analysis, based on considering C_{am} as the solid carbon species with the potential for deposition, indicates that conditions exist where cementite can be stabilized without the risk of carbon deposition.

In Figure 3.5, stability behavior, at two temperatures for amorphous carbon (metastable condition) and graphite (stable condition) when equilibrated with the five gas species, is shown. At low temperatures (below 850 °C) the form of carbon can be considered to be amorphous carbon in initial sequence step for formation of carbon as graphite. The kinetics of the solid-solid transformation controls the meta-stability.

3.2 Carbon Deposition from CH_4.

Pring and Farlie (1912), in their paper on the methane equilibrium cited the research conducted by Mayer and Altamayer (1907). Whereas the work of Spring and Farlie was conducted in the temperature range 1200 to 1500°C, that of Mayer and coworker was a much lower-temperature investigation where measurements were made at temperatures between 250 and 850°C. The significance of this lower temperature investigation is that it is one of the earliest references to amorphous carbon in the context of carbon condensation from gas phase containing carbon-bearing species.

Three decades later, in 1945, F.J. Dent conducted measurements of the gas composition in equilibrium with the concomitant solid-phase. This extensive research project encompassed both CH_4/H_2 and CO/CO_2 equilibration with a condensed carbon-species onto a (Ni (or Mo) on an Al_2O_3 support) catalyst surface. The temperature range of these studies was 410 to 515 °C for the C-H system and 250 to 900 °C for the C-O system. The data presented by Dent for the measurements on the CO/CO_2 system have been amended and recompiled in Table A.6. Perhaps the most significant discovery was that the Gibbs free-energy of the condensed-solid phase, relative to if it were

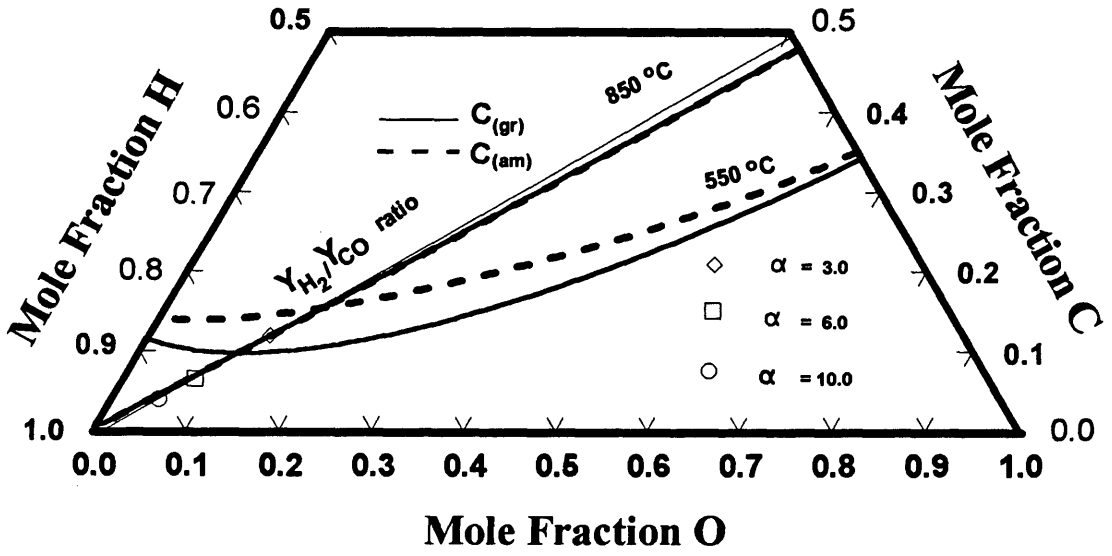

Figure 3.5. Phase Stability Diagram for the System C-O-H 550 and 850 °C at 0.8 atm showing the equilibrium composition of species gas with graphite and amorphous carbon. (above each line the gas phase is saturated with respect to either graphite or amorphous carbon). $\alpha = Y_{H_2} / Y_{CO}$ ratio.

hypothetically graphite, was independent of the gas-phase species that were introduced to effect the equilibration. Thus, it was found that the gas-phase composition in equilibrium with this low-temperature phase of condensed-carbon was at higher carbon-potential than if carbon in the form of graphite was the equilibrated solid species. These data have been utilized in the thermodynamic analysis conducted as part of this research, in order to reevaluated the saturation boundary for carbon condensation from a C-H-O gas phase. The results have now been incorporated in the early ternary gas-phase composition diagrams developed recently by Conejo (1995). The impact of the condensed carbon phase on the location of the saturation boundary for the binary $CH_{4(g)}$-$H_{2(g)}$ gas mixture is illustrated in Figure 3.6. (a) and (b). It is seen that when amorphous carbon is the potential condensed species then a higher carbon-content gas phase can be maintained in the system in comparison to when graphite is the condensed species These boundaries are displayed as a function of temperature for two system total pressure. The data for amorphous carbon by Dent, and listed in Table A.6, were used in the calculations.

3.3 Metastable Field

The metastable Fe-C-H-O ternary diagram was investigated by Conejo (1995). It had been found that for experiments conducted with CO-H_2 gas-mixture compositions located in the region where iron would be expected as the stable phase, iron carbide was formed instead. This metastable solid-phase configuration developed by Conejo (1995) was obtained by extrapolating the boundary for iron carbide into the iron field. A region could then be delineated where iron carbide, in principle, could be produced without carbon deposition at a specific total pressure, on the basis that the equilibrium is achieved in the gas phase between the CH_4, CO, CO_2, H_2O and H_2.

It is also possible to consider the gas phase as being metastable. In this case, equilibration between only four species in the gas phase (CO, CO_2, H_2O and H_2) with the condensed phases is considered. This gas-phase metastable configuration indicates that

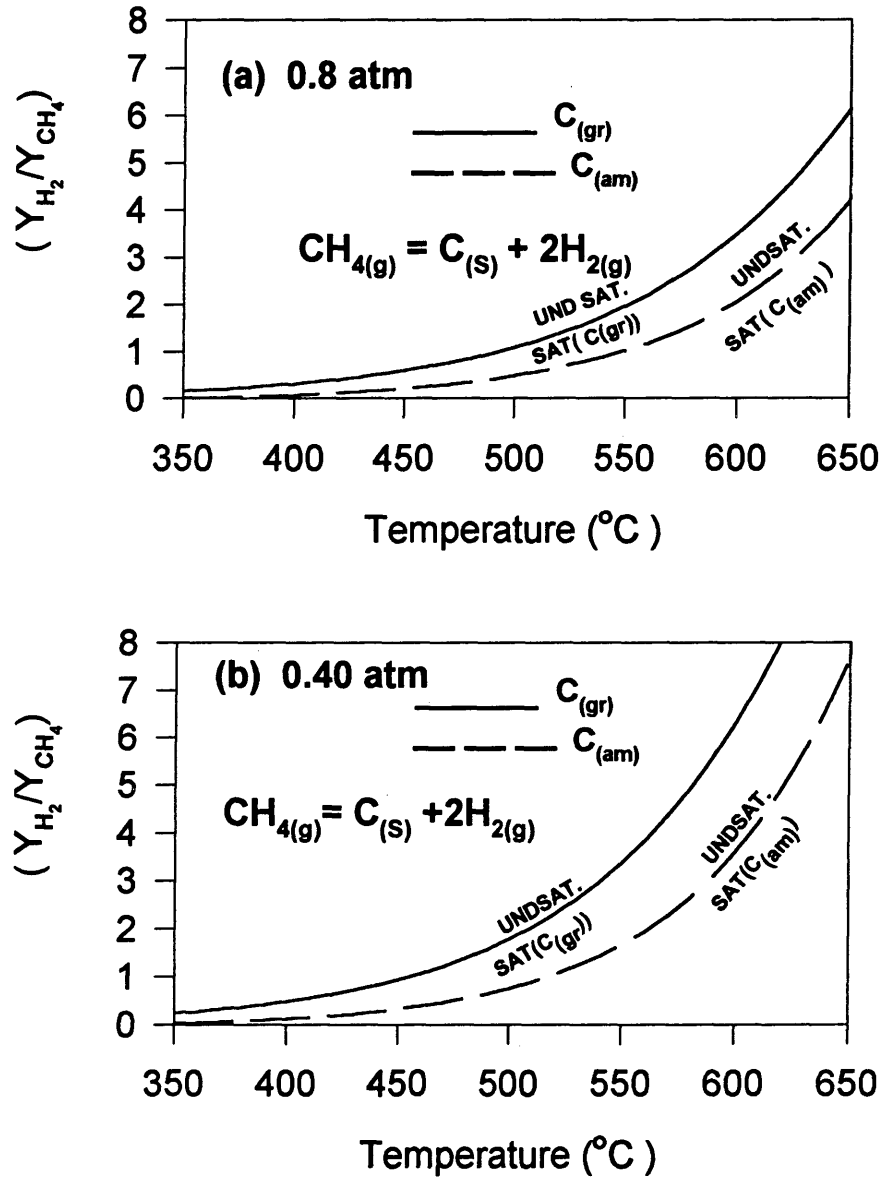

Figure 3.6. Saturation Equilibrium Composition for Y_{H_2} / Y_{CH_4} Gas-mixture at (a) 0.8 atm and (b) 0.4 atm. (above each line the gas phase is undersaturated with respect to either graphite or amorphous carbon).

potential for sooting exists when graphite is the condensed carbon species, in contrast to when amorphous carbon is the condensed carbon species.

The ternary diagrams for this configuration, due to the feed-gas phase not being equilibrated (methane not formed) within the reactor environment, are compared with that for the stable configuration, at 800 and 900 °K (527 and 627 °C) and for 1.0 atm in Figures 3.7 and 3.8. At 900°K and 1 atm, Figure 3.7(a), it is seen that it is possible to select a gas-phase composition for which formation of iron does not incur the potential risk of deposition of carbon. However in Figure 3.7(b), for the metastable gas-phase (CO,CO_2,H_2,H_2O) a C-H-O gas-phase composition on the variable Y_{H_2} / Y_{CO} ratio line, can now be selected within the Fe_3C phase field. However, if the condensed carbon-species is selected as $C_{(gr)}$ the gas-phase is saturated, whereas if $C_{(am)}$ is selected instead is undersatured. At lower temperature of 800 °K and the same total pressure similar remarks is hold as shown in Figure 3.8.

On analyzing the C-H-O system independently, at 900 °K and 0.8 atm., Figure 3.9, it is seen that for certain Y_{H_2} / Y_{CO} ratios larger than 3.0, when amorphous carbon is the condensed carbon species then, in addition to the expanded undersaturated region compared to when $C_{(gr)}$ is the condensed carbon-species, both phase boundaries undergo a shift such that undersatured regions now lie below the "Y_{H_2} / Y_{CO}" tie line. At the same time, the undersaturated region associated with $C_{(am)}$ is still larger than that associated with $C_{(gr)}$.

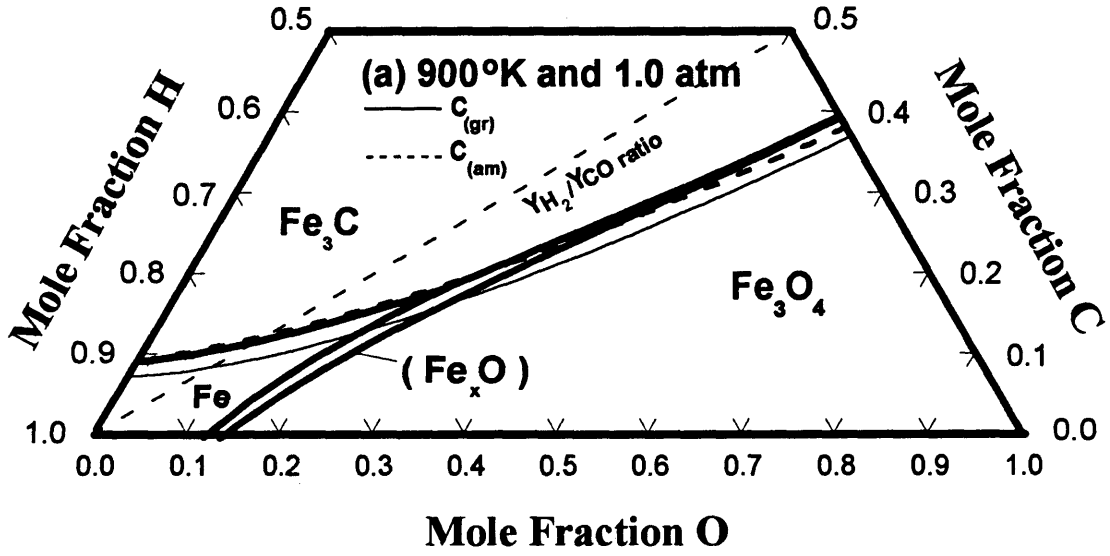

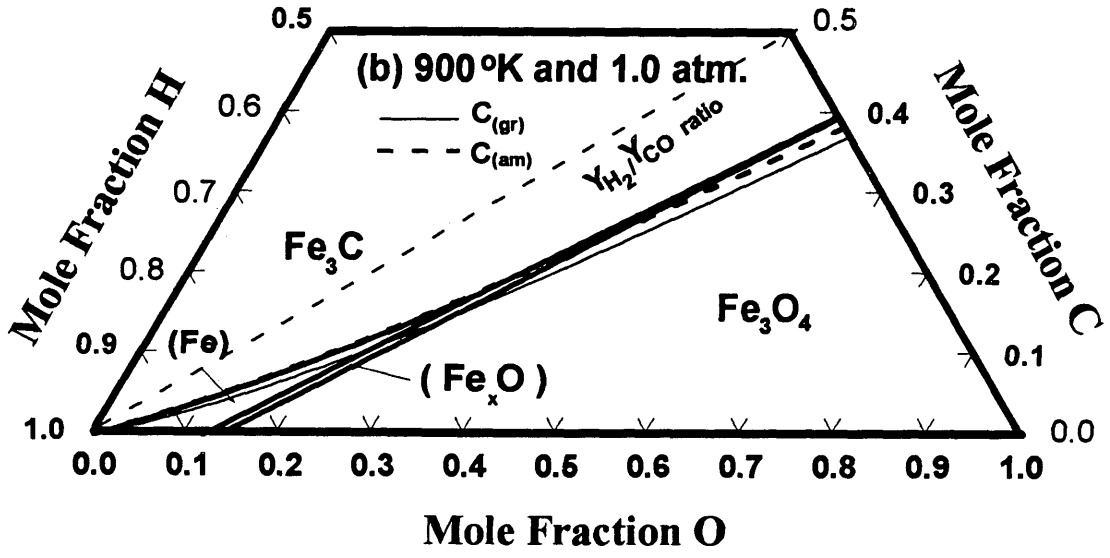

Figure 3.7 Phase stability diagrams for the system Fe-C-H-O at 900 °K and 1.0 atm. (a) Stable gas-phase configuration, (b) metastable gas-phase configuration.

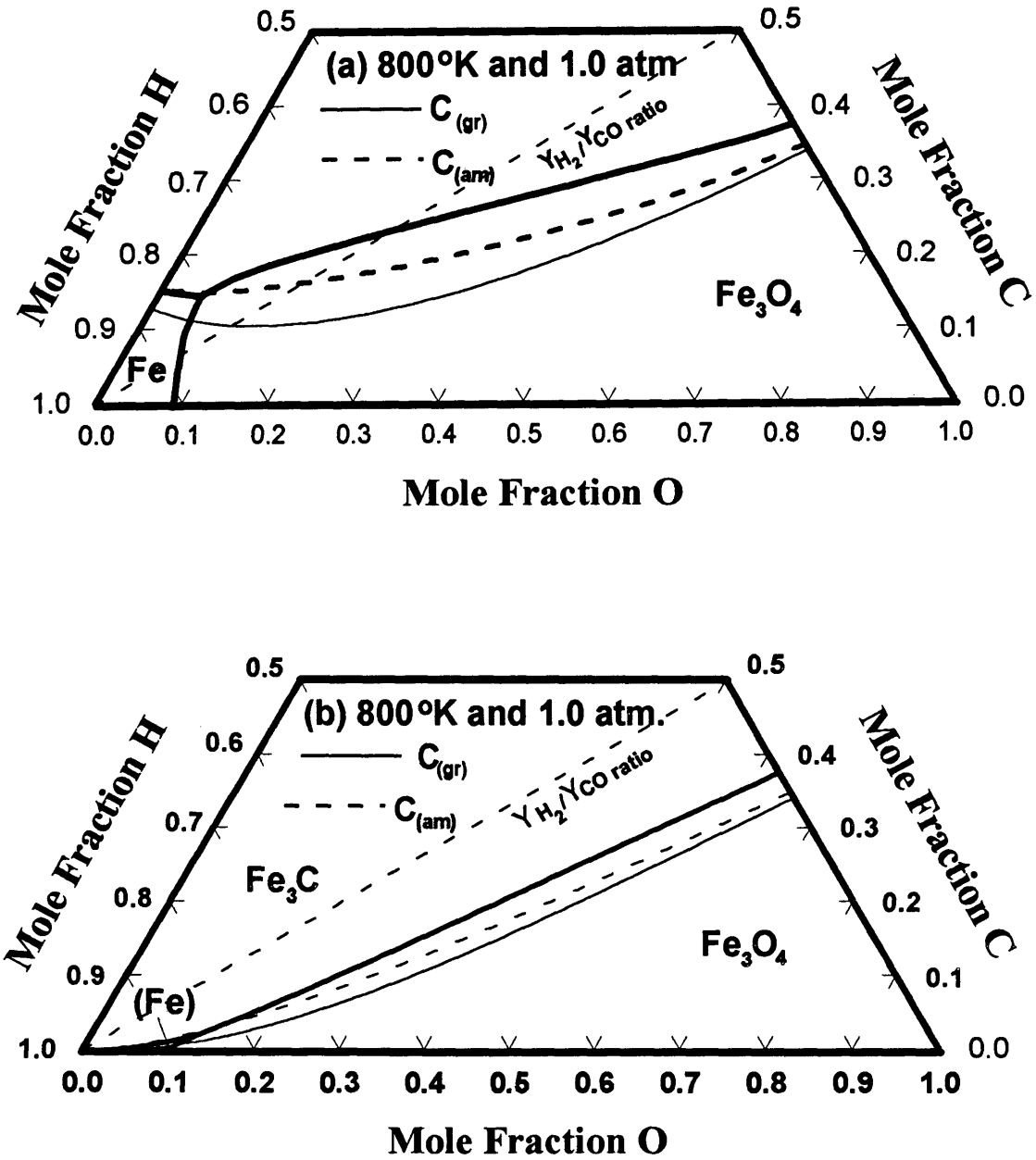

Figure 3.8 Phase stability diagrams for the system Fe-C-H-O at 800 °K and 1.0 atm. (a) Stable gas-phase configuration, (b) metastable gas-phase configuration.

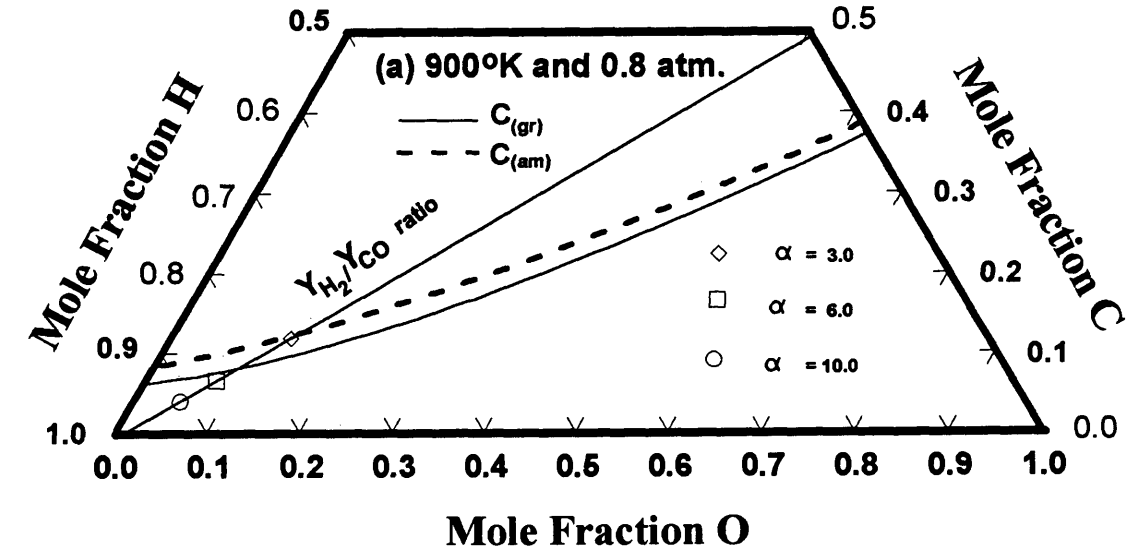

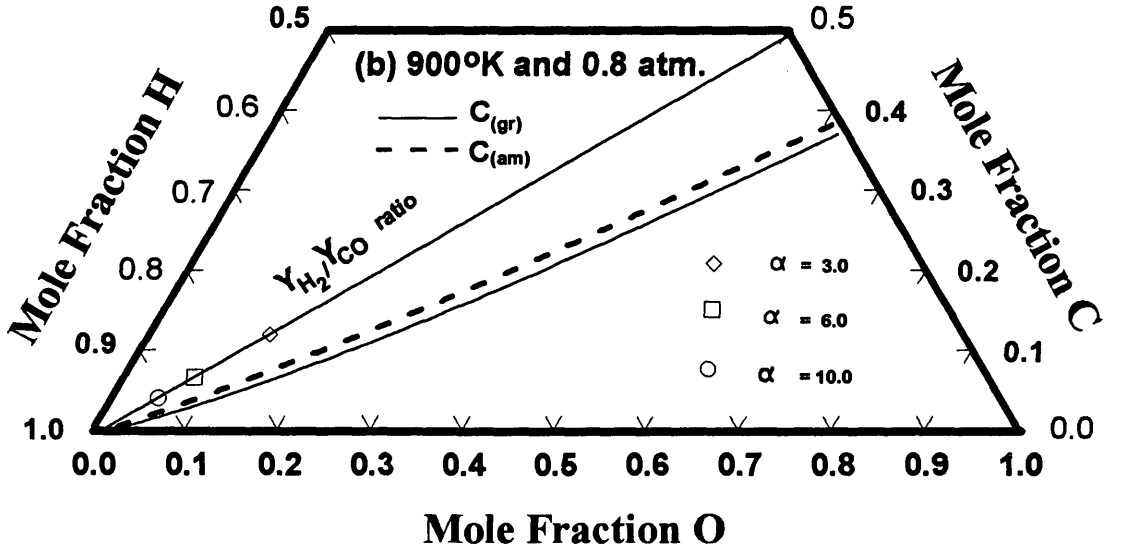

Figure 3.9 Phase stability diagrams for the system C-H-O at 900 °K and 0.8 atm $\alpha = Y_{H_2} / Y_{CO}$ ratio in the feed gas. a) stable gas phase configuration, (b) metastable gas-phase configuration.

3.4 Adsorption Model for Carbidization by H_2-CO Gas Mixture

A mechanism for carbidization can be developed on the basis of fundamental concepts of adsorption kinetics. Conejo (1995) has previously considered adsorption as the rate-limiting step during conversion of iron to cementite.

This present investigation has reappraised the model developed previously by including not only chemisorption of CO but H_2 as well onto the surface of iron, the nascent. The adsorption behavior was modeled according to concepts put forth by Turkdogan and Vinters, (1974). Thus, the chemisorption of both CO and H_2 are considered to be at equilibrium

$$CO_{(g)} + 2(*) \leftrightarrow **CO, \quad K_{3.13} \quad \text{.....(3.13)}$$

$$H_{2(g)} + 2(*) \leftrightarrow 2*H, \quad K_{3.14} \quad \text{.....(3.14)}$$

On the surfaces carbon is formed by the dissociate rate-controlling reactions:

$$**CO + **CO \xrightarrow{k_{3.15}} CO_{2(g)} + *C + 3(*) \quad \text{.....(3.15)}$$

and ,

$$2*H + **CO \xrightarrow{k_{3.16}} H_2O_{(g)} + *C + 3(*) \quad \text{.....(3.16)}$$

The symbols appearing in Equations (3.15) and (3.16) indicate the following: the asterisk (*) signifies an unoccupied site and the chemical species with an asterisk refers to an adsorbed state; e.g.; * CO signifies an adsorbed CO molecule.

The carbidization reaction is:

$$3Fe_{(s)} + *C \xrightarrow{k_{3.17}} Fe_3C_{(s)} + (*) \quad \text{.....(3.17)}$$

$$k_{3.17} >> k_{3.15} \text{ and } k_{3.16}$$

since the intrinsic rate of carbidization (i.e. reaction between the adsorbed carbon on the iron surface and the iron itself) is high relative to the rate at which the adsorbed carbon is created on the iron surface. Then the overall rate of carbidization is controlled by the combined rates of the heterogeneous irreversible Reactions (3.15) and (3.16)

This overall rate of carbidization is given by the following expression:

$$r''_{Fe_3C} = -r''_c = r''_{c(3.15)} + r''_{c(3.16)} \quad \text{.....(3.18)}$$

and therefore,

$$r''_{Fe_3C} = k_{3.15}(\theta_1)^4 + k_{3.16}.(\theta_2)^2.(\theta_1)^2 \quad \text{.....(3.19)}$$

where, $1 \equiv CO$; $2 \equiv H_2$; and θ_i refers to the concentration of sites occupied by species i (CO or H_2).

The equilibrium state of Reactions (3.13) and (3.14) may be represented by:

$$K_{3.13} = \frac{a_1^2}{p_1} \quad \text{.....(3.20)}$$

and,

$$K_{3.14} = \frac{a_2^2}{p_2} \quad \text{.....(3.21)}$$

in which, p_i is the partial pressure of the gas species i (i =1 or 2); and a_i is the surface activity of the adsorbed species i.

Also, according to(Altrup and Tavares, 1992):

$$a_i = \frac{\theta_i}{\theta_*} \quad (i = 1\&2) \quad \text{.....(3.22)}$$

where, θ_i is the concentration of unoccupied sites. Furthermore, since the concentration of sites occupied by carbon (i.e. *C) is negligibly small (because of the high intrinsic rate of Reaction (3.17)), then:

$$\theta_1 + \theta_2 + \theta_* = 1 \qquad \text{.....(3.23)}$$

Thus, on combining the two relationships expressed by Equation (3.22) with Equation (3.23) the following expression is obtained for the concentration of unoccupied sites :

$$\theta_* = \frac{1}{(1 + a_1 + a_2)} \qquad \text{.....(3.24)}$$

On substituting into the Equation (3.22), it is found that:

$$\theta_1 = \frac{a_1}{(1 + a_1 + a_2)} \qquad \text{.....(3.25)}$$

and,

$$\theta_2 = \frac{a_2}{(1 + a_1 + a_2)} \qquad \text{.....(3.26)}$$

When these expression (Equations (3.24), (3.25) and (3.26)) are incorporated into Equation (3.19) together with the equilibrium relationships (Equations (3.20) and (3.21)) where a_i is replaced by the site-concentration, then

$$r''_{Fe_3C} = k_{3.15}\left[\frac{(K_{3.13}\cdot p_1)^2}{\left(1+(K_{3.13}\cdot p_1)^{1/2}+(K_{3.14}\cdot p_2)^{1/2}\right)^4}\right] +$$

$$k_{3.16}\left[\frac{(K_{3.14}\cdot p_2)}{\left(1+(K_{3.13}\cdot p_1)^{1/2}+(K_{3.14}\cdot p_2)^{1/2}\right)^2}\right]\left[\frac{(K_{3.13}\cdot p_1)}{\left(1+(K_{3.13}\cdot p_1)^{1/2}+(K_{3.14}\cdot p_2)^{1/2}\right)^2}\right] \ldots (3.27)$$

It is seen that when p_2 (p_{H_2}) is equal to zero, then only CO is the reactant gas species, and the equation above becomes:

$$r''_{Fe_3C} = k_{3.15}\left[\frac{(K_{3.13}\cdot p_1)^2}{\left(1+(K_{3.13}\cdot p_1)^{1/2}\right)^4}\right] \qquad \text{.....(3.28)}$$

Obviously, when p_1 is zero (no carbon bearing species present) then $r''_{Fe_3C} = 0$

Equation (3.28) can be recast in a linearized form by inverted this Equation .

Thus,

$$\frac{p_1^{1/4}}{\left(r''_{Fe_3C}\right)^{1/4}} = \left(\frac{1}{k_{3.15}K_{3.13}^2}\right)^{1/4} + \frac{K_{3.13}^{1/2}}{\left(k_{3.15}K_{3.13}^2\right)^{1/4}}\bullet p_1^{1/2} \qquad \text{.....(3.29)}$$

which can be stated as :

$$y = a + b\bullet x \qquad \text{.....(3.30)}$$

in which,

$$y = \frac{p_1^{1/4}}{\left(r''_{Fe_3C}\right)^{1/4}}, \quad \text{and} \quad x = p_1^{1/2}$$

The coefficients a and b are then related to the rate parameters and equilibrium constant according to:

$$a = \left(\frac{1}{k_{3.15} K_{3.13}^2} \right)^{1/4} \quad \text{and} \quad b = \frac{K_{3.13}^{1/2}}{\left(k_{3.15} K_{3.13}^2 \right)^{1/4}}$$

Therefore

$$K_{3.13} = \left(\frac{b}{a} \right)^2 \quad \text{and } k_{3.15} = \left(\frac{1}{b^4} \right)$$

3.5 Iron-Bearing Phase Prediction from Gravimetric Analysis.

In order to predict the distribution of the iron-bearing phases in the reaction product from measurements of the masses of the precursor Fe_2O_3 and the product, the following equations were developed.

The interpretation of the grade of the conversion (f) with the fraction of loss in mass (f_L) as function of the phase present is detailed next. The following calculation is only valid after complete reduction. This indicates a complete transformation of hematite into Fe.

for 100 % of Hematite (Fe_2O_3)

$$f = \left[\frac{a - (f_L - b)}{a} \right] \quad \text{.....(3.31)}$$

$$f_L = \frac{m_i - m_f}{m_i} \quad \text{.....(3.32)}$$

where

f = fraction of conversion

f_L = fraction of loss in mass

m_i = mass of precursor.

m_f = mass of product.

a = f_L for 100 % reduction - f_L for 100% conversion, for example : 0.30 - 0.25 = 0.05 for Fe_3C.

b = f_L for 100 % conversion, for example: 0.25 for Fe_3C.

This indicates that a 25 % loss in mass is equivalent to 100 % conversion of Fe_2O_3 to Fe_3C. In Table 3.1, The constant values used in Equation (3.31) are describe.

Table 3.1 Constant Values used in Equation (3.31) for grade of conversion f

Phase	f_L for 100 conversion (b)	0.30 - b (a)	wt%C
Fe	0.30	0.00	0.00
Fe_3C	0.25	0.05	6.67

The relationship of f_L in order to determine the mass fraction of cementite and Fe for the standard initial condition of 100 % Fe_2O_3 in the initial sample is :

$$f_{Fe_3C} = \left[\frac{m_f - m_i \dfrac{2M_{Fe}}{M_{Fe_2O_3}}}{m_f} \right] \cdot \frac{M_{Fe_3C}}{M_C} \qquad \text{.....(3.33)}$$

where

f_{Fe_3C} = mass fraction of Fe_3C

m_i = mass of precursor.

m_f = mass of product.

M_{Fe} = Molecular weight of Fe.

M_{Fe_3C} = Molecular weight of Fe_3C.

$M_{Fe_2O_3}$ = Molecular weight of Fe_2O_3.

from Equation (3.32)

$$m_f = m_i(1 - f_L) \qquad \text{.....(3.34)}$$

then Equation (3.33) yields;

$$f_{Fe_3C} = \left[\frac{1 - \frac{2M_{Fe}}{M_{Fe_2O_3}} - f_L}{(1 - f_L)}\right] \cdot \frac{M_{Fe_3C}}{M_C} \qquad \text{.....(3.35)}$$

and,

$$f_{F_e} = f_{Fe_T} - f_{Fe_3C} \bullet \frac{3M_{Fe}}{M_{Fe_3C}} \qquad \text{.....(3.36)}$$

where

f_{Fe} = mass fraction of Fe

f_{Fe_T} = mass fraction of total iron in the product

The equations above mentioned are only used in the range for f_L between 0.30 and 0.25

If the initial sample has some impurities, the mass fraction of Fe_3C and Fe must be calculated by using the following expression:

$$f_{Fe_3C} = \left[\frac{1 - \frac{m_i}{m_f} \bullet f_{ar}}{1 - \frac{3M_{Fe}}{M_{Fe_3C}}} \right] \cdot \frac{M_{Fe_3C}}{M_C} \qquad \text{.....(3.37)}$$

and

$$f_{Fe} = f_{Fe_T} - f_{Fe_3C} \bullet \frac{3M_{Fe}}{M_{Fe_3C}} \qquad \text{.....(3.38)}$$

where

f_{ar} = mass fraction of product after reduction is completed.

CHAPTER 4
DETAILS OF EXPERIMENTS CONDUCTED

This chapter describes the equipment and measurement techniques used for the experiments conducted. The reaction experiments were conducted in a tubular (batch) reactor system with sample boat. The solid reactant (hematite) and reaction product were analyzed by use of scanning electron microscopy to examine morphological features and a combination of x-ray diffraction and Mössbauer spectrometry for phase analysis.

4.1 Tubular Reactor System.

The tubular reactor system consisted of three primary components: the gas supply system, the temperature controller and the horizontal tube-furnace with a quartz tube. A schematic of this configuration is shown in Figure 4.1. The horizontal tube-furnace was of split configuration, with electrical-resistance heating elements. The outer dimensions of the semi-cylindrical halves of the furnace were: a radius of 3¼ inches and a length of 13 inches. The quartz reactor tube (1 in. O.D. x 7/8 in. I.D. x 16 in. long) was inserted into the concentric heated region, 1¼ in. in diameter. To avoid condensation of water, hot water (80 °C) from a water bath was circulated through copper coils soldered to the stainless steel end-closures. The two end-closures, respectively, also served as gas inlet and gas effluent for the quartz-tube reactor. The sample to be processed was placed in an alumina boat (65 mm long x 13 mm wide x 10 mm deep), then inserted into the center of the quartz tube. Power to the furnace was regulated by the temperature controller (ATHENA Series 6080 P.I.D. controller). A stainless steel (304 SS) sheathed, ungrounded alumel (type K) thermocouple was used to monitor the temperature

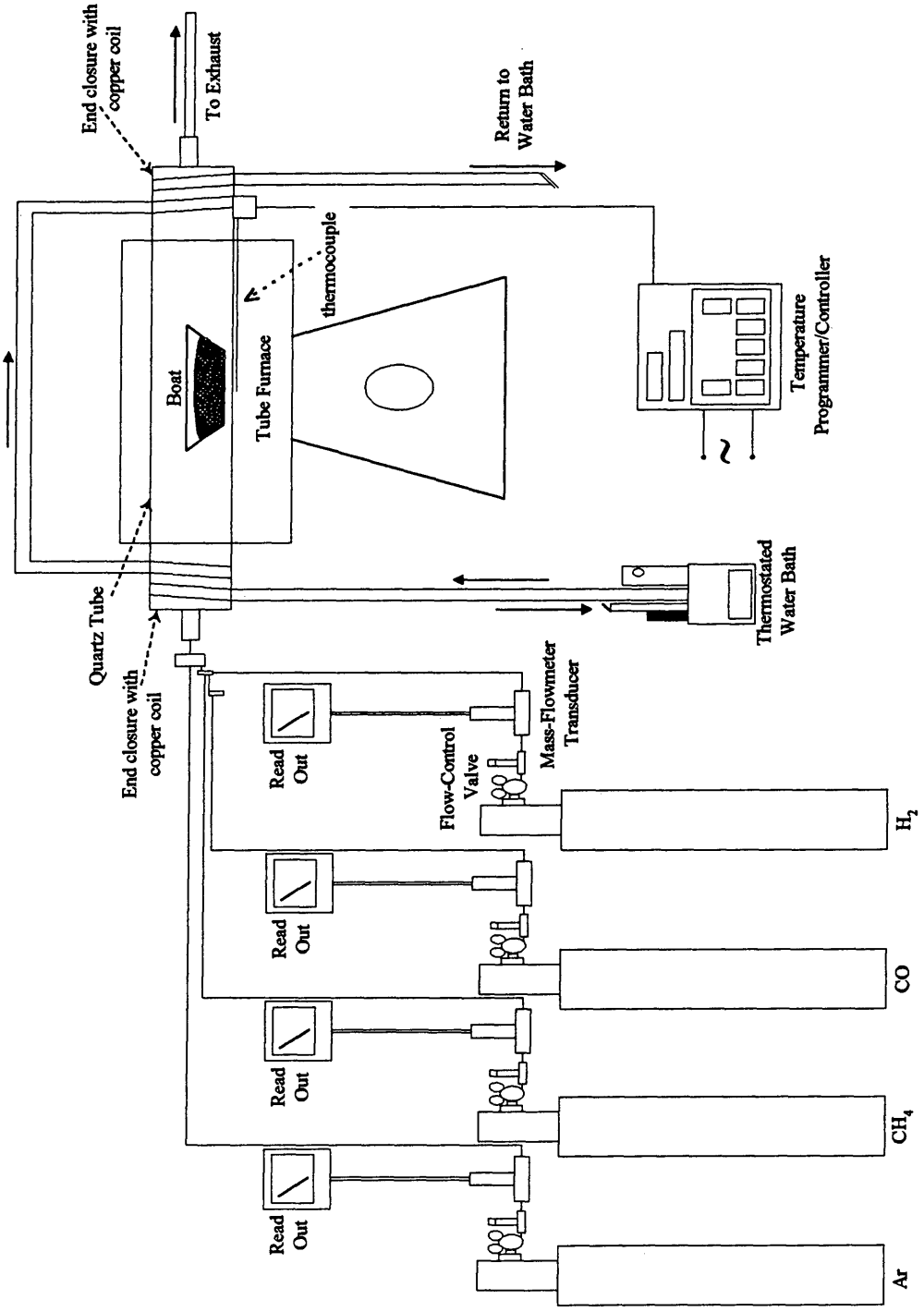

Figure 4.1 Schematic of tubular reactor system.

and provide the control-signal for the temperature controller. The thermocouple was placed in an open-end alumina tube (1/4 in. O.D) and positioned next to the electrical resistance heating elements, with the thermocouple tip at the center of the furnace. The various gas flowrates were controlled by Hasting mass flowmeters (range 0-1000 SCCM).

4.2 Chemical Reagents.

Iron-bearing precursor: Since one of the primary objectives was to re-establish the intrinsic kinetics of the conversion process, oxide reduction intermediate solid-species carbidization, the same quality of Fe_2O_3 (reagent grade, from the Baker Company, lot No 37199, with chemical composition listed in Table 4.1), which had been used by Conejo was employed. The powder consists of particles, including clusters, in the size range of 0.2 - 0.4 μm. Its x-ray diffraction pattern is shown in Figure 4.2.

Table 4.1 Chemical Composition of Iron-bearing Precursor. (Hematite)

Component	wt %
Fe_2O_3	**99.4**
Insoluble in HCL	0.15
Phosphate	0.01
Sulfate	0.16
Copper	0.002
Manganese	0.04
Zinc	0.002

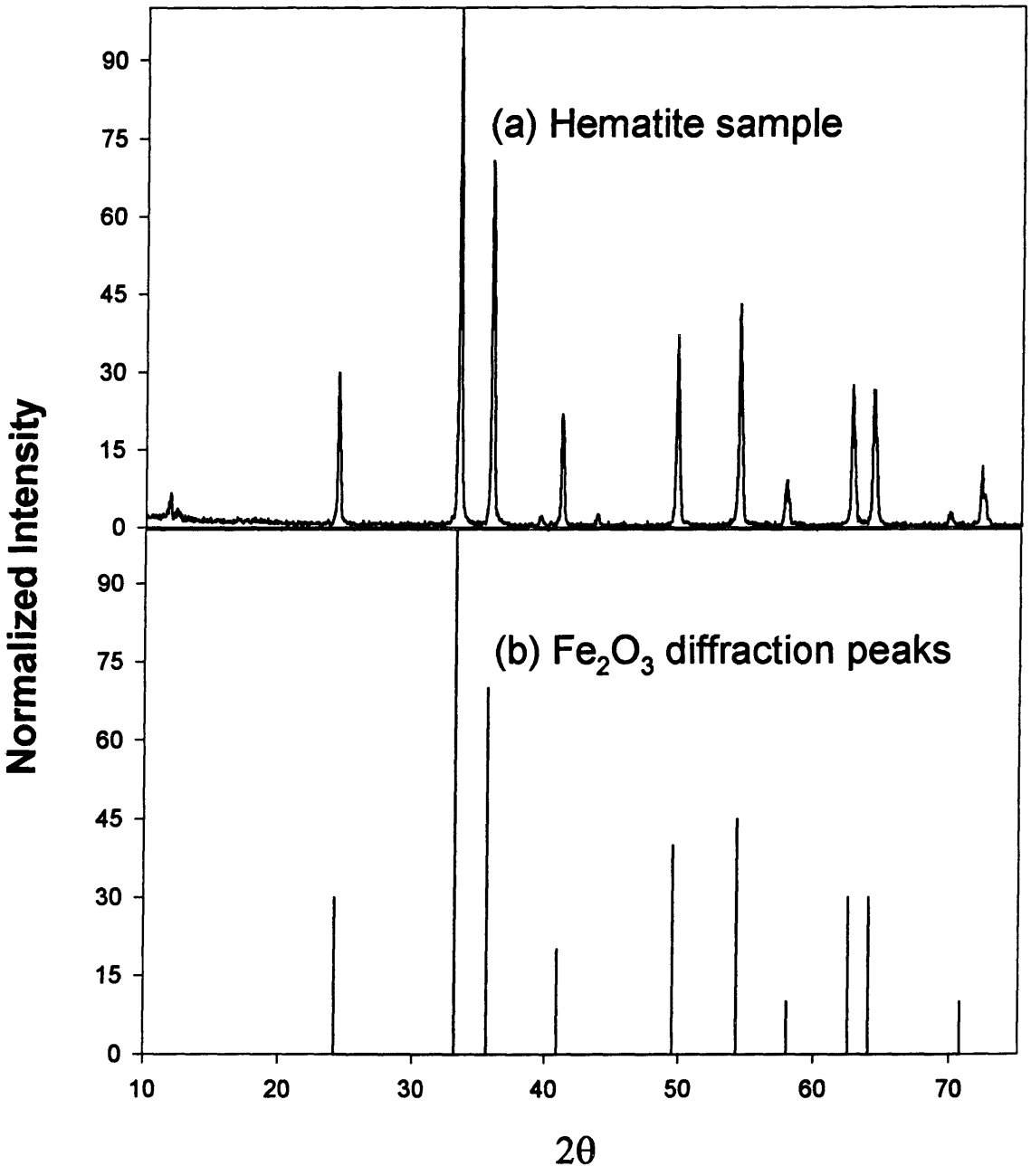

Figure 4.2 XRD pattern of hematite used in this research.

Gases: Commercial grade of carbon monoxide (CO), hydrogen (H_2), methane (CH_4), oxygen (O_2) and argon (Ar) were used.

4.3 Chemical Analyses and Equipment Employed

The equipment and techniques employed for analyzing samples are described in the following sections. Morphology characterizations and particle-size determinations, described in Section 4.3.1, were conducted with a JEOL Scanning Electron Microscope, Model JXA 840. Semiqualitative chemical composition of the precursor powder and the reaction products from the experiments conducted, were obtained by x-ray diffraction analysis. The method used for this analysis is described in Section 4.3.2 . The Mössbauer technique, described in Section 4.3.3, was used for phase analyses of the reaction products.

4.3.1 Scanning Electron Microscopy (SEM):

Using SEM, sample magnification in the range from 0 to 300,000X, with a resolution of 60 Å., can be achieved. The electron accelerating voltage is variable between 1 keV and 35 keV. The instrument also incorporates Wave Dispersive Spectroscopy (WDS) and Energy Dispersive Spectroscopy (EDS) which, in conjunction with Nortran software were occasionally used for chemical analysis. The powder samples were sprinkled onto carbon adhesive tape and coated with gold .

4.3.2 The X-Ray Diffraction (XRD) Analysis.

A Rigaku model RU-200 x-ray diffractometer was used in this research. The instrument is located in the Physics Department of the Colorado School of Mines. It features a rotating anode copper source for Cu-Kα radiation, and a standard $\theta/2\theta$ diffractometer. The comminuted powders were either tightly packed in an aluminum

sample-holder frame or uniformly sprinkled onto double adhesive tape attached to a glass slide, which was then placed into the spring clamp of the diffractometer. The samples were scanned from 30 to 90° 2θ at a step size of 0.05°, and a count time of 1 second per step. The x-ray photon detector generated an electronic signal, which was processed into a sample-analysis data file of photonic (x-ray) counts per second for each value of 2θ.

4.3.3 The Mössbauer Spectrometer System.

The Mössbauer effect, employed in this spectrometer, is a phenomenon associated with the recoilless emission and absorption of gamma-ray photons. A schematic illustrating the key components of a Mössbauer spectrometer is shown in Figure 4.3. In the arrangement shown the gamma ray source is provided with an oscillatory motion relative to the wafer sample . The spectrometer detects the number of photon counts per second over a spectrum of gamma-ray frequencies generated by Doppler shift effect. The photon counts are accumulated in a series of 256 data channels, representing 256 Doppler velocities, by a multi-channel analyzer, controlled by a personal computer. The velocities that show the lowest photon counts correspond to the maximum absorption by the Mössbauer effect. Each iron-containing phase present in the sample has a specific spectrum of absorption lines that can be represented as the summation of a series of Lorentzian absorption curves.

Sample preparation for Mössbauer analysis consisted of first comminuting the sample and then mixing it uniformly with a powdered-sugar binder. This mixture was then pressed into a wafer that acted as the gamma-ray beam absorbing element of the Mössbauer-analysis system. A 100 mg sample was taken from (typically) 350 mg of reaction product and mixed with 500 mg of powdered sugar using a "wigglebug" mixer in a plastic capsule. The blended mixture was pressed in a punch and die arrangement to produce a 1 inch diameter cylindrical wafer. Two Avery adhesive paper circles (adhesive

surface in contact with the powder) were placed at each end of the punch, so as to maintain the integrity of the wafer during and after extraction from the die.

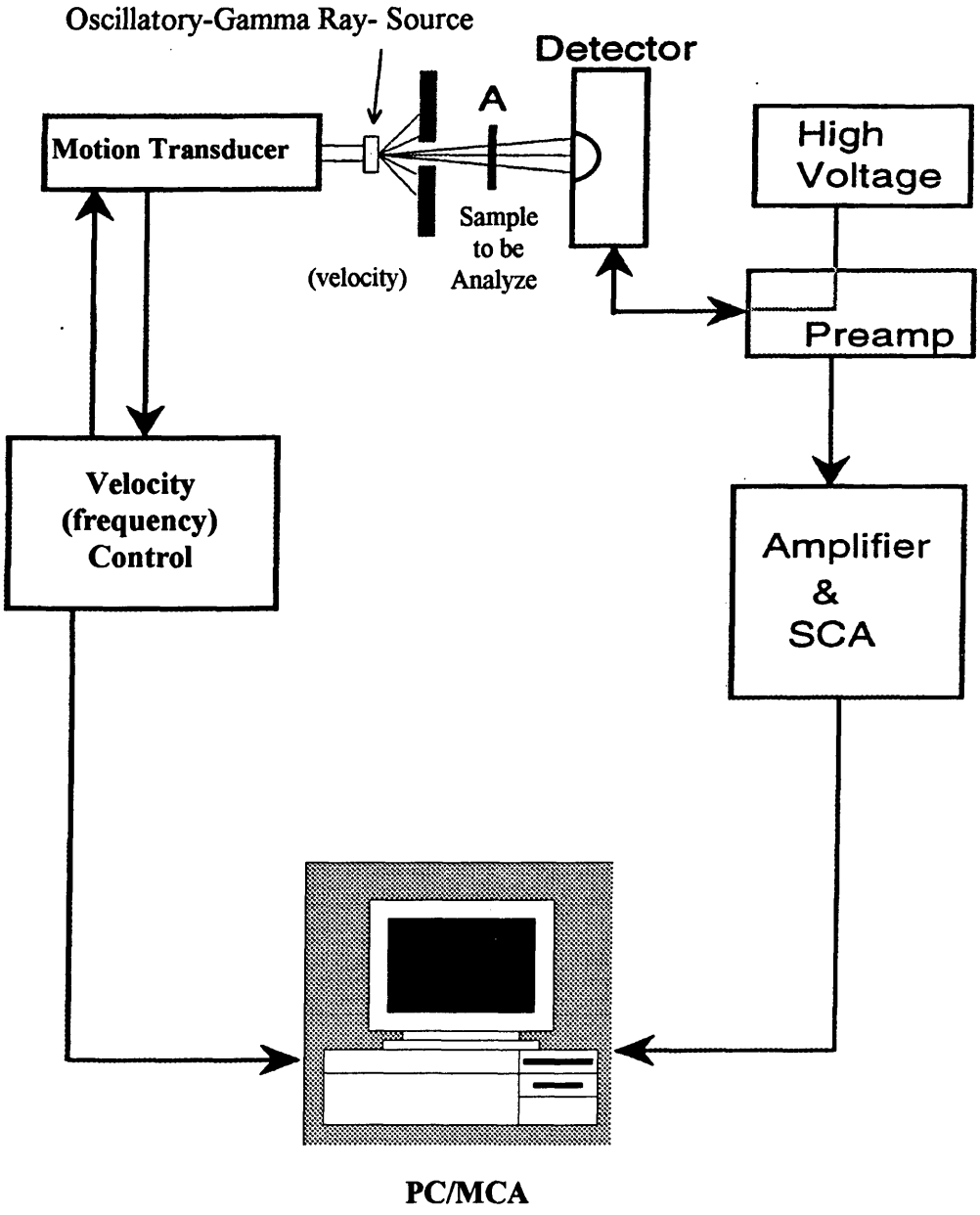

Figure 4.3 Schematic of a Mössbauer spectrometer system

4.4 Procedures Employed.

The procedures employed for performing the experiments are now described. Specific details are provided of the procedures employed for preliminary experiments, experiments on conversion with methane, and experiments for testing the adsorption rate-model.

Except for the preliminary experiments, 500 mg of precursor hematite was loaded into a alumina boat (35 mm long x 10 mm wide x 6 mm deep) which was then placed in a larger size boat (65 mm long x 13 mm wide x 10 mm deep). This arrangement allowed for the discrimination as to whether carbon deposition was located on the alumina (boat) surface or the reaction product when and if it occurred.

4.4.1 General Procedure.

In each of the experiments, the temperature controller was programmed to provide the following sequence: ramp to 650 °C at a ramp rate of 30 °C/min; hold at 650 °C for a pre-established time; cool down to ambient temperature at the "natural" rate of the system. At the start of each experiment, while at ambient temperature, the reactor was purged with argon for approximately 10 minutes, after which the reactant gas-mixture was introduced into the quartz reactor tube. The cool-down sequence was initiated by shutting down the flow of the gas mixture and the power supply, and reintroducing argon into the reactor. When the temperature was approximately 400 °C, the flowrate was reduced from 1000 SCCM to 200 SCCM and the split furnace was opened to increase the cool-down rate. When the reactor reached ambient temperature the argon flow was disconnected, the end-closure removed, and the boat containing the reaction product removed. On the basis of a prior calibration, it was determined that the actual sample temperature was approximately 625 ± 5 °C

4.4.2 Preliminary Experiments.

These experiments were conducted according to the general procedures already described. The gas mixture investigated was H_2/CO. After the initial argon purge at ambient temperature, the carbidizing gas mixture, composed of a pre-established flowrate of CO and a pre-established flowrate, of H_2 was introduced into the reactor by shutting down the flowrate of argon. Once the hold temperature of 650 °C was obtained a pre-establish reaction time was allowed to elapse. After that, the cool-down sequence was initiated by shutting down the power supply. When the temperature was approximately 400°C, argon was reintroduced by shutting down flowrate of CO and H_2 and the split furnace was opened to increase the cool-down rate. When the reactor reached ambient temperature the argon flow was disconnected, the end-closure removed, and the boat containing the reaction product removed.

4.4.3 Experiments with Methane.

These experiments were also conducted according to the general procedures described in section 4.4.1. The first series of experiments were conducted with a binary H_2/CH_4 gas mixture. Conejo (1995) had reported that for this gas reactant, reduction of hematite to iron was observed but subsequent carbidization was absent. In an attempt to modify the gas-phase composition a fixed flowrate of oxygen was introduced into the reactor. The rationale was that CH_4 did not appear to be adsorbed onto the iron surface and perhaps CO was the "surface-active" species required for carbidization.

4.4.4 Experiments for Validating Adsorption Rate-Model.

Once again these experiments were conducted according to the general procedures described previously. The exception was in how the reactant gas was introduced into the reactor. After the initial argon purge ambient temperature, H_2 was introduced at a flowrate of 800 SCCM to reduce the sample, hematite, to iron. Once the hold

temperature of 650 °C was obtained an additional 5 minutes was allowed to elapse. This elapsed time had been pre-established as being suitable for complete reduction to iron. After this period, the argon purge was re-established for 5 minutes by shutting down the flow of H_2 and reintroducing argon into the reactor to flush H_2 from the system. After that, by shutting down the flow of argon and introducing the carbidizing gas mixture, composed of pre-established flowrates of CO and H_2, was then introduced at 650 °C for a pre-established time. After the reaction time had elapsed, the purge argon was re-introduced for 5 minutes, shutting down the flowrates of H_2 and CO, in order to chemically quench the gas-solid reaction. Next, the cool-down sequence described in the general procedures was initiated.

CHAPTER 5
RESULTS AND DISCUSSION

The objectives of the experiments conducted were to determine reaction rates and in conjunction therewith elucidate mechanisms primarily associated with the conversion of iron to cementite. In the first section, the results of preliminary experiments conducted in the tubular-reactor system are presented. In the second section , results of a set of experiments conducted to corroborate the characteristic of the adsorption rate-model developed in Chapter 3 are presented. In the third section, SEM photomicrographs of the morphologies of the precursor iron obtained by hydrogen reduction of hematite and the cementite produced therefrom are presented. Finally, in the fourth and last section, details of additional experiments which were conducted so as to either validate or corroborate various results previously obtained.

5.1 Preliminary Experiments.

These preliminary experiments were conducted in order to reassess conditions for carbidization of iron oxides without the potential risk of deposition of carbon. Some of the findings of the previous investigation by Conejo (1995) were first corroborated. A particularly curious aspect was that Conejo had discovered that there was no carbidization of iron-from-hematite in runs where CH_4-H_2 gas mixtures were employed (including reduction of hematite. In the second part, the introduction of new gas (CO or O_2) in addition to the H_2-CH_4 gas-mixture investigated by Conejo, was added to the gas mixture to determine if this species would serve to initiate the carbidization reaction.

5.1.1 Carbidization with CO-H_2 Gas Mixture.

These experiments, conducted in the tubular-reactor system, were performed in order to corroborate some of the findings of the previous investigation by Conejo (1995). The precursor employed was reagent grade Fe_2O_3 (hematite) whose characteristics were described in Chapter 4.

In principle several iron carbides phase may be present in the reaction product. Consequently, in Figure 5.1 the XRD patterns for Fe_3C, $Fe_{2.5}C$ and Fe_2C are displayed which served to identify the phases present in the reaction product.

Conversion of Reagent Grade Fe_2O_3 with CO-H_2 Gas Mixture. These runs were conducted according to the procedure described in Chapter 4. The reducing/carbidizing gas-mixture was composed of CO-H_2 . The reaction time and specific features of each experiment are described in table 5.1.

Table 5.1 Experimental data of carbidization of Fe_2O_3 with H_2-CO gas mixture at 625 °C and 0.8 atm total pressure.

Run No	Y_{H_2} / Y_{CO}	Reaction Time (min)	Cool-down Condition	Observation
A1	3	30	with carbidizing gas	Fe_3C with carbon deposit
A2	3	30	with argon	Fe_3C with carbon deposit
A3	3	15	with argon	Fe_3C with carbon deposit

Run A1 was conducted with a reaction time of 30 minutes at 625°C; The sample was then cooled, in contact with the reactant gas-mixture, to approximately 400°C. The initial sample mass was ~ 1300 mg and Y_{H_2} / Y_{CO} = 3. It was

discovered that carbon had deposited in the boat on the upstream-facing end. The XRD analysis of this product, displayed in Figure 5.2, revealed nearly complete conversion

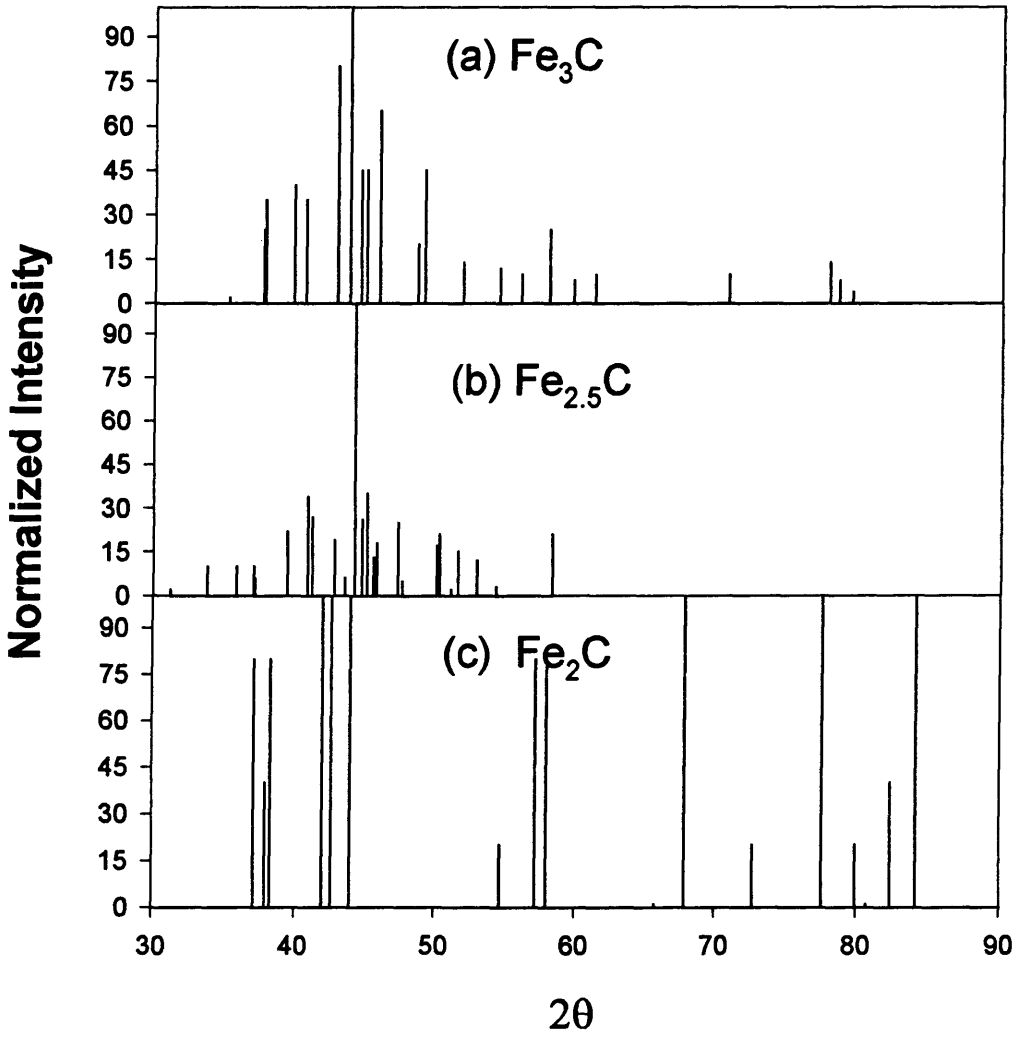

Figure 5.1 JCPDS diffraction reference peaks. for a) Fe_3C, b) $Fe_{2.5}$ C and c) Fe_2C.

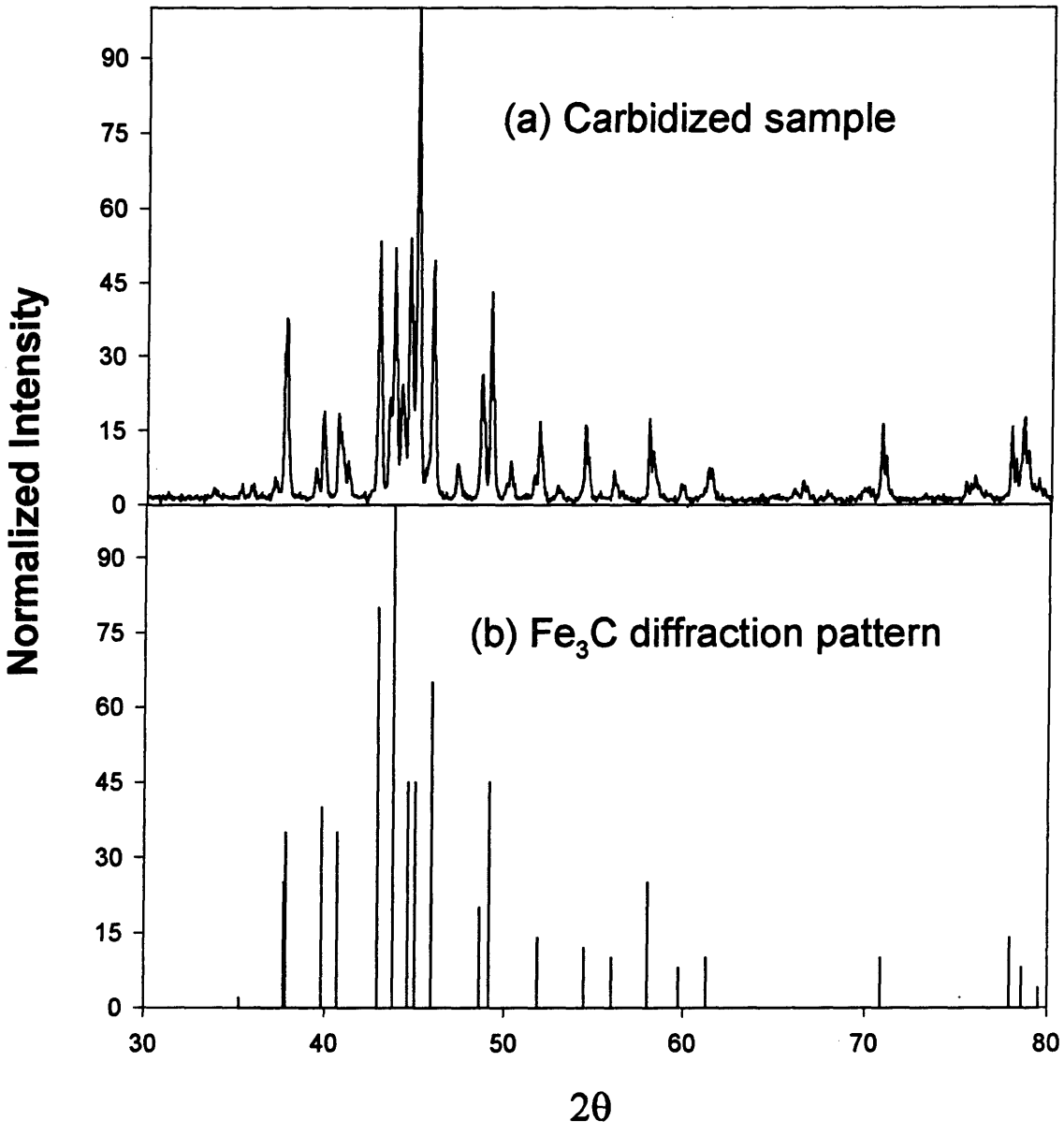

Figure 5.2 XRD pattern of: a) Carbidized sample with 25% CO-75% H_2 mixture; $P_{tot.}$ = 0.8 atm.; at 625 ° C for 30 minutes, cool down under reactant gas-mixture; and, b) JCPDS diffraction reference peaks for Fe_3C.

to Fe_3C. The gravimetric analysis of 26.11% loss in mass (rather than ~25 %), included the carbon deposit in the product.

Run A2 was conducted according to the previous run, except that argon was used during the cool down. The behavior observed was the same, including the carbon deposit with the reaction product. The XRD analysis (Figure 5.3) revealed complete conversion, with cementite as the prominent carbide phase.

In the Run A3, the procedure was again identical, except that the reaction time at temperature was reduced to 15 minutes. In this case, the amount of deposited carbon with the reaction product was less than for the experiments before. The XRD analysis again revealed complete conversion to cementite as evidenced by the diffraction pattern in Figure 5.4 — iron or other phases could were not detected. The smaller amount of carbon in this experiment provided evidence that it was likely that the carbon deposited was initiated after complete reduction (transformation of Fe_2O_3 to Fe), and subsequently iron carbide served as a catalyst for the decomposition of CO.

A series of experiments was now performed in order to identify the stage at which carbon precipitated occurred. In order to distinguish whether iron or iron carbide catalyzed the precipitation of carbon; these experiments were conducted using two alumina boats. A small boat with approximately 500 mg of sample (hematite) was placed towards the down stream end within a larger boat and some experiments used two boats without a sample. Table 5.2 describes the results obtained.

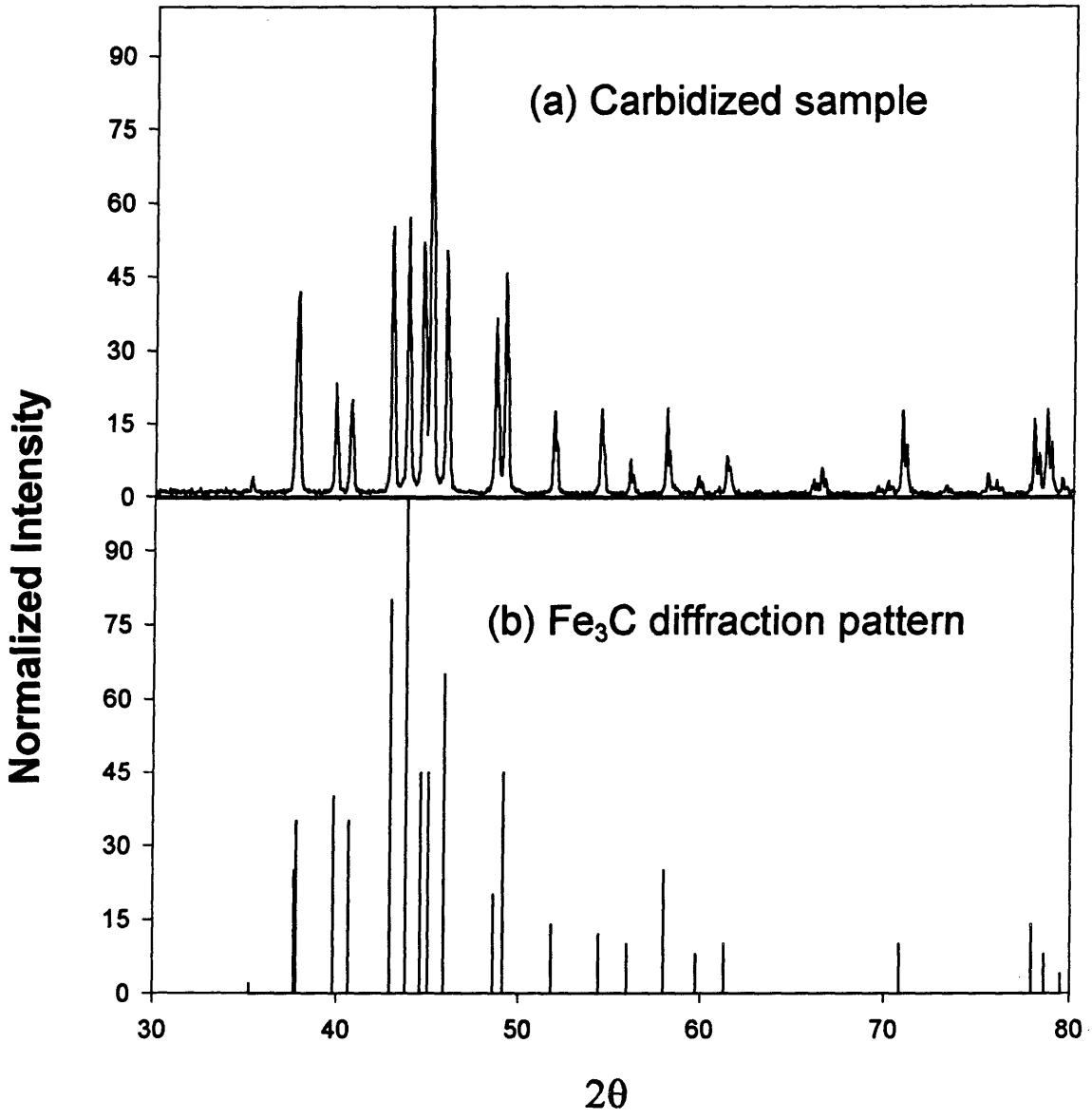

Figure 5.3 . XRD pattern of: a) Carbidized sample with 25% CO-75% H_2 mixture; $P_{tot.}$ = 0.8 atm.; at 625 ° C for 30 minutes, cool down under argon; and, b) JCPDS diffraction reference peaks. for Fe_3C.

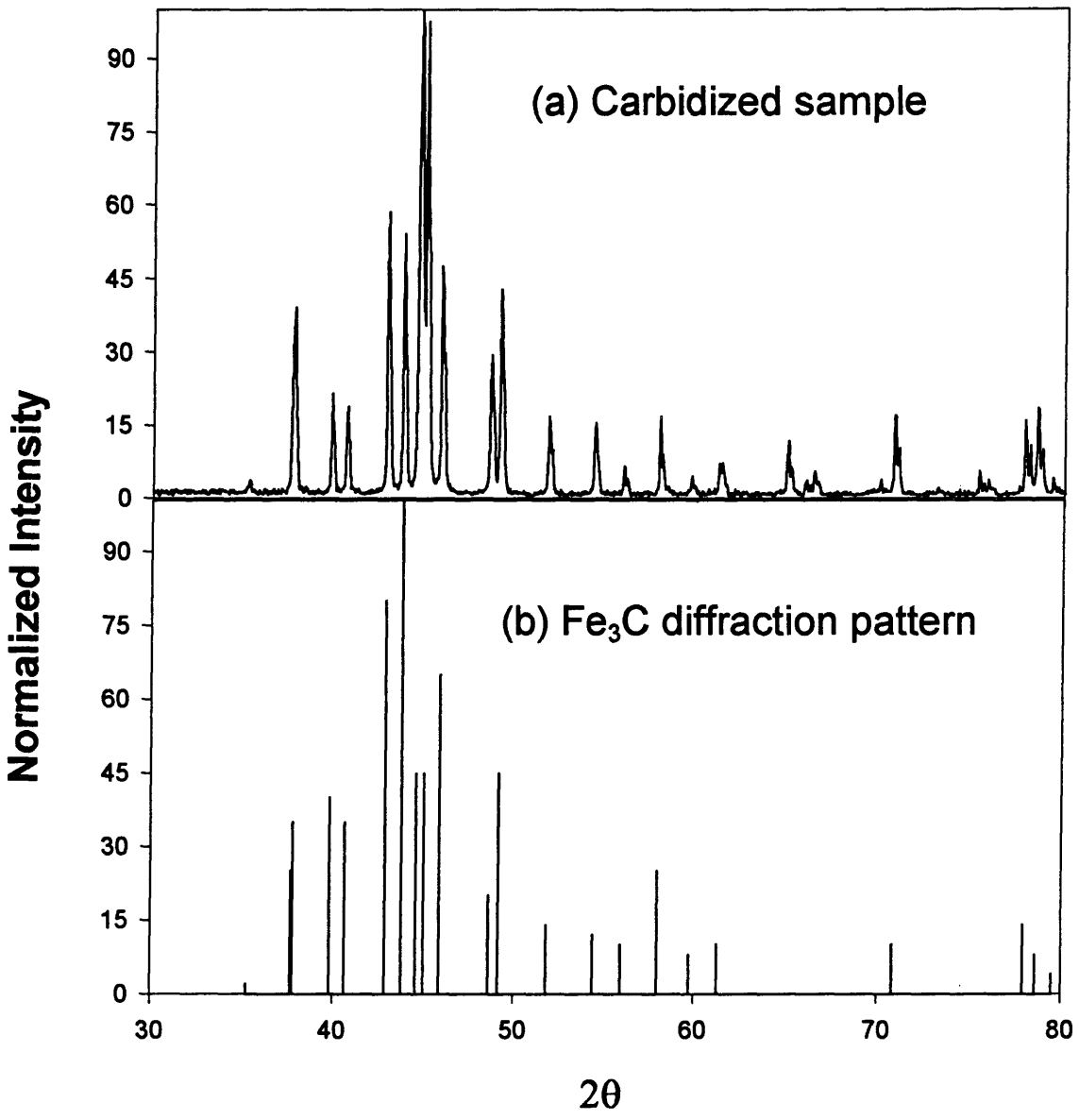

Figure 5.4. XRD pattern of: a) Carbidized sample with 25% CO-75% H_2 mixture; P_{tot} = 0.8 atm.; at 625 ° C for 15 minutes and b) JCPDS diffraction reference peaks. for Fe_3C.

Table 5.2 Experimental data of carbidization of Fe_2O_3 with H_2-CO gas mixture at 625 °C and 0.8 atm total pressure. Configuration with two Al_2O_3 boats.

Run No	Y_{H_2} / Y_{CO}	Reaction Time (min)	Sample container & reactant	Observations
B1	3	10	two boats and sample	Fe_3C with carbon deposit. No Fe detected
B2	3	15	two boats (no sample)	no carbon
B3	5	15	two boats (no sample)	no carbon
B4	pure CO	10	two boats (no sample)	no carbon
B5	8	10	two boats and sample	Fe_3C with carbon No Fe detected

The procedure for Run B1 used a reaction time of 10 minutes. Complete conversion to Fe_3C had occurred (determined subsequently) with deposition of carbon over the reaction product in the small boat only. These results verified that iron carbide catalyzed the deposition of carbon. Run B2 was now conducted without Fe_2O_3 reactant in the small boat, and with $Y_{H_2} / Y_{CO} = 3$ and a reaction time of 15 minutes. There was no carbon deposition in the boats.

In Run B3 the same result was obtained for $Y_{H_2} / Y_{CO} = 5$. By using pure CO without Fe_2O_3 reactant in Run B4 with reaction time for 10 minutes, again there was no carbon deposition in the boats. Finally, in Run B5 with sample, $Y_{H_2} / Y_{CO} = 8$ and reaction time was 15 minutes, there was carbon with reaction product. Thus, it was established that for a reaction time of less than 10 minutes no carbon with will be found with the reaction product.

Experiments with CH_4-H_2 Gas Mixture. In these experiments also at 625°C, the procedure employed was the same as before, except that a reaction time was selected on the basis of the runs with CO-H_2 where complete conversion had occurred. In table 5.3, the details and results of each experiment are described.

In the Run C1, the reaction time was 20 minutes and the Y_{H_2} / Y_{CH_4} ratio was 3.25 which corresponded from the thermodynamic data to the equilibrium for the reaction : $CH_{4(g)} + Fe_{(s)} = Fe_3C_{(s)} + 2H_{2(g)}$ at 0.8 atm of total pressure. The gravimetric analysis indicated 6.16 % Fe_3C in the reaction product. However, XRD and Mössbauer analyses revealed only one solid-phase, metallic iron, as shown in Figure 5.5. This indicates that the carbon deposited was not in a iron-bearing species (iron carbide) and may have been amorphous. Therefore, 0.41 % C in the sample (~1.43 mg of carbon in ~350 mg of reaction of product) could not be identified by XRD analysis.

Table 5.3 Experimental data of carbidization of iron with H_2-CH_4 mixture at 625 °C and 0.8 atm total pressure. Configuration with two Al_2O_3 boats

Run	Y_{H_2} / Y_{CH_4}	Reaction Time (min)	Observations
C1	3.25	20	reduction to Fe, no carbidization
C2	3.00	10	reduction to Fe, no carbidization
C3	1.00	10	reduction to Fe, no carbidization
C4	1.00	20	reduction to Fe, no carbidization
C5	1.00	10	sample (Fe_3C), no carbon deposit
C6	1.00	10	. sample (Fe_3C+ Fe), no carbidization no carbon deposit

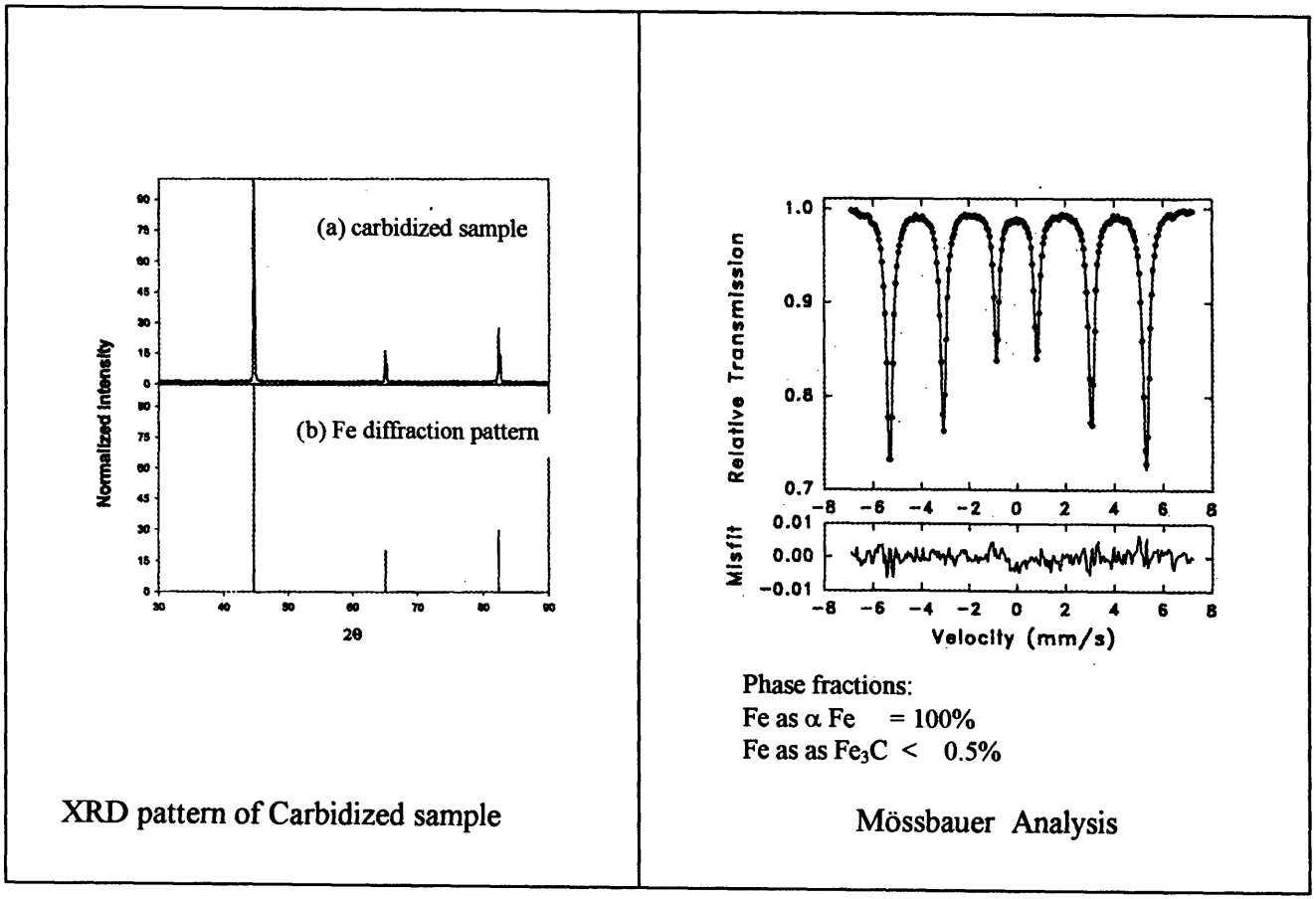

Figure 5.5 Carbidized sample with 23.53% CH_4-76.47% H_2 mixture; P_{tot} = 0.8 atm.; at 625 ° C for 10 minutes a) XRD pattern of: Carbidized sample; b) JCPDS diffraction reference peaks for Fe and c) Mössbauer Analysis.

In the Run C2, where Y_{H_2} / Y_{CH_4} was reduced to a value of 3 (increased relative methane content) and for a reaction time of 10 minutes, the gravimetric analysis indicated 5.7% Fe_3C in the reaction product,. However, as in C1 run, the XRD revealed only the presence of Fe and no carbon containing phase was observed with the reaction product.

In the Run C3, the methane concentration was increased still further — Y_{H_2} / Y_{CH_4} = 1.0 — and the reaction time was again 10 minutes. Gravimetric analysis indicated 10.2 %Fe_3C but no carbon phase was observed with the reaction product.

In the Run C4, the Y_{H_2} / Y_{CH_4} ratio was 1.0 and the reaction time was 20 minutes. This was performed in order to increase the reaction time between the metallic iron formed after reduction by the carburizing gas. The XRD and Mössbauer analyses of this reaction product revealed only one solid-phase species, as can be observed in Figure 5.6, metallic iron. According to gravimetric analysis the result was Fe and Fe_3C, with 91.73 and 7.40 % respectively. In order to demonstrate that CH_4 was unreactive the iron carbide produced from a previous experiment with CO-H_2 gas mixture was used in Run C5. In the Run C5, the Y_{H_2} / Y_{CH_4} = 1.0 and the reaction time was 10 minutes. No significant change on mass of the reaction product from the mass of the original sample could be discerned. This indicated no carbon deposition or decomposition of original sample.

Another experiment, Run C6, was performed except that the sample was iron carbide plus metallic iron in identical proportion (250 mg of Fe and 250 mg of Fe_3C). The reaction product of this experiment did not present appreciable change in mass from the original sample. From the thermodynamic data, the equilibrium Y_{H_2} / Y_{CH_4} for the reaction : $CH_{4(g)} + Fe_{(s)} = Fe_3C_{(s)} + 2H_{2(g)}$ was equal to 3.25. This indicates that the

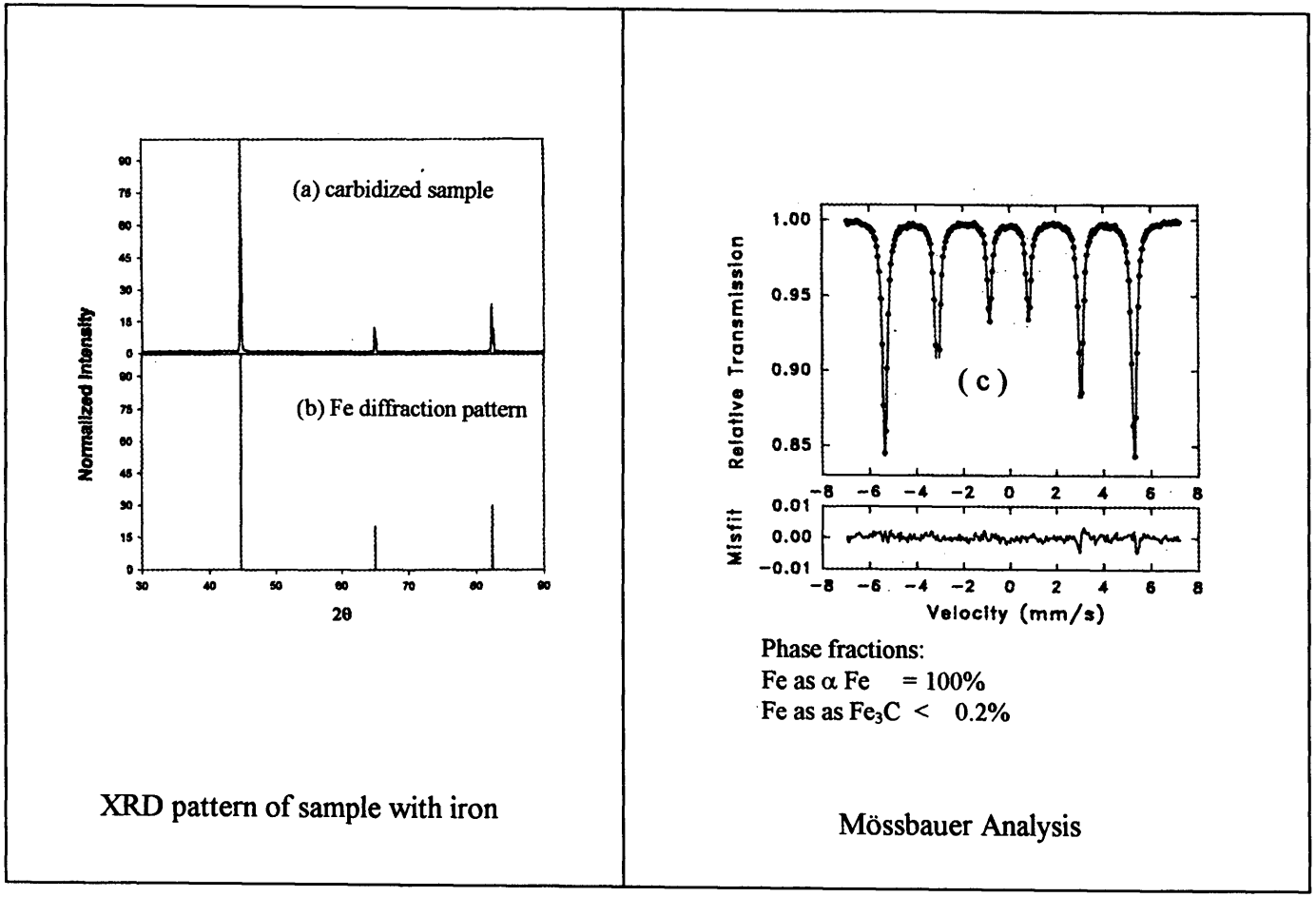

Figure 5.6 Carbidized sample with 25% CH_4-75% H_2 mixture; P_{tot} = 0.8 atm.; at 625 °C for 20 minutes. a) XRD pattern of: sample ; b) JCPDS diffraction reference peaks for Fe. and c) Mössbauer Analysis production of H_2 is required by equilibrium condition.

In C5 and C6 Runs, the H_2-CH_4 gas-mixture was "inert" under the condition specified.

Conversion with CH_4-H_2-O_2 Gas Mixture . The objective of these experiments was to examine whether a the H_2-CH_4-O_2 gas mixture could be equilibrated to produce a carbidizing gas which reacts with iron and to produce iron carbide. In principle, by including O_2 in the gas phase, an equilibrated gas phase containing CO would be produced which could allow for the formation of Fe_3C.

In Table 5.4 presents a summary of these experiments. The gas-mixture utilized $Y_{H_2} / Y_{CH_4} = 1$ with ~ 2.0 mole % O_2. The reaction time for Run D1 was 10 minutes at 625 °C and 0.8 atm of total pressure. A ~ 25% loss in mass indicated complete conversion to cementite from gravimetric analysis. However, the XRD analysis revealed the presence of the metallic iron metallic plus wüstite (FeO) as displayed in Figure 5.7. Therefore, it verified incomplete reduction. As a result, carbidization was not possible, even though metallic iron was present under a carbidizing gas.

Table 5.4 Experimental data of carbidization of iron with H_2-CH_4-O_2 mixture at 625 °C and 0.8 atm total pressure. Configuration with two Al_2O_3 boats.

Run No	Y_{H_2} / Y_{CH_4},(% O_2)	Reaction Time	Observations
D1	1.00, (2.0)	10	no carbidization, Fe & FeO in the product
D2	1.00, (2.0)	15	no carbidization, only Fe

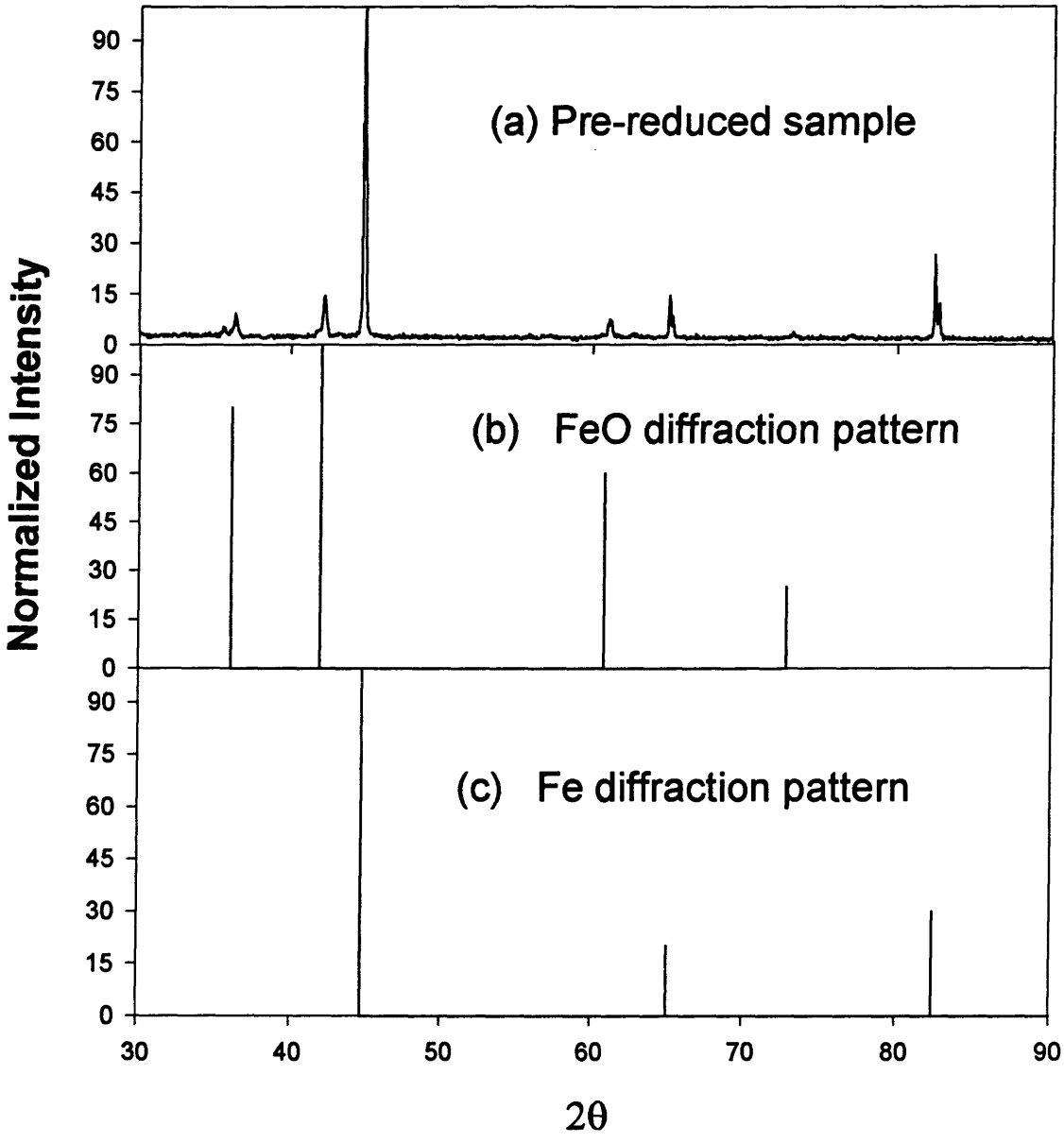

Figure 5.7 XRD pattern of: a) Carbidized sample with 49% CH_4-49% H_2-2% O_2 mixture; $P_{tot.}$ = 0.8 atm.; at 625 °C for 10 minutes. b) JCPDS diffraction reference peaks for FeO and c) JCPDS diffraction reference peak. for Fe.

One additional experiment, Run D2, was performed under the same conditions, except that the reaction time was 15 minutes. The gravimetric analysis indicated 25.4% Fe_3C. However, the XRD analysis revealed the presence of Fe and no-Fe_3C as displayed in Figure 5.8. As indicated before, 25.36 % Fe_3C is equivalent to 1.69 % C in the reaction product, which could not be identified by XRD analysis. Wüstite did not appear to be present and the pattern only revealed Fe. The FeO/Fe equilibrium requires that p_{O_2} = 1.24 x 10^{-24} atm whereas the feed gas contained p_{O_2} of 1.5 x 10^{-2} atm. It is apparent that reaction of oxygen with either H_2 or CH_4 must have occurred, and with the premise that CO is the species required for carbidization, then the reaction must be primarily with CH_4 rather than H_2.

Conversion with CH_4-H_2-CO Gas Mixture. The following experiment was performed under the same conditions as the D experiments except in this case O_2 was replaced by CO. The details of this experiment are described in the table 5.5. The gravimetric analysis indicated 10.6% Fe_3C. However, the XRD of this reaction product revealed only Fe as shown in Figure 5.9. In this Figure, Mössbauer analysis revealed the presence of a small amount of Fe (1.5 %) as Fe_3C and a small amount of Fe (1.2 %) as non-magnetic phase. The latter may be duè to the presence of austenite (fcc-Fe stabilized by carbon in solution). This Run verified the results obtained in previous experiments that CO in the gas-phase was the active carbidizing gas.

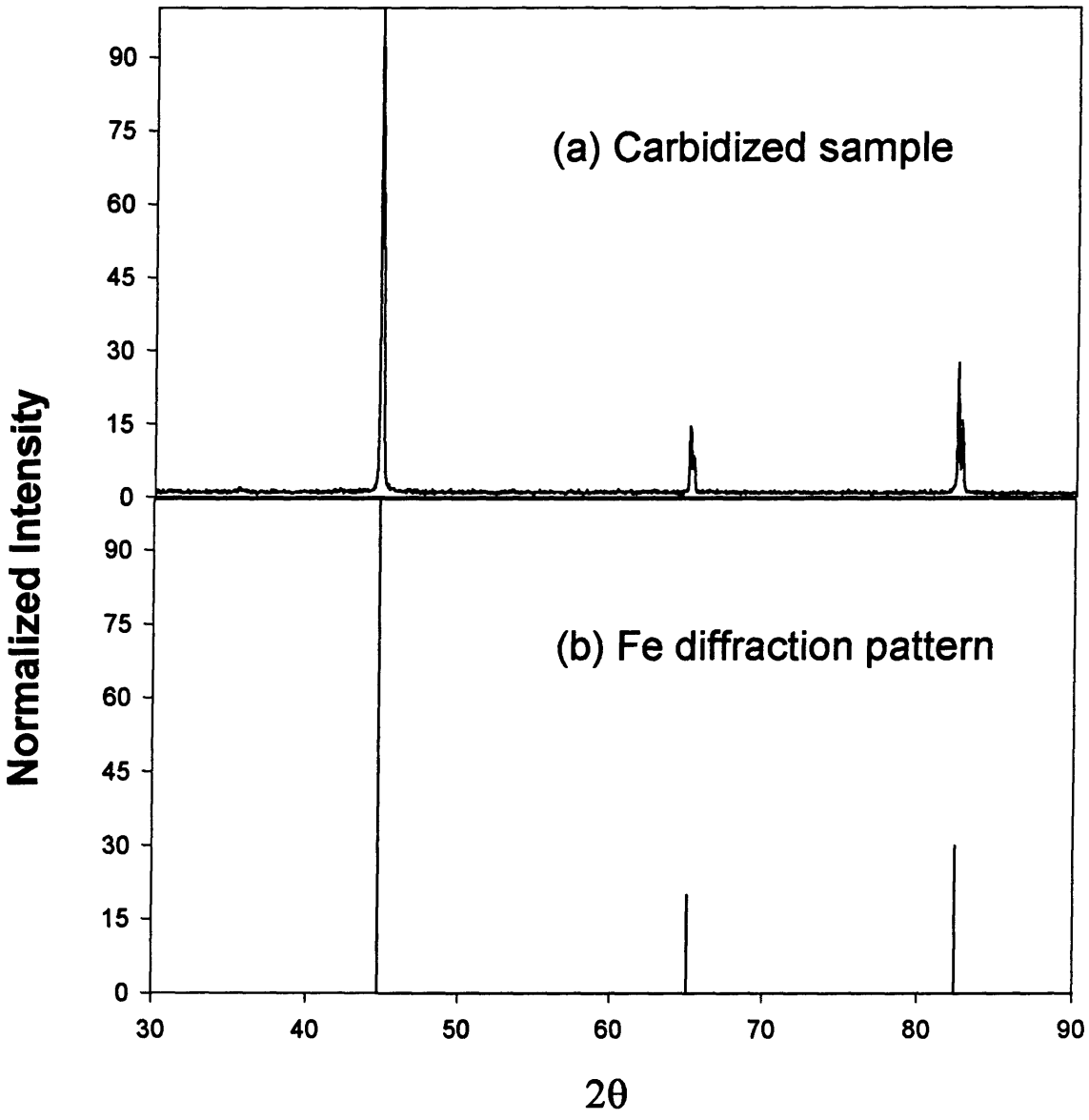

Figure 5.8 XRD pattern of: a) Carbidized sample with 49% CH_4-49% H_2-2% O_2 mixture; P_{tot} = 0.8 atm.; at 625 °C for 15 minutes. b) JCPDS diffraction reference peaks for Fe.

Table 5.5 Experimental data of carbidization of iron with H_2-CH_4-CO mixture at 625 °C and 0.8 atm total pressure. Configuration with two Al_2O_3 boats.			
Run	Y_{H_2} / Y_{CH_4}, (% CO_2)	Reaction Time (min)	special Condition observed
E1	1.00, (2.5)	10	no carbidization, presence of Fe

5.2 Validation Experiments for Adsorption Rate-Model.

These experiments were performed so that the parameters of the equation developed to model the rate of carbidization could be measured. The parameters obtained are strictly for the carbidization of iron (produced by hydrogen reduction of hematite) by a CO-H_2 gas phase. It is recalled that these gas species are adsorbed onto active sites of the metallic iron (Fe°, at equilibrium or close to equilibrium) and subsequently a carbon species is created on these sites by two reaction paths :

i) a surface Boudouard reaction ($2CO_{(g)} = C_{(s)} + CO_{(g)}$) and

ii) a surface shift water gas reaction ($H_{2(g)} + CO_{(g)} = H_2O_{(g)} + C_{(s)}$).

This surface carbon is then consumed at an intrinsically higher rate, relative to the growth of carbon, to produce cementite (until 90-95 % of the iron is converted to cementite). The asymptotes defined by the rate equation occur when the gas phase contains either pure hydrogen (no carbidization) or pure carbon monoxide (where the surface Boudouard-reaction controls the carbidization rate). On increasing the carbon monoxide content of the gas mixture from zero, the rate of carbidization would be expected to increase progressively to a maximum value and then decrease progressively to a value where the rate is controlled solely by the surface Bouduard reaction.

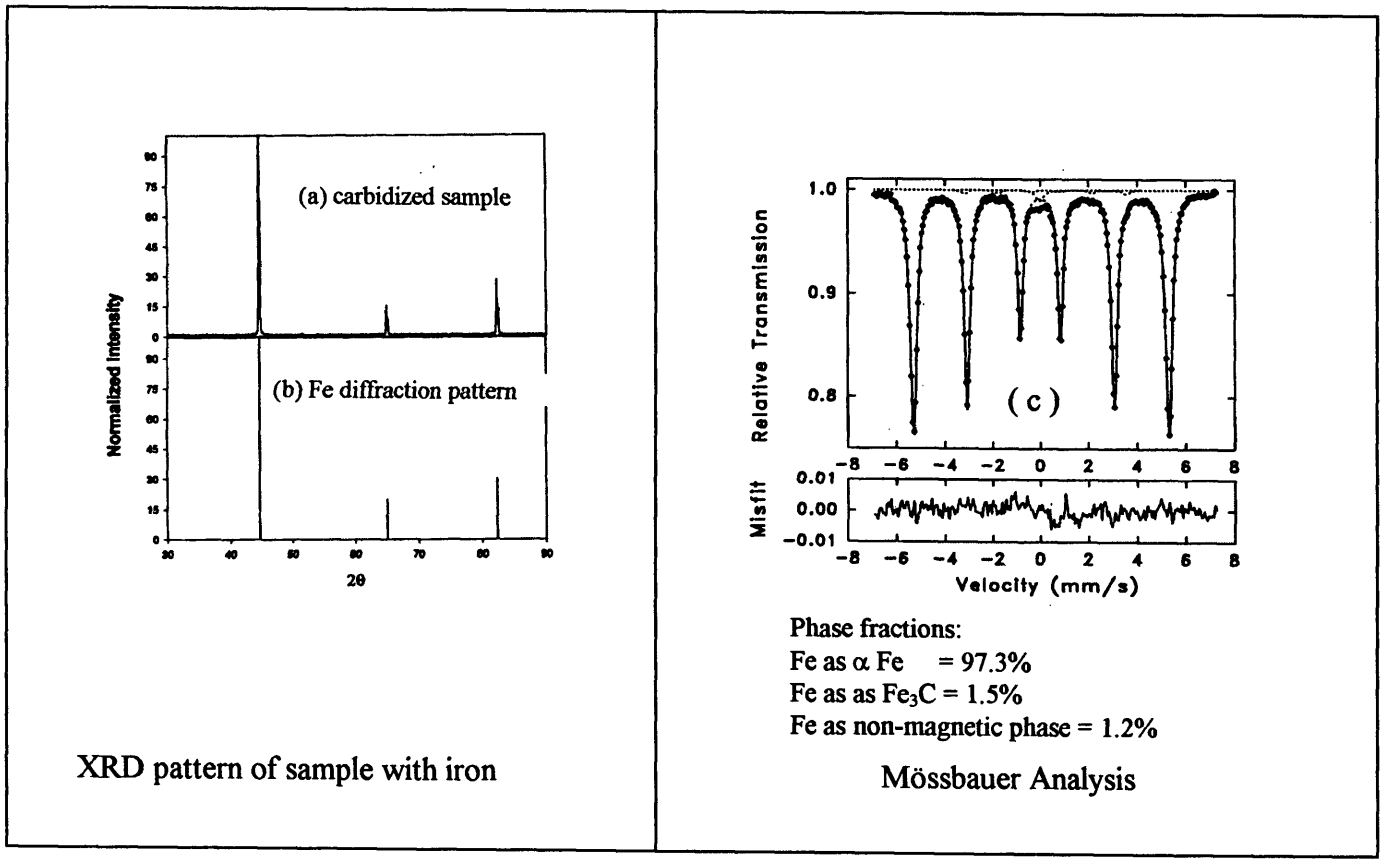

Figure 5.9 Carbidized sample with 48.75% CH_4-48.75% H_2-2.5% CO mixture; $P_{tot.}$= 0.8 atm.; T = 625 ° C and reaction time = 10 minutes. a) XRD pattern of sample; b) JCPDS diffraction reference peaks for Fe. c) Mössbauer analysis.

5.2.1 Fractional Conversion of Iron and Mass Fraction of Cementite in The Reaction Product.

The heterogeneous specific reaction-rate equation can, most conveniently, be related to the fractional conversion of iron to cementite. The relationship between this parameter and the rate of formation of cementite is now developed.

The fractional conversion is defined by:

$$\chi_A = \frac{Moles\ of\ iron\ converted}{Moles\ of\ iron\ present\ initially} \quad \text{.....(5.1)}$$

$\chi_A = \chi_{Fe}$ (fractional (mass or moles) conversion of Fe to Fe_3C); for $0 \leq \chi_A \leq 1$

or, $$\chi_A(t) = \frac{N_{Ao} - N_A(t)}{N_{Ao}} \quad \text{.....(5.2)}$$

also, from the stoichiometry of cementite:

$$N_A(t) = N_{Ao} - 3N_B(t) \quad \text{.....(5.3)}$$

in which, B ≡ Fe_3C

or, $$\left(N_{Ao} - N_A(t)\right) = 3N_B(t) \quad \text{.....(5.4)}$$

Thus,

$$\chi_A(t) = \frac{3N_B(t)}{N_{Ao}} \quad \text{.....(5.5)}$$

In addition, $N_{Ao} = \frac{m_{Ao}}{M_A}$. In which , m_{Ao} is the mass of A present initially and M_A its molecular weight.

Therefore,

$$\chi_A(t) = \frac{3N_B(t)}{\frac{m_{Ao}}{M_A}} \quad \text{.....(5.6)}$$

or,

$$\frac{dN_B}{dt} = \frac{1}{3}\frac{m_{Ao}}{M_A}\frac{d\chi_A}{dt} \quad \text{.....(5.7)}$$

The mass fraction of cementite (B) in the reaction product is given by:

$$f_B(t) = \frac{m_B(t)}{m_B(t) + m_A(t)} \quad \text{.....(5.8)}$$

Also,

$$m_B(t) = N_B(t) \cdot M_B \quad \text{.....(5.9)}$$

$$m_A(t) = N_A(t) \cdot M_A \quad \text{.....(5.10)}$$

Thus, on combining equations (5.6) , (5.8), (5.9) and (5.10) the following expression is obtained:

$$\chi_A(t) = \frac{1}{\left(\frac{M_B}{3M_A}\right)\left(\frac{1}{f_B(t)} - 1\right) + 1} \quad \text{.....(5.11)}$$

Equation (5.11) can then be used to convert $f_B(t)$.to $\chi_A(t)$.

5.2.2 Heterogeneous Rate-Expression Development

The heterogeneous specific reaction rate is defined as follows:

$$r_B'' \equiv \frac{1}{S}\frac{dN_B}{dt} \quad \text{.....(5.12)}$$

in which S is the "surface area" of the solid phase in contact with the gas phase and N_B is the moles of B (Fe_3C) in the reaction product at *t*.

Also, it is recalled that :

$r_B'' \equiv r_{Fe_3C}'' \equiv r_B''(p_1, p_2)$; 1 ≡ CO and 2 ≡ H_2

When Equations 5.7 and 5.12 are combined, the resulting expression in terms of fractional conversion is :

$$\frac{d\chi_A}{dt} = \lambda \cdot r_B''(p_1, p_2) \quad \text{.....(5.13)}$$

in which, $\lambda = \frac{3M_a S_o}{m_{Ao}}$, an invariant quantity.

Upon integration, Equation 5.13 yields:

$$\chi_{Fe}(t) = \lambda \cdot r''_{Fe_3C}(p_{CO}, p_{H_2}) \cdot t \quad \text{.....(5.14)}$$

This equation now allows the parameters of the rate equation to be determined from the measurements performed.

5.2.3 Carbidization of Hematite with CO-Ar Gas Mixture.

The objective of these experiments was to develop rate data which would allow the equilibrium constant for the CO adsorption reaction and the rate parameters for the carbidization reaction to be established.

$$r''_{Fe_3C} = k_{3.15} \left[\frac{(K_{3.13} \cdot p_1)^2}{\left(1 + (K_{3.13} \cdot p_1)^{1/2}\right)^4} \right] \quad \text{..... (5.15)}$$

The fractional conversion time behavior is described by:

$$\chi_{Fe}(t) = \lambda \cdot r''_{Fe_3C(PCO, PH_2)} \cdot t \quad \text{.....(5.16)}$$

Substituting Equation (5.15) into Equation (5.16) yield:

$$\chi_{Fe}(t) = k'_{3.15} \left[\frac{(K_{3.13} \cdot p_1)^2}{\left(1 + (K_{3.13} \cdot p_1)^{1/2}\right)^4} \right] . t \quad \text{..... (5.17)}$$

where $k'_{3.15} = \lambda\, k_{3.15}$ is invariant for a given precursor iron and reaction temperature.

The partial pressure of the CO in the gas phase can be adjusted over a sufficiently wide range by adjusting the composition of the CO-Ar gas mixture, Also, Equation 5.17 can be inverted to give a linearized relationship from which the parameters $k'_{3.15}$ and $K_{3.13}$ can be estimated by standard linear regression analysis.

$$\frac{p_1^{1/2}}{\left(\frac{\chi_{Fe}(t)}{t}\right)^{1/4}} = \left(\frac{1}{k'_{3.15}\ K_{3.13}^2}\right)^{1/4} + \frac{K_{3.13}^{1/2}}{\left(k'_{3.15}K_{3.13}^2\right)^{1/4}} \bullet p_1^{1/2} \quad \text{.....(5.18a)}$$

which is of the from:

$$Y = a + bx \quad \text{.....(5.18b)}$$

The reaction time for the experiments conducted was selected to be 5 minutes, and the CO partial pressure investigated covered the range 0.2 to 0.8 atm.

Because Equation 5.18a is of a form where the dependent variable, Y, contains both χ_{Fe} and p_1 (the original dependent and independent variables, respectively) the values of the parameters obtained are not optimal. Consequently, nonlinear optimization strategy, implemented by a computer program, was devised, based on Equation (5.17) which then "fine-tuned" $k'_{3.15}$ and $K_{3.13}$ obtained from the linear regression analysis of equation 5.18a. This optimization search routine automatically determined values of the parameters such that the sum of the squared of the deviation between the values of $\frac{\chi_{Fe}(t)}{t}$ as measured and as predicted by the right side of the Equation 5.17 was minimum. The final result is displayed in Figure 5.10. The value of CO adsorption equilibrium constants were $K_{3.13} = 1.33 \pm 0.075$ atm^{-1} and for $k'_{3.15} = 0.66 \pm 0.03$ min^{-1}.

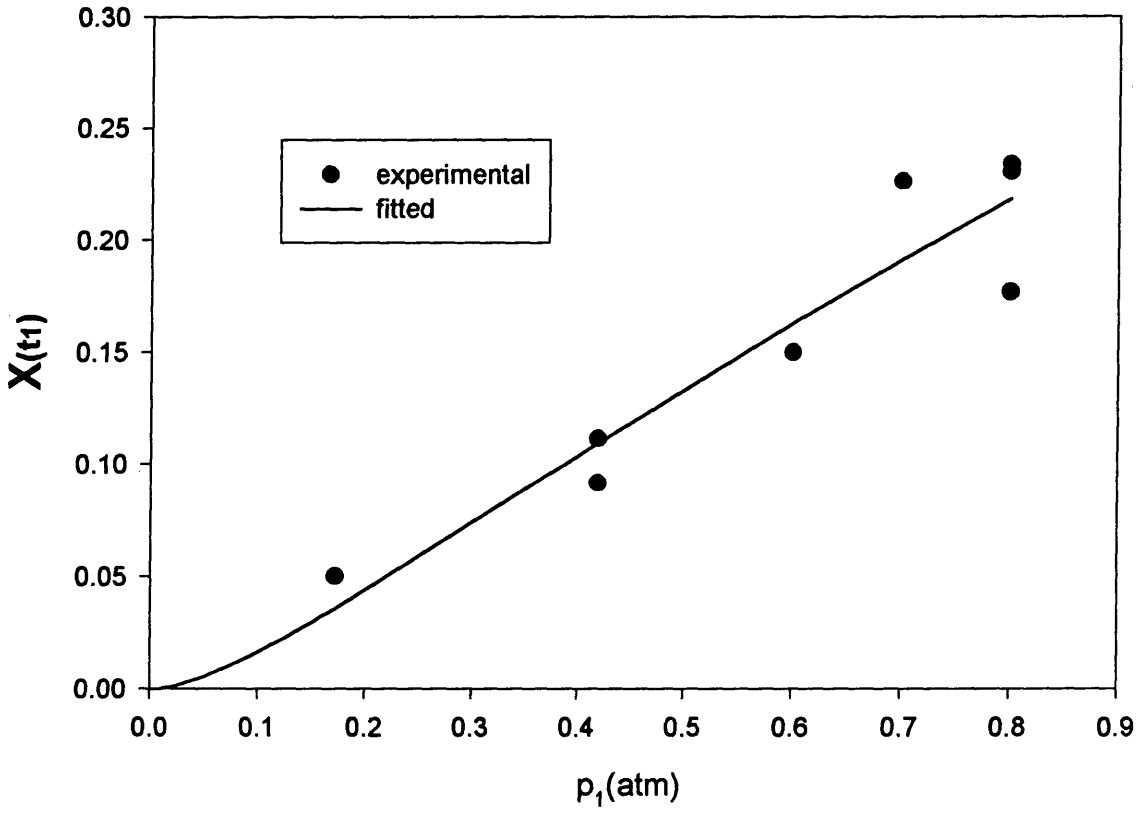

Figure 5.10 Experimental data fitted to the adsorption-rate model. CO-Ar gas mixture. Reaction time: 5 minutes; P_{tot} = 0.8 atm; and, T= 625 °C.

5.2.2 Carbidization of Hematite with H_2-CO Gas mixture.

The corresponding relationship for the conversion-time behavior is :

$$\frac{\chi_{Fe}(t)}{t} = k'_{3.15}\left[\frac{(K_{3.13}\cdot p_1)^2}{\left(1+(K_{3.13}\cdot p_1)^{1/2}+(K_{3.14}\cdot p_2)^{1/2}\right)^4}\right]+$$

$$k'_{3.16}\left[\frac{(K_{3.13}\cdot p_1)}{\left(1+(K_{3.13}\cdot p_1)^{1/2}+(K_{3.14}\cdot p_2)^{1/2}\right)^2}\right]\left[\frac{(K_{3.14}\cdot p_2)}{\left(1+(K_{3.13}\cdot p_1)^{1/2}+(K_{3.14}\cdot p_2)^{1/2}\right)^2}\right] \quad ..(5.19)$$

This is obtained by incorporating Equation (3.27) into Equation (5.14). The optimum values of $k'_{3.15}$ and $K_{3.13}$ previously determined were now maintained in Equation 5.19. The optimum values of $k'_{3.16}$ and $K_{3.14}$ were determined from linear regression of equation (5.19) with experimental data. Consequently an optimum value was establish by use of the least deviation of error. The following resumed expression was used for a multi-linear regression:

$$Z = k'_{3.16}x_1x_2 \quad .....(5.20)$$

in which ,

$$Z = \frac{\chi_{Fe}(t)}{t} - k'_{3.15}\cdot x_1^{1/2}$$

$$x_1 = \left[\frac{(K_{3.13}\cdot p_1)}{\left(1+(K_{3.13}\cdot p_1)^{1/2}+(K_{3.14}\cdot p_2)^{1/2}\right)^2}\right]$$

$$x_2 = \left[\frac{(K_{3.14} \cdot p_2)}{\left(1 + (K_{3.14} \cdot p_1)^{1/2} + (K_{3.14} \cdot p_2)^{1/2}\right)^2} \right]$$

The optimum values of the remaining parameters $k'_{3.16}$ and $K_{3.14}$ are then obtained by a manual search strategy in which the value of $K_{3.14}$ is adjusted while the optimum value of $k'_{3.16}$ is obtained by multivariable regression. Ultimately, the optimum value of $K_{3.14}$ is obtained when the sum of the squares of the deviation between Z and $k'_{3.16} x_1 x_2$ is observed to be a minimum.

The fitted data for the experiments conducted for a reaction time of 5 minutes are displayed in Figure 5.11. It is seen that the model is able to provide a good fit to the measured conversions.

$$K_{3.13} = 1.33 \pm 0.075 \text{ atm}^{-1}$$

$$K_{3.14} = 0.35 \pm 0.02 \text{ atm}^{-1}$$

$$k'_{3.15} = 0.66 \pm 0.03 \text{ min}^{-1}$$

$$k'_{3.16} = 21 \pm 1.5 \text{ min}^{-1}$$

The model with the parameters obtained by fitting of the data from experiments with CO-Ar and CO-H_2 gas mixtures was now used to predict the conversions for experiments with a reaction time of 10 minutes. The predicted behavior is indicated by the line on Figure 5.12. The agreement is reasonably good except for hydrogen fractions between 0.3 and 0.7 where the measured conversions appear to be approximately invariant. This may indicate that the rate of carbidization decreased after carbidization achieved a certain value which could depend on composition of gas-mixture. This behavior can be attributed to the constraint imposed on the " surface area" of the precursor iron reactant being invariant. This feature was introduced into Equation (5.12)

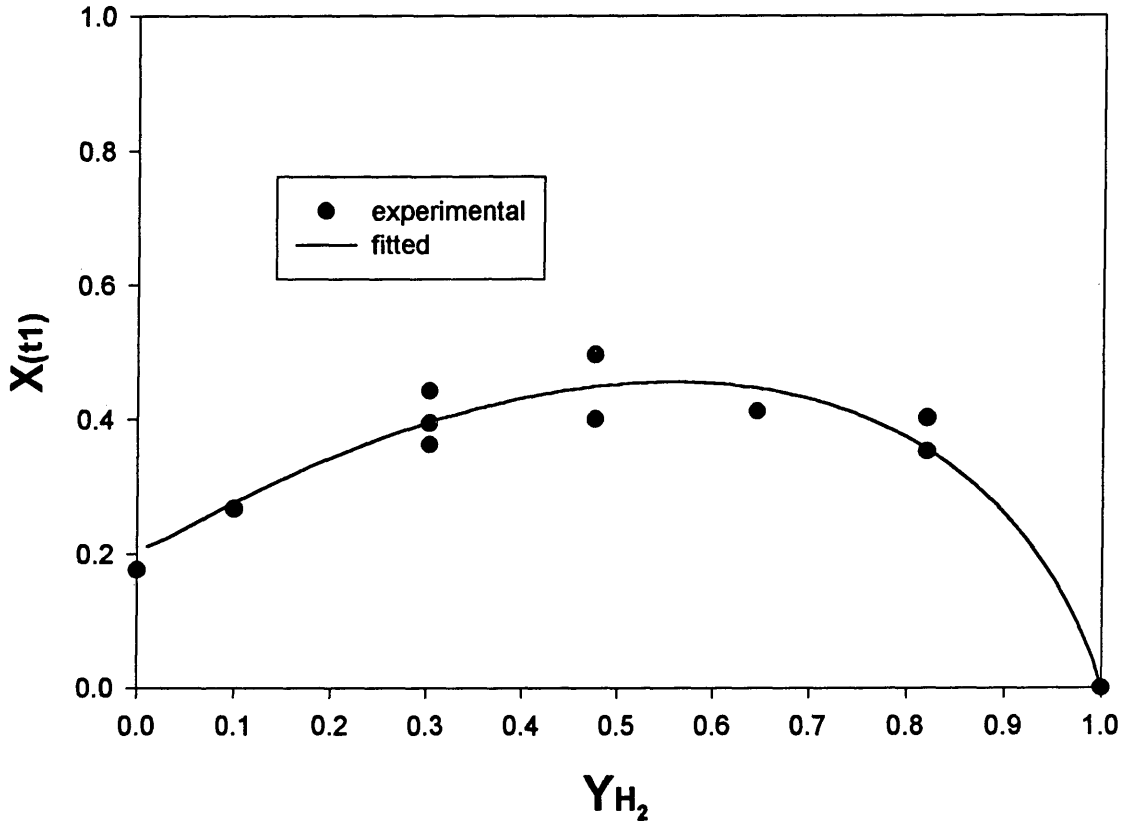

Figure 5.11 Experimental data fitted to the adsorption-rate model. H_2-CO gas mixture. Reaction time: 5 minutes. P_{tot} = 0.8 atm; and, T= 625 °C.

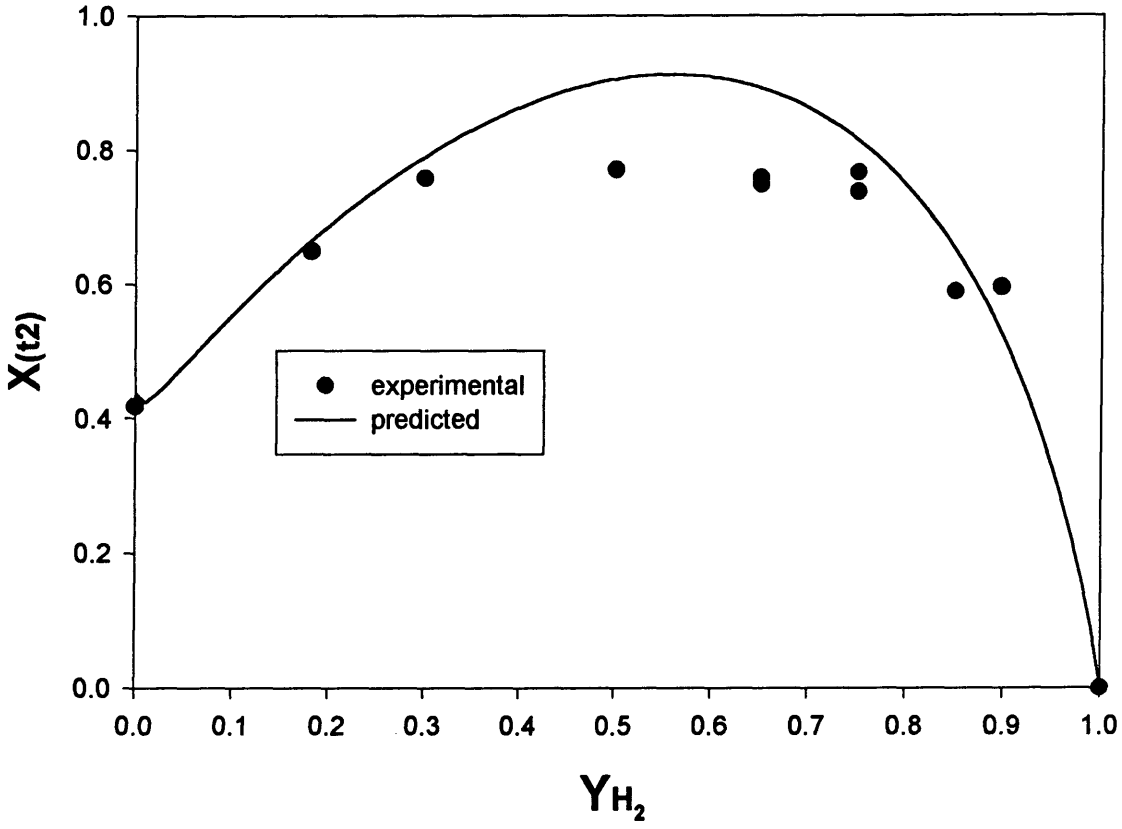

Figure 5.12 Experimental data and fitted values to the adsorption-rate model. H_2-CO gas mixture. Reaction time: 10 minutes. P_{tot} = 0.8 atm; and, T= 625 °C.

where the surface are S was replaced by So, an invariant quantity. It was recognized in the development of the model that the "surface area" associated with the active site would be dependent on conversion. However, the functional form to adopt was not apparent. Conejo (1995) had observed in his TGA experiments that there were two stages of carbidization. A first stage with higher rate of carbidization than that of second the stage after approximately 80% of conversion.

5.3 Morphology of iron and iron carbide produced from carbidizing process.

The precursor iron for carbidizing process comes from the reagent grade hematite which was described in Chapter 4. It was reduced under H_2 for enough time to achieve complete reduction, or complete transformation of hematite in the sample to metallic iron. The morphology of this metallic iron is displayed in Figure 5.13.

In order to determine if some change is evidenced from precursor iron to the iron carbide during the carbidizing process, a SEM analysis was used to check the morphology of the iron carbide product. A Carbidized sample with 25% CO-75% H_2 mixture at 625 °C for 15 minutes was used to characterize the morphology of the iron carbide by SEM. According to Mössbauer and XRD analysis, the iron carbide produced was Fe_3C or θ-carbide. Its morphology is shown in Figure 5.14 at two different magnifications. It was evidenced that there was not appreciable change by SEM analysis after the carbidizing process by comparison Figure 5.13 and Figure 5.14.

The presence of iron carbide with iron as original sample for carbidization with CH_4- H_2 gas mixture was used. This original sample was a mechanical mixture of iron and iron carbide in order to provide a catalytic surface for carbidization from iron carbide which was demonstrated to be active the surface to promote the precipitation of carbon onto reaction product surface, when a CO-H_2 gas mixture was used. The result of this experiment, as explained in section 5.1, was that no appreciable change in mass between original sample and reaction product occurred. Also, the SEM analysis revealed no

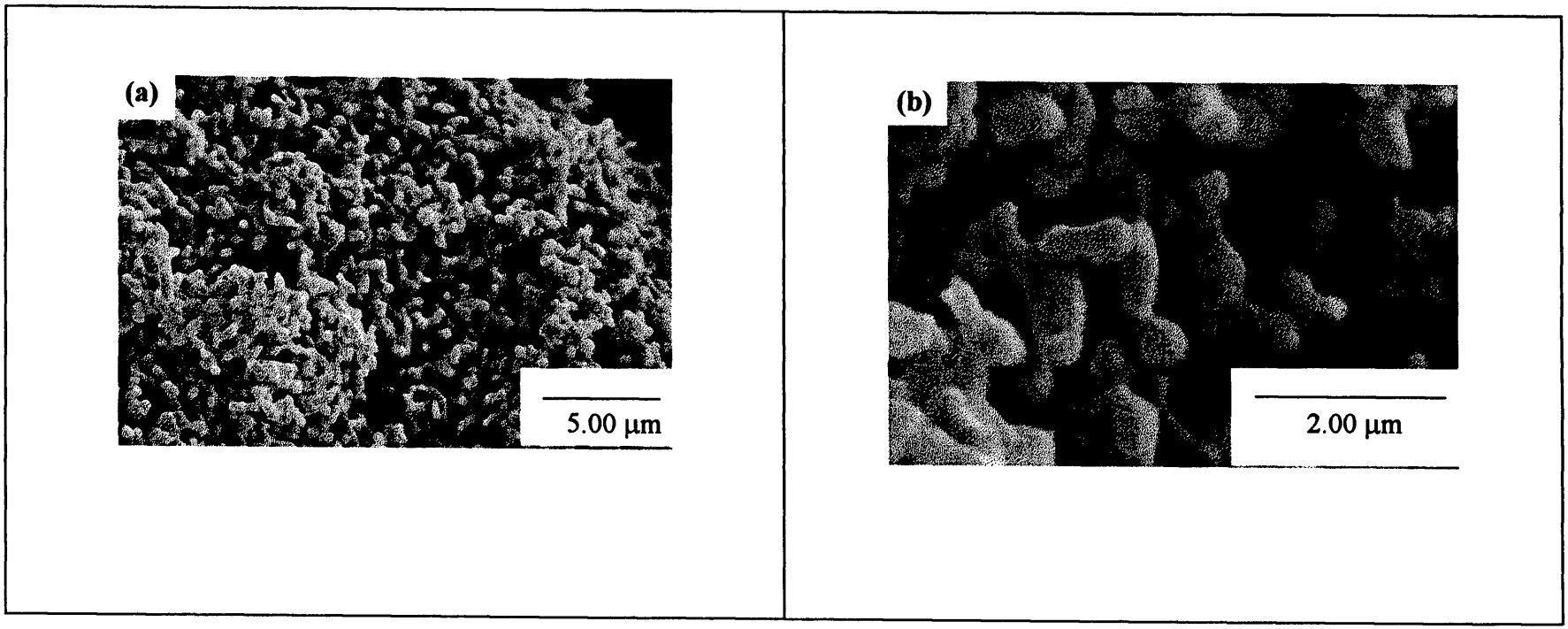

Fig.5.13 Morphology of Fe. Precursor Fe_2O_3. reduction : 75 % H_2, 25 % CH_4; $P_{tot.}$ = 0.8 atm.; T = 625 °C; Reaction time = 15 minutes.a) 5,000X and b) 20,000X

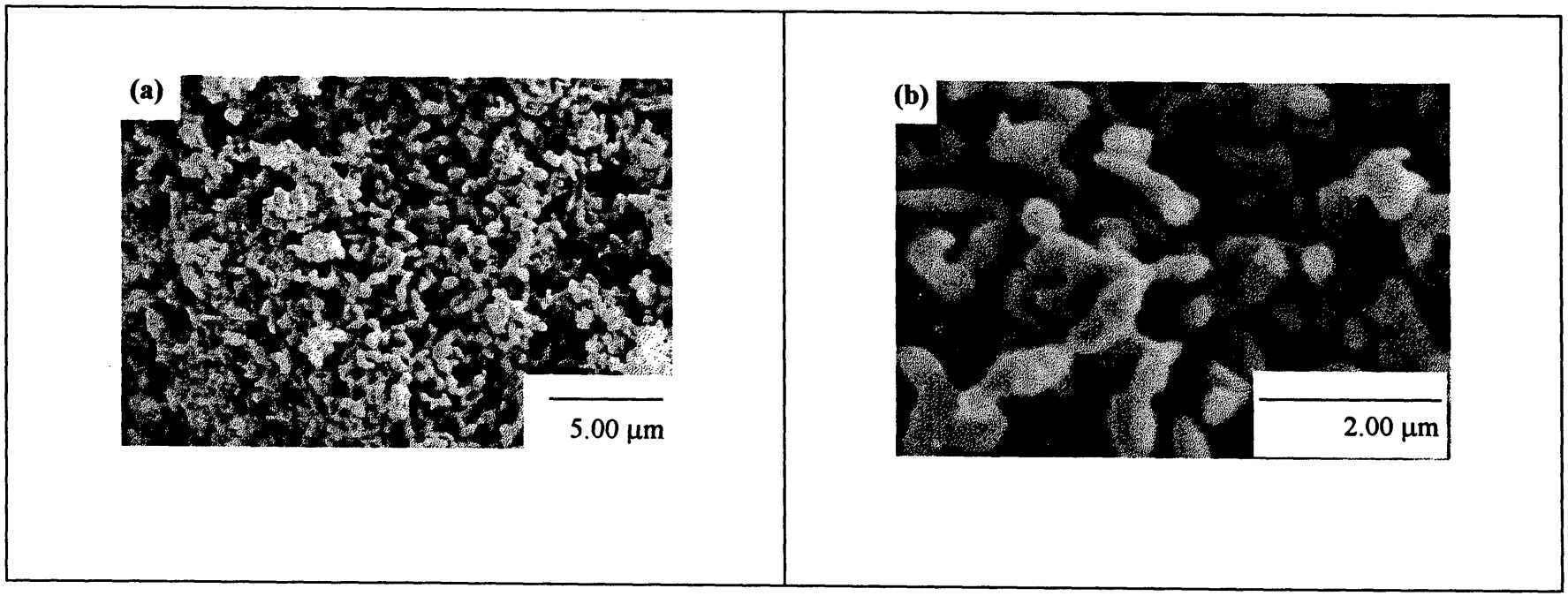

Fig.5.14 Morphology of Fe_3C. Precursor Fe_2O_3. Carbidization : 75 % H_2, 25 % CO; Ptot. = 0.8 atm.; T = 625 °C; Reaction time = 15 minutes. a) 5000X and b) 20,000X

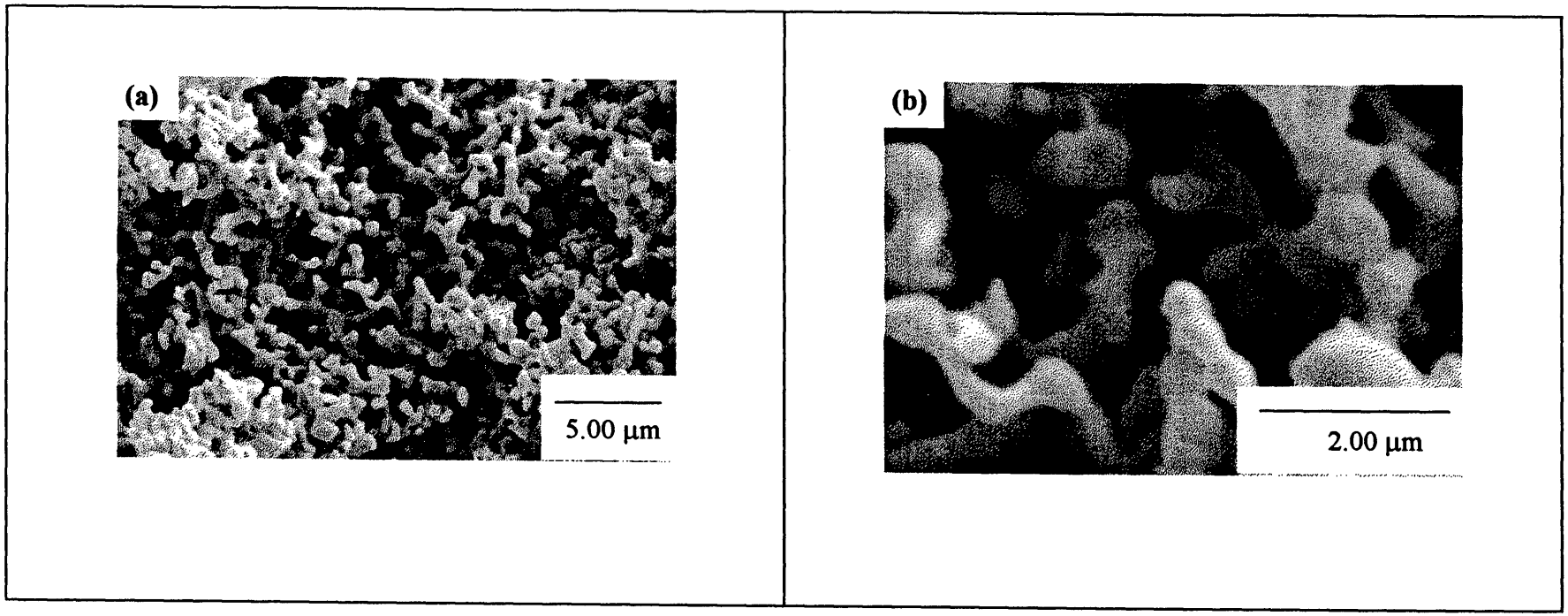

Fig.5.15 Morphology of mechanical mixture of Fe and Fe_3C . 50 % Fe and 50 %Fe_3C.
a) 5,000X and b) 20,000X

appreciable change in morphology as displayed in Figure 5.15. Thus, it is found that there is no appreciable change in morphology of the precursor iron from reagent grade hematite during its conversion to cementite.

5.4 Other Experiments.

In this section, The following set of experiments were realized in order to complement certain information required for a better understanding of the results achieved in this research.. First, iron-bearing phase predictions from gravimetric analysis were validated by use of Mössbauer analysis and how the importance of sampling process in generating representative samples is also explained. In the second section, a reproducibility test to corroborate the procedure performed is described in detail. Finally, the reaction product from reduction by H_2 was verified.

5.4.1 Validation of Iron-bearing Phase Predictions from Gravimetric Analysis by Use of Mössbauer Analysis.

The objective of this section is the validation of iron phase predictions from gravimetric analysis by use of the Mössbauer technique. Recall that the reaction product for partial carbidization revealed the presence of Fe and Fe_3C according to XRD analysis. The gravimetric analyses can predict the mass fraction of the iron phases in the reaction product by use of the mass balance of carbon and iron based on the loss in mass from the original sample . These expressions were developed in section 3.5.

A series of experiments were performed in order to obtain the experimental data that for verification of the results obtained by the gravimetric analysis. In order to obtain a range in the mass fraction of Fe_3C in the reaction product, a gas mixture was selected composed of 80 %-H_2 and 20 % CO for various reaction times (5, 10, 15, 20 and 30 minutes) at 625 °C and 0.8 atm of total pressure. In each experiment, the reaction product was ground to size -270M and analyzed by Mössbauer analysis. At the same

time, the predictions of the presence of Fe and Fe_3C were assessed by gravimetric analysis. The results obtained from both analyses are displayed in Figure 5.16. It can be noted that there were significant difference between the Mössbauer and Gravimetric analyses for the procedure employed. The possibility of a sampling problem was then considered

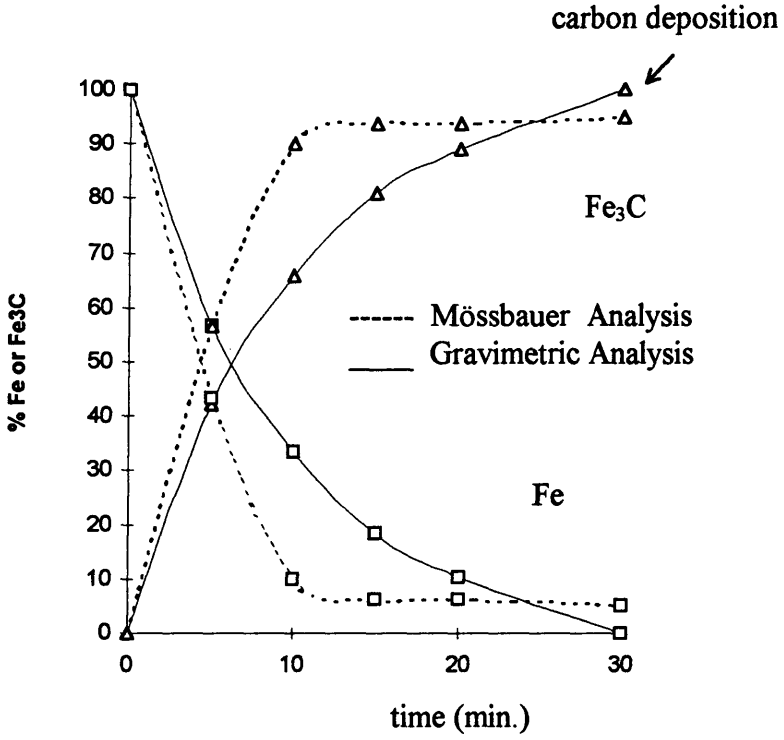

Figure 5.16 % Fe and %Fe_3C obtained from Gravimetric and Mössbauer analysis from reaction products carbidized with 80%-H_2 and 20%CO for: 5, 10, 15, 20 and 30 min. of reaction time; at 625°C and $P_{tot.}$= 0.8 atm.

The selectivity of one phase over the other in the sampling was evidenced in X-ray diffraction and Mössbauer analyses. A sample with size -270M resulted in a level of Fe as Fe_3C (Figure 5.17) higher than that of a sample ground to -325M as shown in Figure 5.18.

The sample ground to -325M resulted in 65.1% Fe as Fe_3C from Mössbauer analysis (according to gravimetric analysis the result was 64.85% Fe as Fe_3C) while the sample ground to -270M resulted in 89.4 % Fe as Fe_3C. All of these results indicated that there existed a sampling problem because of the selectivity of size range during sampling from the sample holder containing size -270M.

The percentage of Fe as Fe_3C in the sample by Mössbauer analysis was higher than that of gravimetric analysis. For example, the content of Fe as Fe_3C in the sample with size -270M was 23 %. The same sample which was split in two sizes, a + 325M/-270M and -325M, resulted in 7.8 and 10.4 % Fe as Fe_3C respectively. These results from Mössbauer analysis are shown in Figure 5.19.a. b and c, respectively.

In order to verify the size distribution present in the sample, a SEM analysis was performed in which were analyzed three sizes, one from the original sample (-270M), +325/-270M and -325M. The heterogeneity of particle size in the sample with size -270M is clearly shown in the Figure 5.20a. It was possible that the selectivity presented in the analyses was correlated with the selectivity of the particle size when a small amount of the sample, 100 mg, was taken for Mössbauer analyses from the main sample holder. For a sample with size -325M, the heterogeneity of the particle size was still quite clear as shown in Figure 5.20.c so that even grinding to this fines size could still lead to sampling problems.

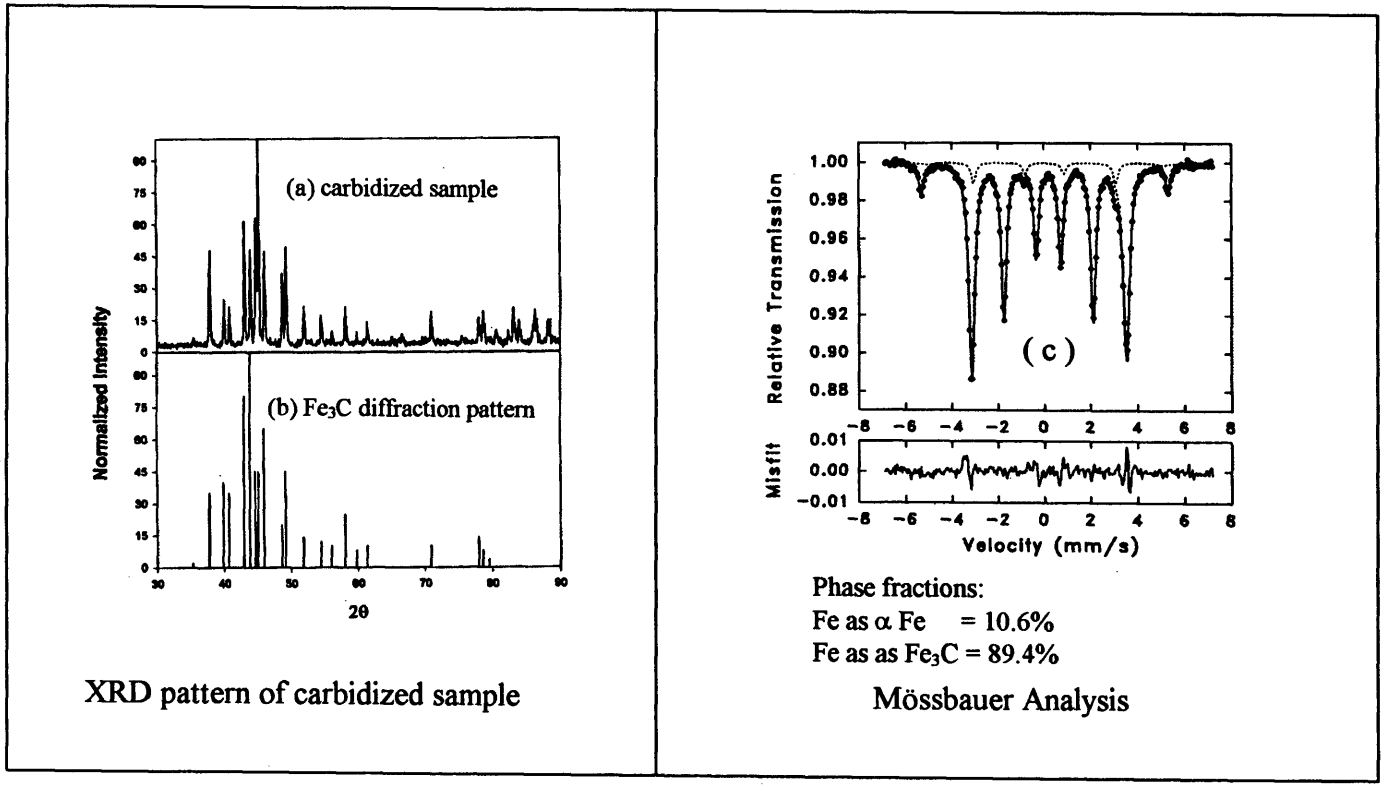

Figure 5.17 Sample precursor Fe_2O_3 reduced with H_2. Subsequent carbidization : 80 % H_2, 20 % CO; $P_{tot.}$ = 0.8 atm.; T = 625°C; Reaction time = 10 minutes. a) XRD for carbidized sample b) JCPDS diffraction reference peaks for Fe_3C. c) Mössbauer analysis.

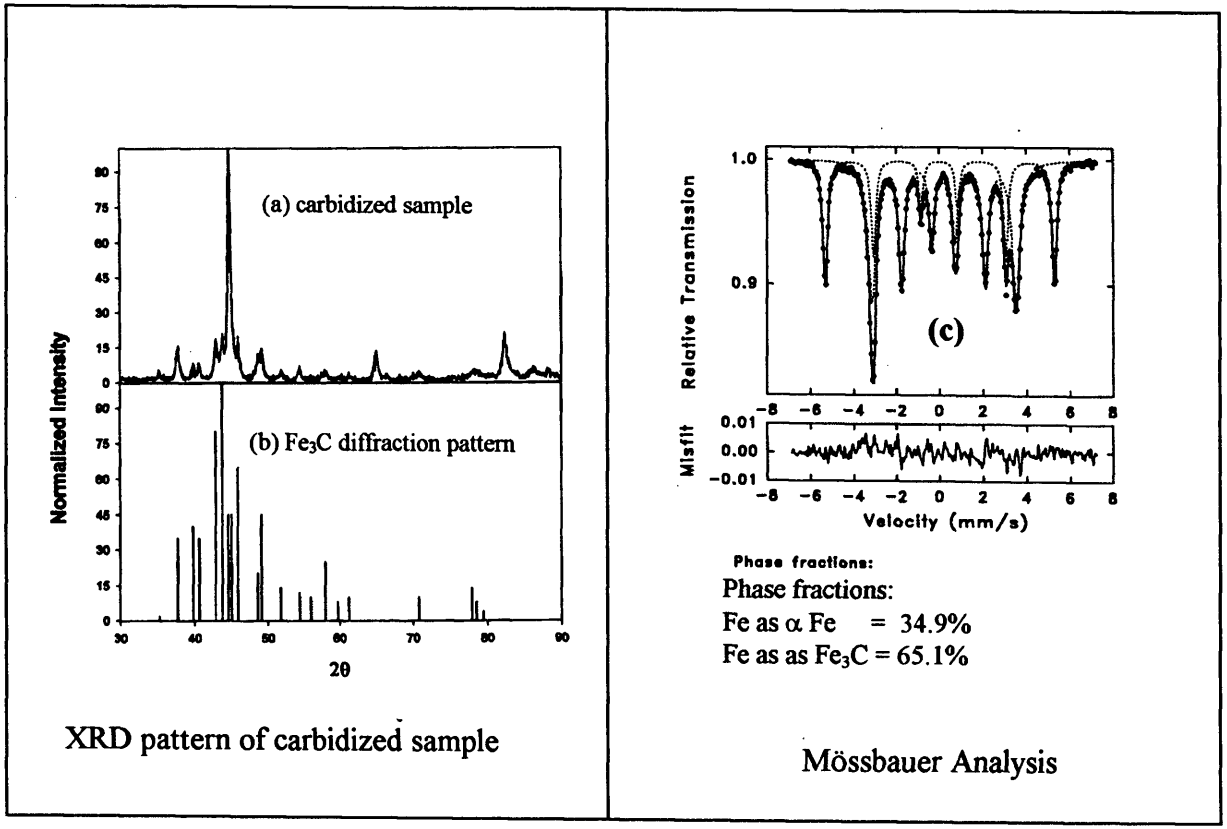

Figure 5.18 Comminuted sample (-325M). Precursor Fe_2O_3 reduced with H_2. subsequent carbidization : 80 % H_2, 20 % CO; Ptot. = 0.8 atm.; T = 625 °C; Reaction time = 10 minutes. a) XRD for carbidized sample b) JCPDS diffraction reference peaks for Fe_3C. c) Mössbauer analysis.

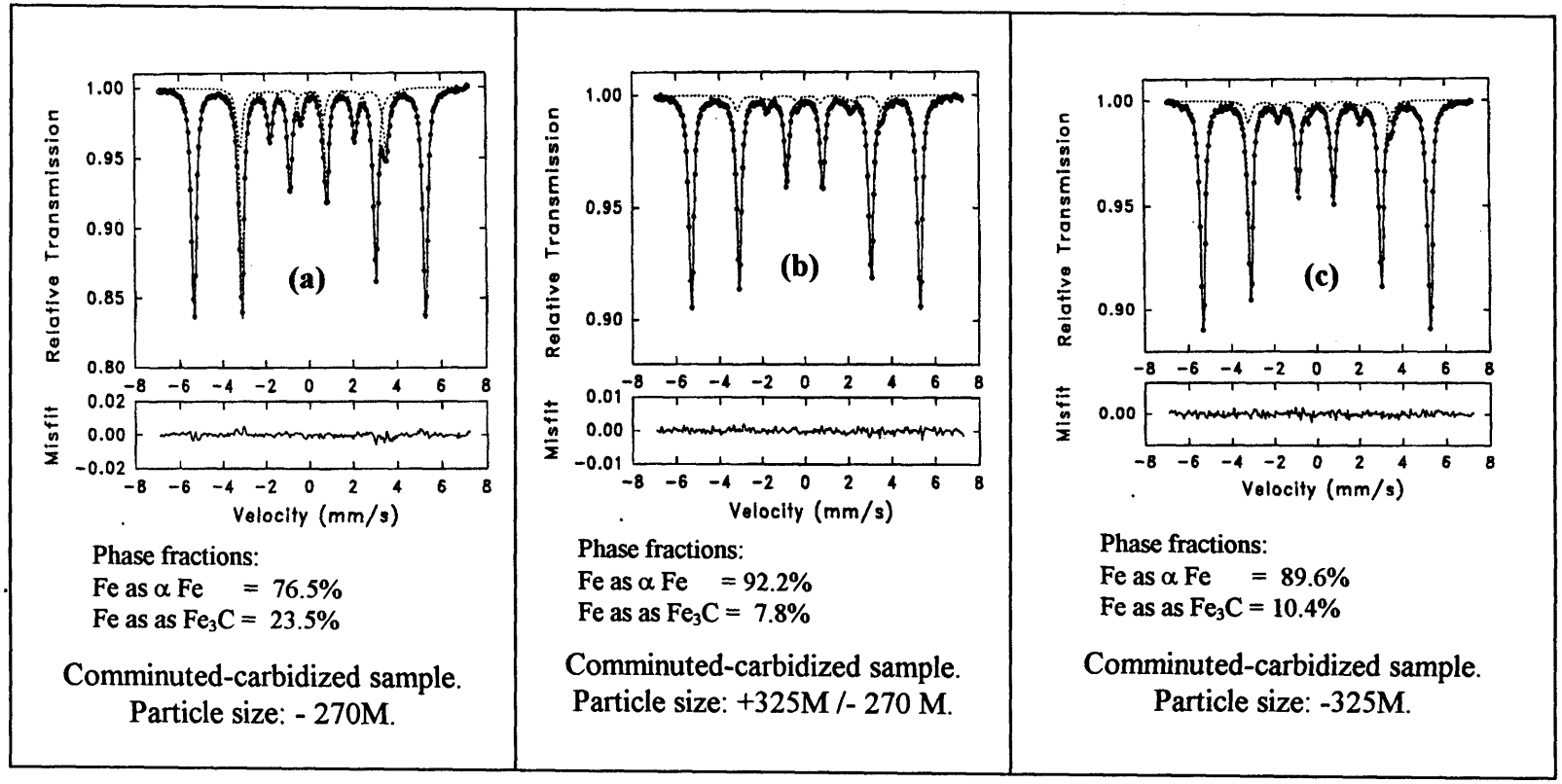

Figure 5.19 Mössbauer analyses of comminuted samples. Precursor Fe_2O_3 reduced with H_2. Subsequent carbidization: 52% CO, 48% Ar; P_{tot}= 0.8 atm.;T = 625°C. Reaction time = 5 minutes. Comminution details are indicated in each frame.

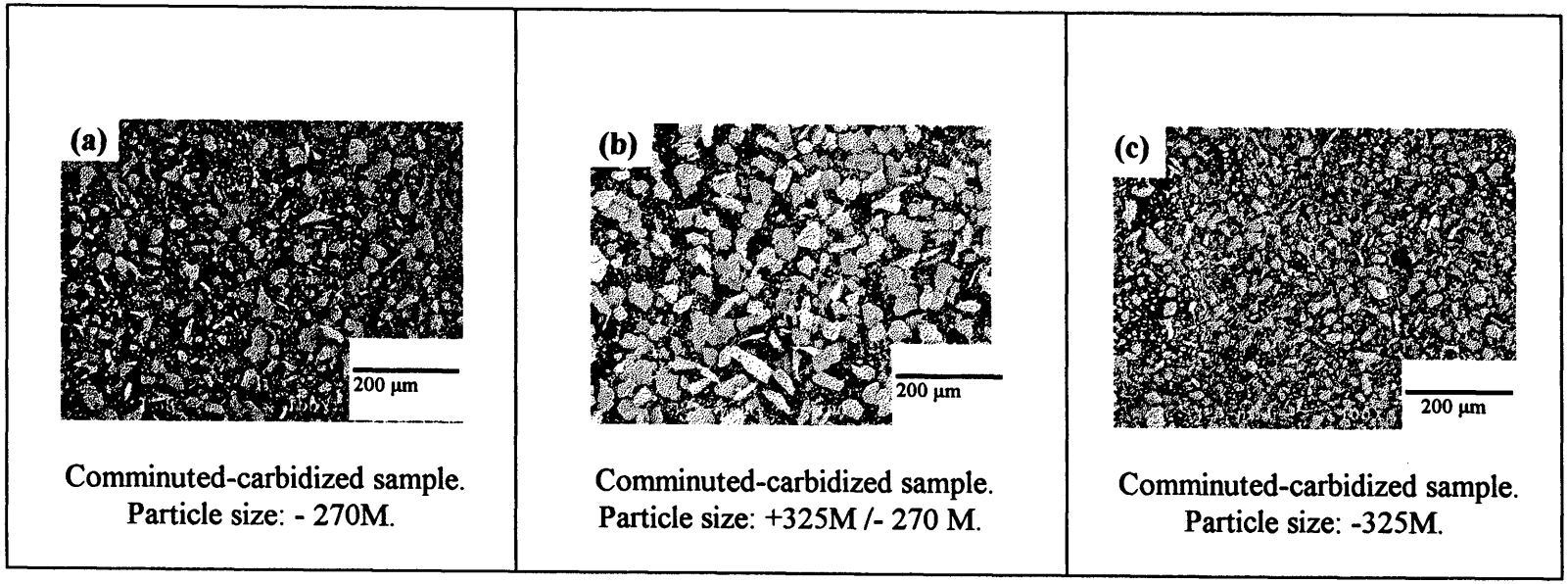

Figure 5.20 SEM photomicrographs of comminuted samples. Precursor Fe_2O_3 reduced with H_2. Subsequent carbidization: 52% CO, 48% Ar; Ptot= 0.8 atm.;T = 625°C; Reaction time = 5 minutes. Comminution details are indicated in each frame.

5.4.2 Reproducibility Test to Corroborate the Procedure used.

During the carbidization process with H_2-CO gas mixture, it was required if the gravimetric analysis was able to reproduce or if the process carbidization was able to be reproduced under the same condition. This was required in order to produce enough reaction product for futures analysis, a amount of the 1,009 mg of reaction product was produced from three consecutive experiments. Each experiment was performed with 80 % H_2 and 20 % CO for 10 minutes. The reduction was with 100 % H_2 and the results are displayed in Table 5.6 in which the percentage of the carbon is the main factor to be assessed since with this percentage, the % Fe_3C was assessed. It was determined previously that the iron carbide present in the reaction product was cementite. The results of Mössbauer analysis for these experiment revealed excellent agreement with theses results of gravimetric analysis.

Table 5.6 Experimental data for replicated experiment carbidization with 80 %H_2 and 20 CO for 10 minutes. (Pre-reduction of Fe_2O_3 with 100 % H_2)

run	initial mass (mg)	final mass (mg)	%C	% Fe_3C (gravimetric)	% Fe_3C (Mössbauer)
A	500.4	364.2	4.24	63.68	66.0
B	501.0	365.1	4.36	65.50	66.5
C	500.7	364.9	4.37	65.57	66.6

5.4.3 The Reaction Product from Reduction by H_2

Two experiment were conducted with 100 % H_2 at 625 °C for 5 min. The heating path from room temperature to 625 °C was realized under H_2 during 20 minutes, and the cool-down path was realized under argon. The mass of the original sample was 500.2 mg and the mass of the reaction product was 348.6 mg. This mass ratio is 0.6969 which can be compared to a ratio of 0.6994 conversion of Fe_2O_3 to Fe

In the second experiments under the same condition for before experiment, the mass of the original sample was 500.7 mg and the mass of the reaction product was 349.9 mg. This indicated that a factor of .6988 was assessed.

This determined that a ratio of 0.697 conversion of Fe_2O_3 to Fe can be used for to assess the amount of the mass of the reaction product after the reduction by H_2 of the original sample. Thus, after the carbidization process, the difference between the mass of final reaction product and the mass of the original sample after reduction, determines the amount of carbon deposit.

CHAPTER 6
CONCLUSION

This final chapter of this thesis includes a summary and discussion of the salient aspects of the research conducted. Enumerated conclusions are listed which highlight the accomplishments of the investigation. Finally, suggestions for further work are provided.

6.1 Summary and Discussion

The research conducted focused on assessing the thermodynamic basis for the production of iron carbides (cementite). In addition, intrinsic measurement of conversion rates of iron to cementite with CO-H_2 gas mixtures have been conducted. These measurements allowed the viability of an adsorption based model, which was developed to describe the conversion kinetics, to be assessed.

The development of phase-stability diagrams has provided a basis for defining limiting operational conditions for cementite stability. In addition to displaying the phase-stability fields on an equilateral triangular diagram where the gas phase composition is represented by C-H-O coordinates, a right-angle triangular diagram was also employed. The latter representation provided for better discrimination in identifying the region, corresponding to a range of gas-phase compositions, where carbidization was possible without the risk of carbon (either as graphite or amorphous carbon, deposition). On the basis that a t "low" temperatures (800-900 °K) the condensed carbon phase is amorphous (Dent) carbon rather than graphite, the thermodynamic (equilibrium) analysis revealed an increased undersaturated field where carbon deposition in principle is absent.

An additional feature of the thermodynamic analysis was regarding the gas-phase equilibration. If the species CH_4 is exclude from the gas phase, so that a metastable gas

phase comprised of CO, CO_2, H_2 and H_2O, then the tie line along which a specified Y_{H_2} / Y_{CO} ratio is defined now lies with the Fe_3C field for a feed gas, where Y_{H_2} / Y_{CO} >3. The ramification is that, in principle, whereas a stable gas-phase comprised of CH_4, CO, CO_2, H_2 and H_2O evolves, the gas-phase composition coordinate would lie within the Fe phase-field, it now lies within the Fe_3C field.

The experiments conducted to provide information on the intrinsic rate of conversion of iron-from-hematite to cementite, relied on the knowledge-base provided by the thermodynamic analysis conducted in this research and the previous investigation by Conejo (1995) as well as previous works in carbidization.

Conejo had found that under equilibrium conditions and for gas-phase total-pressure in the vicinity of 1 atm, that the potential for iron carbide formation and for carbon (graphite) deposition could not be uncoupled. In other words the cementite field in his Fe-C-H-O phase stability diagrams was located in a region where the hypothetical activity of graphite was higher than unity, Thus, the conversion of iron to cementite without "carbon" deposition would imply that metastable conditions were present by which the rate of consumption of carbon on the surface to produce cementite was higher than the parallel competing reaction for carbon condensation and crystallite development. Indeed, his TGA experiment on the in-situ conversion of iron to cementite indicated that carbon deposition did not occur until approximately 80 % conversion of iron had occurred. The iron in his experiments was an intermediate reaction product obtained by the reduction of reagent grade hematite with the feed phase ($CO-H_2$) also employed for carbidization. This behavior reported by Conejo was also observed in the present research.

The rate-model, without consideration of deposition of carbon, for conversion to iron carbide which was developed appears to be viable in describing the conversion behavior up to a fractional conversion of 0.8 to 0.9.

The parameters of the rate-equation were obtained from experiments (at 625 °C, 898 °K) conducted with CO-Ar and CO-H_2 gas mixtures. The composition of the CO-H_2 gas mixtures covered the range from "pure" CO (no H_2 present) to low mole fraction of CO ($Y_{CO} = 0.05$).

The reaction-rate equation developed in conjunction with the measurements of the fractional conversion of Fe to Fe_3C, $\chi_{Fe}(t)$ was:

$$\chi_{Fe}(t) = \lambda \cdot r''_{Fe_3C(P_{CO},P_{H_2})} \cdot t$$

in which,

$$\lambda = \frac{3M_a S_o}{m_{Ao}}$$

$$\lambda \cdot r''_{Fe_3C(P_{CO},P_{H_2})} = k'_{3.15}\left[\frac{(K_{3.13}\cdot p_1)^2}{\left(1+(K_{3.13}\cdot p_1)^{1/2}+(K_{3.14}\cdot p_2)^{1/2}\right)^4}\right]+$$

$$k'_{3.16}\left[\frac{(K_{3.13}\cdot p_1)}{\left(1+(K_{3.13}\cdot p_1)^{1/2}+(K_{3.14}\cdot p_2)^{1/2}\right)^2}\right]\left[\frac{(K_{3.14}\cdot p_2)}{\left(1+(K_{3.13}\cdot p_1)^{1/2}+(K_{3.14}\cdot p_2)^{1/2}\right)^2}\right]..(+$$

and,

$$K_{3.13} = 1.33 \pm 0.08 \text{ atm}^{-1}$$

$$K_{3.14} = 0.35 \pm 0.02 \text{ atm}^{-1}$$

$$\lambda \cdot k_{3.15} = k'_{3.15} = 0.66 \pm 0.03 \text{min}^{-1}$$

$$\lambda \cdot k_{3.16} = k'_{3.16} = 21 \pm 1.5 \text{ min}^{-1}$$

The quantity λ incorporates the Fe stoichiometry of Fe_3C, molecular weight of Fe, the initial mass of iron and the "surface area" of the precursor iron . The latter quantity can not be determined explicitly since it is embedded in the heterogeneous reaction-rate constants of $k'_{3.15}$ and $k'_{3.16}$.

The parallel competing reaction for surface carbon where soot is deposited would also have to be incorporated to provide for a complete description of the behavior observed. However, apparent lack of the equilibration of CO and H_2 in the gas phase (to the extent that neither CO_2 nor H_2O are formed) should be investigated before this effort is initiated.

6.1 Enumerated Conclusions

The following enumerated conclusions represent the primary contributions of this research to the knowledge-base on conversion of iron to cementite by gas-phase carbidization:

1. a) A significant contribution to the research is the development of metastable gas phase configurations for the Fe-C-O-H system, where a binary representation of the equilibrated gas-phase composition by its component mole-fractions (Y_C, Y_H and Y_O) is employed.
   b) Some configurations of the gas phase with cementite provide for conditions where Fe_3C activities higher than unity in conjunction with carbon activities lower than unity are achieved, when amorphous carbon is the condensed carbon phase rather than graphite.
2. Cementite formation without carbon deposition is controlled by the rate at which "carbon" is incorporated into Fe_3C relative to that at which it is incorporated into the carbon deposit assemblage. However, as the carbide content of the reaction product exceeds approximately 80-90 %, carbon (soot) builds up on the surface of converted material. It is not clear whether this phenomenon is due to the Fe_3C serving as a catalyst for the decomposition of CO, which apparently does not equilibrate in the gas phase, or only to the unequilibrated CO. Evidence for the lack of equilibration to the extent that neither CO_2 nor H_2O is formed was obtained from the thermodynamic

analysis where CH_4 was excluded from the gas phase, which then hypothetically provided for conditions where Fe_3C is stable in a region of carbon undersaturation.

3. There is no appreciable change in morphology of the iron particles produced by reduction of the reagent grade Fe_2O_3 with hydrogen, during the subsequent conversion to Fe_3C.

6.3 Recommendations for Further Research

The following recommendations for further research based on the experience gained in conducting the present research are provide:.

a) Explore the non-reactivity of CH_4 in regard to its gas phase equilibration with other species such as CO_2 and H_2O. Its unreactivity with Fe to produce Fe_3C would appear to be now well establish by the results of this research. This would require chromatographic analyses of quenched gas-phase samples.

b) Investigate the intrinsic kinetics of Fe conversion to Fe_3C with CO-H_2 mixtures, similar to this study except that H_2S (or SO_2) would be added to the feed gas. This research would be particularly important in regard to the high-conversion carbon precipitation behavior, in light of recent research conducted in Japan.

c) Conduct experiments, with commercial samples of hematite to obtain data on the conversion rates. These measurements would provide information the influence of particle-size and associated chemical constituents on the conversion rate.

REFERENCES

Alstrup, I., *J. Catal.* **109**, 24 (1988).

Alstrup, I.and Tavares M. T, *J. Catal.* **135**, 147 (1992).

Aparicio, L.M., *J. Catal.* **165**, 262 (1997).

Baker, D. W. (1981), Ph.D Thesis, Colorado School Of Mines.

Bell, A. T.,in E.E. Petersen and A.T Bell (Eds): *Catalyst Deactivation*, Dekker, New York,(1987) , 253.

Chipman, John., Met. Trans., 55, (1972).

Conejo, Alberto., "Conversion of Iron Oxides to Iron Carbides by gas phases carbidization"; Ph.D. Thesis , Colorado School of Mines (1995).

Dent, F. J., L. A. Moignard, A.H. Eastwood, W. H. Blackburn, and D.Hebden : Trans. Inst. Gas Eng., 602 (1945).

Dent, F. J., and CoBB. J, Chem. Soc. **2**,1902 (1929).

Dirand and Afqir, Acta Metallurgica, 983.

Edström, J. O., JISI, November, 289, (1953)

El-Geassy, A. A., Shehata, K. A., and Ezz, S. Y., Trans ISIJ, vol. 17, 629,(1977).

Erley, W., and Wagner, H. J., *J. Catal.* **53**, 287 (1978).

Fruehan R.J. Future steelmaking : "Technologies and the Role of Basic Research" Iron & Steel maker (July, 1996), 25.

Garraway, R.. "Nucor's Startup of the world's first Commercial Iron Carbide Plant". Iron & Steelmaker June (June, 1996), 27.

Grabke, H.J.. "Evidence on the surface concentration of carbon on Gamma iron from the Kinetics of the carburization in CH_4-H_2". Metallurgical Transactions 2972- Volume 1. October 1970.

Gregory, D K. Ferguson, E. Slootman, E. Viraize, J. Luchoff. "Results of ALAR_PC™ . Post-combustion at Cascade Steel Rolling Mills" Iron & Steel maker (May, 1996) * page number.

Hager, J. P., F.A. Stephens, and F, M. Stephens,. "Method for Controlling the Conversion of Iron-Containing Reactor Feed into Iron Carbide" :U.S. Patent 5 366 897, Nov.22,1994.

Hayashi, S. and Y. Iguchi: ISIJ Int, **37**,16(1997).

Hirotsu and Nagakura. Acta Metallurgica ,1972

Jackson, R. S., JISI, May, 375, (1973)

JANAF thermochemical Tables (1986); Third Ed. Editedby Am. Chem. Soc./Am. Onst. Physics/National Bureau of Standars. vol.I. p.600.

Jones, J. A. T.. New steel Melting Technologies . Iron & Steel Maker p. 49 April (1996).

Kawasaki, E. Sanscraine, J. and Walsh, T. J. "Kinetics of reduction of iron oxide with CO and H_2", AIChE Journal, Vol. 8, Nr.3, 1962, pp. 48-54.

Kim, M. S., Rodriguez, N. M., and Baker, R. T. K., *J. Catal.* **134**, 253 (1992).

Kock, A. J. M., De Bokx, P. k., Boellaard, E., Klop, W., and Geus, J. W., *J. Catal.* **96**, 468 (1985).

Königer, A., Hammerl, C., Zeitler M.and Rauschenbach B. (1997); "Formation of metastable iron carbide phases after high-fluence carbon ion implantation iron carbide at low temperatures", Physical Review B, Vol.55. Nr. 13 April 1997, pp. 8143-8147.

Lien, H. O., El-Mehairy, E. and Roos, H. U. (1971).; "A Two-zone theory of iron oxide reduction", JISI, July 1971, pp. 541-545.

Ma, C-B., Ando, T., Williamson, D. L., and Krauss, G., Met, Trans 14A, 1039 (1983)

Mayer, M., and Altamayer, V., Chemische Berichte **40**,2134 (1907).

McManus, George J., Steel Editor: *Re-engineering The Steel Industry*. Newsteel, p. 17, January, (1994).

Niels R. Udengaard, Jens-Henrik Bak Hensen, David C. Hanson and Joseph A. Stal "Sulfur passivated reforming process lowers syngas H_2/CO ratio". Oil Gas journal , March.(1992), pp. 62-67.

Olsson, G. and Turkdogan, E. T: "Catalysis of Iron Decomposition Of carbon Monoxide. Part II: Effect of additions of H_2, H_2O, CO_2 and SO_2 Mixtures", Met. Trans, Vol.5, (1974), pp. 21-26.

Pankratz, L. B. (1982); "Thermodynamic Properties of elements and Oxides". U.S. Bureau of Mines, Bulletin ^72, 1982.

Park, C., Rodriguez, N. M., and Baker, R. T., *J. Catal.* **169**, 212 (1997).

Pring and Fairle : J.Chem. Soc. 2, 1903 (1929)

Rao, M. N. y López Hércules, Jesús Ramón "Precipitación del carbono y formación de carburos en el hierro esponja durante el proceso de reducción Directa". Latin American Journal of Metallurgy and Materials. Vol 5, No 1,p.52 (1985).

Roe, Lawrence A. "Iron Ore Beneficiation" (1957).

Rosei, R., Ciccacci, F., Memeo, R., Mariani, C., Caputy, S., and Papagno L., "Kinetics of Carbidic Carbon Formation from CO in the 10^{-6} Torr range on Ni (110)" *Journal of Catalysis* **83**, 19-24 (1983).

Rostrup-Nielsen, J. R. "Sulfur-passivated nickel catalysis for carbon-free steam reforming of methane" J. Catal. **85**, (1984), pp. 31-43.

Rostrup-Nielsen, J. R., "Sulfur-Passivated Nickel Catalyst for Carbon-Free Steam reforming of Methane". *J. Catal.* **85**, 35 (1984).

Rostrup-Nielsen, J. R: Steam Reforming Catalysts, Danish technical Press, Copenhagen (1975).

Rostrup-Nielsen, J. R., and Trimm, D. L., *J. Catal.* **48**, 155 (1977).

Sacco, A., Jr., Geurts, W. A., Jablonski, G. A., Lee, S., and Gately, R. A., *J. Catal.* **119**, 322 (1989).

Sakai, N., Chida, T.,Tadaki, T., and Shimoizaka, J., *J.Chem. Eng. Japan* **18**, 199 (1985).

Schouten, F. C., Kaleveld, E. W., and Bootsma, G. A., Surf. Sci. **63**, 460 (1977).

Scriefer, John Pittbursgh Editor.: "Alternative irons for electric and blast furnaces". Newsteel (February, 1995),16

Senateur, J.P. "Contribution a l'etude magnetique et structurale du carbure de Hagg". Ann. Chim. Vol.2, (1967), pp 103-122.

Shultz, J. F., Karn, F. S., Anderson, R. B., and Hofer, L. J., "A New Type of Catalyst-Carbon-expanded Iron". *Fuel* **40**, 181 (1961).

Snoeck, J.-W., Froment, G. F., and Fowles, M., *J. Catal.* **169**, 240 (1997).

Stephens, F. A., Williamson, D. L. and Hager, J. P. "Application of Mössbauer spectroscopy to the development and commercialization of the iron carbide process", EPD Congress,TMS, (1993), 633.

Tavares, M.T; I. Alstrup, C. A. Bernando, and J. R. Rostrup-Nielsen "CO Disproportionation on Silica-Supported Nickel and Nickel-Copper Catalysis". *Journal of Catalysis* **147**, 525-534 (1994).

Tavares,; I. Alstrup, C. A. Bernando, and J. R. Rostrup-Nielsen "CO Disproportionation on Silica-Supported Nickel and Nickel-Copper Catalysis in CO + H_2 mixtures". *Journal of Catalysis* **158**, 402-410 (1996) .

Templeton, Bryan P.: "Microstructural Characterization of Rapidly Quenched and Anneled Nd-Fe-B Hard Magnetic Alloys Using Mössbauer Spectroscopy and X-ray Diffraction"; Msc Thesis , Colorado School of Mines (1998).

Tottrup, P. B., *Journal of Catalysis* **42**, 29 (1976).

Turkdogan, E. T and J.V. Vinters: "Catalysis of Iron Decomposition of carbon Monoxide. Part I: Carbon Deposition in H_2-CO Mixtures", Met. Trans, Vol.5, (1974), pp. 11-19.

Yang, R. T., and Chen, J. P., *J. Catal.* **115**, 52 (1989).

APPENDIX

Table A.1 Equilibration of Oxygen			
Reaction	Standard Gibbs Free Energy Relationship (kJ/mol) *	Temp. range (°K)	Reference
$C_{(s,\,gr)} + \frac{1}{2} O_{2(g)} = CO_{(g)}$	$-107.177 + 0.00178 \bullet T \bullet \ln T + 1.95 \bullet 10^{-6} \bullet T^2 - 394.76 \bullet T^{-1} - 0.1068 \bullet T$	298 - 2000	Janaf 1985 p 626
$C_{(s,\,gr)} + O_{2(g)} = 2CO_{(g)}$	$-393.714 - 0.0004 \bullet T \bullet \ln T + 9.67 \bullet 10^{-7} \bullet T^2 - 25.9408\, xT^{-1} - 0.00052 \bullet T$	298 - 2000	Janaf 1985 p 628
$H_{2(g)} + \frac{1}{2} O_{2(g)} = H_2O_{(g)}$	$-238.618 + 0.011711 \bullet T \bullet \ln T - 2.41 \bullet 10^{-6} \bullet T^2 - 6.9036 xT^{-1} - 0.03263 \bullet T$	373 - 2000	Pankratz Bull. 672,1982 p 181

(*) Modified from kcal/mol to kJ/mol

Table A.2 Equilibration of Carbon			
Reaction	Standard Gibbs Free Energy Relationship (kJ/mol)*	Temp. range (°K)	Reference
$C_{(s,gr)} + H_{2(g)} = CH_{4(g)}$	$- 393.714 - 0.0004 \bullet T \bullet \ln T + 9.67 \times 10^{-7} \bullet T^2 - 25.9408 \bullet T^{-1} - 0.00052 \bullet T$	100 -2000	Janaf Vol 14, 1985 p 600
$2CO_{(g)} = C_{(s,gr)} + CO_{2(g}$	$- 179.36 - 0.00395 \bullet T \bullet \ln T - 2.92 \bullet 10^{-6} \bullet T^2 + 815.4616 \bullet T^{-1} + 0.213087 \bullet T$	298 - 2000	
$H_{2(g)} + CO_{2(g)} = H_2O_{(g)} + C_{(s,gr)}$	$- 131.44 + 0.009933 \bullet T \bullet \ln T - 4.36 \bullet 10^{-6} \bullet T^2 + 401.664 \bullet T^{-1} + 0.074178 \bullet T$	373 - 2000	

(*)Modified from kcal/mol to kJ/mol

Table A.3 Equilibration of Iron Oxides			
Reaction	Standard Gibbs Free Energy Relationship (kJ/mol)*	Temp. range (°K)	Reference
$3Fe_{(s)} + 2O_{2(g)} = Fe_3O_{4(s)}$	$-1135.03 - 0.02203 \bullet T \bullet \ln T - 3.23 \bullet 10^{-5} \bullet T^2 + 1074.87 \bullet T^{-1} + 0.524678 \bullet T$	298- 1043	Coughlin 1951
$3Fe_{(s)} + 2O_{2(g)} = Fe_3O_{4(s)}$	$-954.144 + 0.007623 \bullet T \bullet \ln T + 4.42 \bullet 10^{-5} \bullet T^2 - 41526.2 \bullet T^{-1} - 0.104127 \bullet T$	850 - 1043	Coughlin 1951
$0.947Fe_{(s)} + \frac{1}{2} O_{2(g)} = Fe_{0.947}O_{(s)}$	$-278.721 - 0.03522 \bullet T \bullet \ln T + 2.13 \bullet 10^{-5} \bullet T^2 + 572.7687 \bullet T^{-1} + 0.300503 \bullet T$	850 - 1043	Coughlin 1951
$0.947Fe_3O_{4(s)} + 0.788CO_{(g)} = 3Fe_{0.947}O_{(s)} + 0.788CO_{2(g)}$	$-158.38 - 0.11458 \bullet T \bullet \ln T + 2.12 \bullet 10^{-5} \bullet T^2 + 41375.13 \bullet T^{-1} + 0.886651 \bullet T$	850 - 1043	
$Fe_{0.947}O_{(s)} + H_{2(g)} = 0.947Fe_{(s)} + H_2O_{(g)}$	$+40.10364 + 0.046928 \bullet T \bullet \ln T - 2.4 \bullet 10^{-5} \bullet T^2 + 565.865 \bullet T^{-1} - 0.31939 \bullet T$	850 - 1043	

(*)Modified from kcal/mol to kJ/mol

Table A.4 Equilibration of Iron Carbide			
Reaction	Standard Gibbs Free Energy Relationship (kJ/mol)	Temp. range (°K)	Reference
$3Fe_{(s)} + C_{(s,\,gr)} = Fe_3C_{(s)}$	$-9.23953 - 0..10269 \bullet T \bullet \ln T + 7.43 \bullet 10^{-5} \bullet T^2 + 1492.32 \bullet T^{-1} + 0.643876 \bullet T$	298-1000	Darken and Gurry, 1953, table 16-3, p 401
$3Fe_{(s)} + 2CO_{(g)} = Fe_3C_{(s)} + CO_{2(g)}$	$-188.599 - 0.10664 \bullet T \bullet \ln T + 7.14 \bullet 10^{-5} \bullet T^2 + 2307.781 \bullet T^{-1} + 0.856963 \bullet T$	298-1000	
$3Fe_{(s)} + CH_{4(g))} = Fe_3C_{(s)} + 2H_{2(g)}$	$+56.043 - 0.13919 \bullet T \bullet \ln T + 8.6365 \bullet 10^{-5} \bullet T^2 + 1511.27 \bullet T^{-1} + 0.79926 \bullet T$	298-1000	
$Fe_3O_{4(s)} + 5H_{2(g)} + 2CO_{(g)} = Fe_3C_{(s)} + 5H_2O_{(g)}$	$+39.88063 - 0.02388 \bullet T \bullet \ln T + 9.26 \bullet 10^{-5} \bullet T^2 + 846.7286 \bullet T^{-1} + 0.062869 \bullet T$	298-1000	
$3Fe_{0.947}O_{(s)} + 3.947H_{2(g)} + 0.947CO_{(g)} = 0.947Fe_3C_{(s)} + 3.947H_2O_{(g)}$	$+12.9129 + 0.052946 \bullet T \bullet \ln T - 4.86 \bullet 10^{-6} \bullet T^2 + 96.00745 \bullet T^{-1} - 0.0.31939 \bullet T$	850-1000	

(*)Modified from kcal/mol to kJ/mol

Table A.5 Equilibration of Gas Species			
Reaction	Standard Gibbs Free Energy Relationship (kJ/mol)*	Temp. range (°K)	Reference
$CO_{(g)} + 3H_{2(g)} = CH_{4(g)} + H_2O_{(g)}$	$-196.723 + 0.046438 \bullet T \bullet \ln T - 1.64 \bullet 10^{-5} \bullet T^2 + 382.7105 \bullet T^{-1} - 0.08123 \bullet T$	373 - 2000	
$2CO_{(g)} + 2H_{2(g)} = CH_{4(g)} + CO_{2(g)}$	$-244.64 + 0.03255 \bullet T \bullet \ln T - 1.495 \bullet 10^{-5} \bullet T^2 + 796.50 \bullet T^{-1} + 0.0576 \bullet T$	298 - 2000	
$H_2O_{(g)} + CO_{(g)} = H_{2(g)} + CO_{2(g)}$	$-47.9194 - 0.01389 \bullet T \bullet \ln T + 1.43 \bullet 10^{-6} \bullet T^2 + + 413.7976 \bullet T^{-1} + 0.138909 \bullet T$	373 - 2000	

(*)Modified from kcal/mol to kJ/mol

Table A.6 Standard Gibbs free Energy and Enthalpy Change, at the Temperature and Pressures Indicates, for the reaction: $2CO_{(g)} = CO_{2(g)} + C_{(s)}$; where $C_{(s)}$ is either amorphous carbon or graphite, $C_{\beta(s)}$ or $C_{c(s)}$, respectively. Data for amorphous carbon computed from gas-phase composition measurements for equilibration of gas-phase with condensed solid phase. Columns (6) and 9 are, respectively, the Standard Gibbs Free Energy and Enthalpy Change for the reaction
$C_{\beta(s)} = C_{c(s)}$.(abstracted from Dent; 1945).

Temperature (°C)	Total Pressure (atm.)	$Log_{10}(K_p)$ Kp [=] atm^{-1} $Kp = \frac{P_{CO_2}}{P_{CO}^2}$ (Measured)	$\Delta G°_{Rxn}$ (cal.)		$\Delta G°_{Rxn}$(graphite) minus $\Delta G°_{Rxn}$(meas.) (5)-(4) (cal.)	$\Delta H°_{Rxn}$ (cal.)		$\Delta H°_{Rxn}$(graphite) minus $\Delta H°_{Rxn}$(meas.) (8)-(7) (cal.)
			Determined from Measurements	For reaction with Graphite		Determined from Measurements	For reaction with Graphite	
(1)	(2)	(3)	(4)	(5)	(6)	(7)	(8)	(9)
350	1.00	3.48	-9,910	-14,660	-4,750	-16,960	-41,870	-24,910
400	1.00	2.97	-9,137	-12,550	-3,413	-22,410	-41,590	-19,180
450	1.00	2.40	-7,930	-10,475	-2,545	-27,850	-41,320	-13,470
500	1.00	1.86	-6,572	-8,587	-2,015	-31,900	-41,040	-9,140
550	20.00	1.28	-4,815	-6,207	-1,392	-34,630	-40,760	-6,130
600	1.00	0.75	-2,993	-4,070	1,077	-34,830	-40,490	-5,660
700	1.00	-0.08	356	133	-233	-34,670	-39,940	-5,270
700	20.00	-0.13	578	133	-445	-34,670	-39,940	-5,270
800	20.00	-0.89	4,163	4,163	0	-36,520	-39,390	-2,870
800	20.00	-1.53	7,853	8,111	258	-38,840	-38,840	1,300